STUDY OF AN IRON/NITROGEN/GRAPHENE CATALYST FOR POLYMER ELECTROLYTE MEMBRANE FUEL CELLS

Pierre-Alexandre Pascone

Department of Chemical Engineering
McGill University
Montréal, Québec, Canada

February 2018

A thesis submitted to McGill University in partial fulfillment of the requirements of the degree of Doctor of Philosophy

Abstract

The work of this thesis is in the field of non-noble metal catalysts for the oxygen reduction reaction (ORR) of a polymer electrolyte membrane fuel cell (PEMFC). The ORR requires a catalyst, platinum providing presently the highest level of catalytic activity and being used in essentially all PEMFC applications. Platinum is however a very expensive metal that has hindered the large scale production of PEMFCs in everyday products, generating a desire to develop a low-cost alternative. In this thesis, the proposed catalyst is composed of iron coming from a salt and a carbon nanomaterial with nitrogen functionalities, with one important goal being to improve the time stability of such iron-based catalyst materials. The carbon nanomaterial used is stacked graphene structures having 5 – 20 atomic layers, referred to as graphene nanoflakes (GNFs).

The GNFs were produced in-house through gas phase homogeneous nucleation following the plasma decomposition of a carbon-containing feedstock in an inductively coupled plasma torch reactor. By introducing nitrogen gas, either directly during GNF structural growth or in a second treatment step following growth, nitrogen functional groups are bonded to the surface and edges of graphene in different amounts. Iron acetate was used as the source of iron and added to the GNF structures before being heat-treated to generate the final ORR catalysts.

Another recipe for producing the catalyst included phenanthroline as an added nitrogen source. An electrochemical study performed in neutral media was used as a screening technique to determine the effect of nitrogen functionalization on the GNF support system and its interaction with phenanthroline in producing an active catalyst. The best candidate proved to be the catalyst derived from using GNFs with high levels (15 – 20 atomic percent on the surface) of nitrogen, further referred to as high-nitrogen GNFs (HN-GNFs), and without phenanthroline added. This modified synthesis recipe was used for the duration of the thesis. The catalyst`s surface was also characterized with x-ray photoelectron spectroscopy and imaged with electron microscopy.

Catalysts with three different iron concentrations were then synthesized and put through another electrochemical study to investigate the effect of the iron weight percent on the catalyst in different media (acidic, neutral, basic). The catalysts performed well in acidic media, which is vital for a PEMFC catalyst; this result indicated that PEMFC testing should proceed. Additionally, having more iron present allowed a characterization study to be carried out to explore what the shape, location, and bonding of the iron nanoparticles were. It was seen that the majority of the iron is in the form of nanoparticles and are not found on the surface, but encapsulated by the graphene sheets of the HN-GNFs.

The best materials produced throughout the thesis and evaluated through the electrochemical study were tested in a single-cell PEMFC as the ORR catalyst. Although the current density being drawn from the cell was low when compared to other iron-containing catalysts being developed in other research groups around the world, the catalyst developed effectively showed good stability over the 200 hours of testing.

Résumé

Les travaux de cette thèse sont dans le domaine des catalyseurs à base de métaux non-nobles, en particulier dans le contexte de la réaction de réduction de l'oxygène (RRO) d'une pile à combustible à membrane électrolyte polymère (PCMEP). La RRO nécessite l'utilisation d'un catalyseur, celui-ci étant typiquement à base de platine. Le prix du platine constitue un des freins majeur à l'utilisation des piles à combustibles, en particulier dans le secteur des transports. Cette contrainte a rendu nécessaire la synthèse et le développement de catalyseurs à faible coût et à haute performance électrochimique. Le catalyseur développé dans cette thèse est composé de fer, provenant d'un sel, et d'un nanomatériau à base de carbone sur lequel des groupes fonctionnels azotés y sont greffés. Le nanomatériau à base de carbone est consistué de couches de graphène empilées (typiquement 5 – 20 épaisseurs atomiques), nommé nano-flocons de graphène (NFG). Un des buts premier des structures développées est, en plus d'obtenir des catalyseurs à base de fer ayant une bonne activité dans les piles à combustible, d'optimiser leur niveau de stabilité afin de maintenir la RRO sur des bases de temps plus longs.

La synthèse des NFG est faite par nucléation homogène dans un gaz issu de la décomposition thermique d'une matière première à base de carbone dans un plasma thermique. Le réacteur de synthèse est composé d'une torche à plasma à couplage inductif et d'une paroi conique refroidie à l'eau. Les groupes fonctionnels azotés sont greffés à la surface des couches de graphène, en quantités différentes, suite à l'addition de l'azote soit durant la croissance des NFG, ou dans une étape de fonctionnalisation suivant la croissance. Finalement, l'addition d'acétate de fer aux NFG et l'application d'un traitement thermique permettent de compléter le processus de synthèse du catalyseur pour la RRO.

Une recette de synthèse du catalyseur RRO utilise également de la phénanthroline comme source additionnelle d’azote. Une étude électrochimique en milieu neutre a été réalisée afin de déterminer l’effet qu’ont les groupes fonctionnels azotés sur les NFG, ainsi que leur interaction avec la phénanthroline. Les résultats de cette étude montrent que le meilleur échantillon est un catalyseur à base de NFG, sans phénanthroline, et qui a un haut niveau d’azote en surface de 15 – 20 % atomique. Ce dernier est dorénavant nommé NFG à haute teneur en azote (NFG-HTA). Le protocole de synthèse permettant d’optimiser les échantillons de catalyseurs est par la suite utilisée d’abord pour les analyses de surface en microscopie électronique et spectrométrie photoélectronique X, puis pour les analyses électrochimiques.

Des catalyseurs à trois teneurs différentes en fer ont été évalués par essais électrochimiques en milieu acide, neutre et basique. Ces essais ont permi d’examiner l’effet du pourcentage massique en fer du catalyseur sur la performance électrochimique de ce dernier. Les catalyseurs montrent une bonne performance en milieu acide. Ce résultat est un atout pour un catalyseur de type PCMEP et il montre l’intérêt de poursuivre les essais dans le cadre d’une pile à combustible. La teneur augmentée en fer du catalyseur développé a également permis d’entreprendre une étude de caractérisation afin d’observer la géométrie, l’emplacement et les liaisons chimiques des nanoparticules de fer. Il a été observé que la majorité du fer se trouve en forme de nanoparticules et que ces dernières se trouvent encapsulées par les couches de graphène des NFG-HTA, plutôt qu’en surface.

La structure optimum de catalyseur RRO produite et évaluée par méthodes électrochimiques a été testée dans une cellule PCMEP simple. Bien que la densité de courant mesurée reste faible comparée aux catalyseurs développés ailleurs dans le monde, ce catalyseur a effectivement montré un niveau de stabilité dans le temps pour toute la durée des essais sur plus de 200 heures.

Acknowledgements

I would like to begin by first thanking my supervisors Dr. Dimitrios Berk and Dr. Jean-Luc Meunier. My project was in a slightly different field than what they were used to with their previous students, but they trusted me with it and allowed me to see it through. They knew exactly when I needed guidance, encouragement, direction, or the freedom to work independently, and this blend of supervision over the past five years made me a stronger scientist. I appreciate all the time and effort that they put into having me as their graduate student.

There are many different members of the McGill chemical engineering department that I would like to acknowledge for their various forms of help over the years. To Dr. Sasha Omanovic, thank you for answering all my random questions over the years concerning electrochemistry. To Dr. Milan Maric and Dr. Anne-Marie Kietzig, thank you for allowing me to use the hot press in your respective labs. To Dr. Jeff Gostick, thank you for providing me with gas diffusion layers and discussing with me while I was troubleshooting the fuel cell testing station. To Frank Caporuscio, thank you for your beautiful work with the installation of gas delivery lines on the fuel cell testing station and for brightening my day whenever you walked by. To Jo-Ann Gadsby, Louise Miller-Aspin, and the rest of the chemical engineering staff, thank you to all of the many administrative tasks that you performed over the years that were always of tremendous help. To Dr. Sylvain Coulombe, thank you for always being available for a quick chat and for creating the PPL family, which granted me the opportunity to meet and interact with so many of my colleagues.

I had a fantastic time during my PhD and one reason for that is because of the wonderful colleagues that I overlapped with during my time here. To Adya, Alex, Aqeel, Ben, Cristina, Daniel, Deepak, Elena, Eva, Felipe, Hayat, Kathryn, Mahdi, Marisol, Mark, Max, Mitch, Nathan, Norma, Remi, Seyed, Valentin, and anyone else I missed, thanks for all the great times. I would like to thank Matt Kok for his friendship and for being my fuel cell brother from another lab. To Pablo Diaz, thank you for coming into my life and being the most fascinating person I have ever met. Jasmin de Campos, I always took great pleasure in seeing you go from being my summer student (twice) to becoming a graduate student yourself. Thank you for aiding me with my initial PhD work, being a fantastic office mate, and introducing me to knowledge of the youth to make me feel less old.

To Larissa and Evelyne, thank you for being my first coffee break every morning and for allowing me the pleasure of being a hopefully welcome distraction. As Larissa would say, you are both ‘good people’ and it was wonderful working together. I also would like to apologize to Larissa that my distinctive laugh can be heard from 3 offices down the hall.

Mathew Evans, you are in my opinion the quintessential example of a well-balanced graduate student. I have never met a harder worker in the lab nor a better guy to share a drink with after a hard day of work. Our friendship is one of my personal highlights of the last few years of grad school and I owe a lot of my sanity to you. I look forward to being invited to be a co-creator if you ever do decide to go forward with your sitcom idea.

To Dr. Ulrich Legrand, you have been my closest colleague all these years and the best office mate someone could ask for. I’m not sure if you learned more from me or vice versa, but it was an absolute pleasure to work with you on similar projects. I’ll always remember our

conversations in the office, whether they were about science or just life in general. Thank you for always being there for me and for being my brother in arms as we made our way through grad school together.

To my wonderful family, thank you for all the moral support over the years. To my amazing wife Katie, you are everything to me. Thank you for your patience and understanding and allowing me to pursue this degree with your full support. Without you by my side, I would not have been able to make it through this degree.

Finally, this research would not be possible without the financial support of the Natural Science and Engineering Research Council of Canada (NSERC), the Fonds de recherché du Québec sur la Nature et les Technologies (FRQNT), the Eugenie Ulmer Lamothe fund, Hydro-Quebec, and McGill University.

Table of Contents

Chapter 4: Iron Incorporation on Graphene Nanoflakes for the Synthesis of a Non-noble Metal Fuel Cell Catalyst 54

List of Figures

List of Tables

List of Equations

Nomenclature

°	Arcdegree
°C	Degrees Celsius
/	Per
%	Percent
±	Plus or minus
µA	Microamps
µL	Microliter
µm	Micrometer
AFC	Alkaline fuel cell
Ag/AgCl	Silver/silver chloride
BET	Brunauer-Emmett-Teller
cm	Centimeter
C	Carbon
eV	Electron volts
E	Potential
Fe	Iron
FEG	Field emission gun
g	Gram
GNF	Graphene nanoflakes
H_2SO_4	Sulfuric acid
HN	High nitrogen

ICP	Inductively coupled plasma
K	Kelvin
kPA	Kilopascal
kV	Kilovolts
kW	Kilowatt
L_a	Average in-plane length
L_{eq}	Average continuous graphene length
LN	Low nitrogen
m	Meter
M	Molar
mA	Milliamps
mg	Milligram
MHz	Megahertz
mm	Millimeter
mV	Millivolts
N	Nitrogen
NAA	Neutron activation analysis
NaOH	Sodium hydroxide
Na_2SO_4	Sodium sulfate
NIST	National Institute of Standards and Technology
nm	Nanometers
ORR	Oxygen reduction reaction

PEMFC	Polymer electrolyte membrane fuel cell or proton exchange membrane fuel cell
pH	Potential of hydrogen
PTFE	Polytetrafluoroethylene
RDE	Rotating disk electrode
RF	Radio frequency
RHE	Reversible hydrogen electrode
rpm	Rotations per minute
s	Seconds
slpm	Standard litre per minute
sccm	Standard cubic centimeters per minute
SEM	Scanning electron microscopy
TEM	Transmission electron microscopy
wt%	Weight percent
XPS	X-ray photoelectron spectroscopy

Chapter 1: Introduction

1.1 Problem definition

Our current dependency on fossil fuels is unsustainable due to the amount of greenhouse gases and polluting emissions produced from their use. The international community, as evidenced through the signing of the Paris accord of 2015, has acknowledged that clean energy development is vital. Current lesser-used renewable energy sources will eventually replace oil as the primary supply of energy, but work must be done to improve these technologies to the point where they are cost efficient. Polymer electrolyte membrane fuel cells (PEMFCs) represent an alternative energy technology that is clean, has a high power density, operates at relatively low temperatures, and is generally small. One of the present barriers to the emergence of PEMFCs into mass usage is the high cost, which stems from their use of platinum as a catalyst for the oxygen reduction reaction (ORR). By developing a lower-cost alternative to platinum, PEMFCs could take one step closer to becoming an economically viable option to rival the internal combustion engine.

The electrocatalyst (the term given for a catalyst used for a reaction where electrons are transferred) is a material that aids the reaction by opening up alternative reaction mechanisms, thus lowering the activation energy. A metal, such as platinum, can be used as a catalyst by itself, but its effectiveness can be augmented when dispersed on a secondary material as it reduces agglomeration and exposes more surface area of the metal to trigger the electrochemical reaction. This secondary material, referred to as a support system, would ideally have a large surface area on which to disperse the metal, high conductivity for the electron transport to/from the reaction site, and be porous for a good transfer of the reactants and products to/from the reaction sites. For the ORR, an electrocatalyst composed of a transition metal bonded to 4 pyridinic nitrogen atoms with an aromatic carbon support system has already been identified as a promising cost-effective alternative to platinum [1]. Heme, the coordination complex found in hemoglobin, is an example of this structure and is effectively active for the ORR (Figure 1).

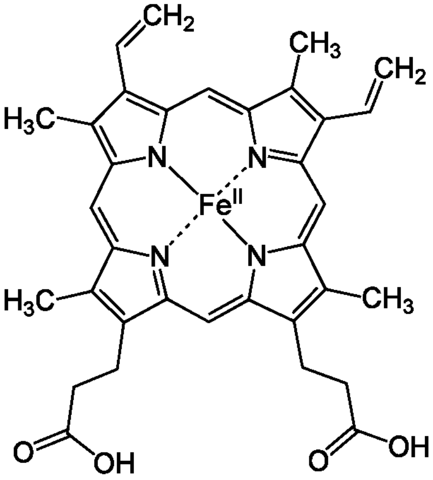

Figure 1. Heme structure [2]

This family of electrocatalysts can be synthesized in various ways, provided a suitable metal, nitrogen source, and carbon support system is in place and the synthesis procedure involves a high-temperature heat-treatment to finalize the chemical structure. The novel electrocatalyst developed in this thesis uses iron from an iron salt and incorporates it into a stacked-graphene nanomaterial whose surface is functionalized with nitrogen. The carbon support system, referred to as graphene nanoflakes (GNFs), is produced in-house through the plasma decomposition of methane and nitrogen through an inductively coupled plasma torch with a conical water-cooled reactor [3].

This doctorate project extends the work previously done during my master's thesis project in which GNFs with low amounts of nitrogen were generated [4]. In this initial project, the iron incorporation method used by Lefèvre *et al.* [5] and based on ball milling of carbon black carbon sources and heat treatments was used without modifications, with the final catalyst being characterized and tested in a PEMFC [4]. This initial work showed that the use of GNFs as a carbon support system for ORR catalysts was worthy of future investigation, particularly in view of catalyst structural evolution and increased stability in time. In this thesis, the iron incorporation method is modified and tuned to the highly crystalline GNF material generated with increased nitrogen functionalization. The synthesized electrocatalysts are characterized and the best candidates are screened using electrochemical studies. The most active electrocatalysts are tested in a single cell PEMFC.

1.2 Thesis objectives

The overall objective of this thesis is to synthesize and comprehend the final structure of a non-noble metal catalyst as an alternative to platinum that is both active to the ORR and stable in a PEMFC environment and is composed of iron, nitrogen, and a carbon support system. The specific objectives for this thesis are:

1) To evaluate if producing a carbon support system and functionalizing it with a large amount of nitrogen on its surface and edges during nanomaterial growth in a plasma process produces more favorable catalyst sites than using phenanthroline as a nitrogen source in a non-plasma secondary step after growth
2) To understand the effect of iron loading as it pertains to both the structure of iron in the carbon support system and the overall catalyst activity towards the ORR.

3) Achieve a stable catalyst by simplifying the catalyst synthesis procedure to prevent damaging the crystalline structure of the carbon support system.

The methodologies for reaching these objectives include:

i) Determine correlations between the synthesis parameters and the overall nitrogen functionalization on the surface of the catalyst relative to the overall composition (atomic percent), covalent bond type to carbon, and interaction with iron nanoparticles.
ii) Investigate the resulting structure and composition of iron within the nitrogen/carbon framework at increased iron salt concentrations in the modified catalyst synthesis method.
iii) Optimize the activity towards the ORR of the novel catalyst based on iron and nitrogen contents and nanomaterial structures through electrochemical studies at various pH environments.
iv) Validate the performance of the catalyst towards the ORR in a single cell PEMFC.

1.3 Organization of the thesis

The thesis is comprised of 8 chapters and an appendix and is written in the manuscript (article) based style. Care has been taken to ensure the requirements set forth by the university and Library and Archives Canada have been met. Chapter 1 introduces the thesis topic and specifies the scientific objectives. Chapter 2 provides an introduction into fuel cells to better understand the final application of this work and highlight the chemical reaction being studied. This chapter also contains a literature review on fuel cell catalysts and relevant carbon nanoparticles used in this field. Chapter 3 is broken down into 3 sections. The first section describes the production of the novel nanomaterial and synthesis of the non-noble catalyst, while the second section offers a review of the characterization techniques used throughout the course of study. Finally, the last section details the experiments used to measure catalytic performance. Chapter 4 is a published manuscript that characterizes differently prepared catalysts to both simplify the iron incorporation method of catalyst synthesis and gain knowledge on what level of nitrogen functionalization yields the best catalyst performance. Chapter 5 is another published manuscript that focuses on the iron content of the catalyst, namely its location within the nanomaterial structure and its weight percent, and presents the catalytic performance within acidic, basic, and neutral electrolyte solutions. The work presented in this chapter directly builds off of the work in chapter 4 as only high nitrogen graphene nanoflakes with the simplified iron incorporation method was used from this point on. Chapter 6 is a manuscript that has been submitted for publication and is the culmination of the thesis work as the best performing catalysts are tested in a fuel cell. Chapter 7 presents fuel cell results of different synthesized catalysts that show the improvement of the base material over the course of the thesis. Chapter 8 summarizes major findings and conclusions, while also addressing the contributions to the scientific field and proposals for further research. The appendix is the operation procedure for growing graphene nanoflakes, provided as additional information to the first section of chapter 3.

Chapter 2: Literature Review

2.1 Classification, introduction, and brief history of fuel cells

An electrochemical cell is a device that either generates electrical energy from redox reactions or uses electricity to drive a nonspontaneous redox reaction. A redox reaction is a chemical reaction where the exchange of electrons between two species results in one species being oxidized (losing electrons) and the other being reduced (gaining electrons). Examples of redox reactions that are found in everyday life are photosynthesis, combustion, and corrosion. Electrochemical cells are classified as either galvanic cells or electrolytic cells. The word ‘galvanic’ comes from the Italian physicist and physician Luigi Galvani who first noticed that energy was released during spontaneous redox reactions and that such release could be used to generate electricity [6]. The first cell to demonstrate this phenomenon was created by the Italian physicist Alessandro Volta, thus inspiring the name ‘voltaic’ cell [6]; ‘voltaic’ and ‘galvanic’ are used interchangeably in the scientific community. The common example of a galvanic cell is a battery, where electrical energy is stored in the form of chemical energy and converted into electricity. The other class of electrochemical cells is an electrolytic cell, when the redox reaction is nonspontaneous and electrical energy from an external source is required. Uses of electrolytic cells in industry are a) in the production of aluminum, sodium, and calcium, b) electroplating metals such as chromium, nickel, or gold, and c) electrolysis in the chlor-alkali industry to make chlorine and caustic soda. Fuel cells are specific types of electrical devices that convert chemical energy into electrical energy. They are classified as a galvanic cell, but are different than batteries in that they do not store energy and instead require a constant external supply of reactants because their reaction products are continuously removed.

The origin of fuel cells goes back to 1839 when scientist William Grove studied reversing the electrolytic process (combining oxygen and hydrogen) to generate electricity [7]. He created the first fuel cell by inserting two platinum electrodes in a sulphuric acid and water solution; at the time, he referred to this device as a 'gas battery' (Figure 2). In 1889, scientists Ludwig Mond and Charles Langer improved Grove's gas battery by adding a clay barrier soaked in sulphuric acid and called their device a 'fuel cell' [7]. In 1937, Francis Bacon used nickel gauze electrodes for his fuel cell that was later used for NASA's Apollo space program [8]. Since the 1980s, fuel cell development has been growing steadily as they are seen as the future replacement of the internal combustion engine and batteries for portable power sources.

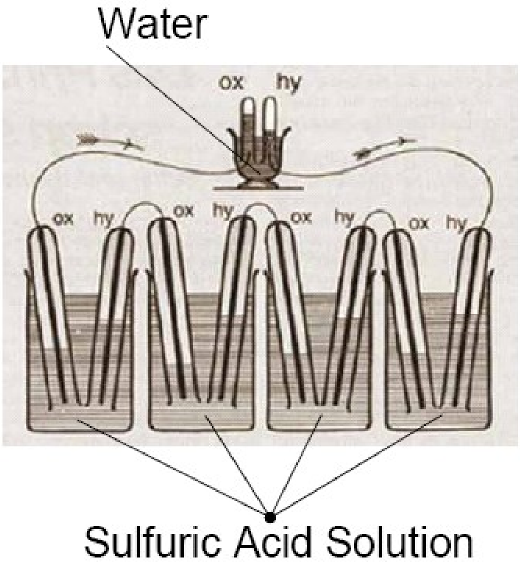

Figure 2. Grove's gas battery diagram [9]

Fuel cells are classified by the type of electrolyte that they use. An electrolyte is a material that produces an electrically conducting solution. Types of fuel cells include: alkaline fuel cells (AFCs), molten carbonate fuel cells (MCFCs), phosphoric acid fuel cells (PAFCs), solid oxide fuel cells (SOFCs), direct methanol fuel cells (DMFCs), and polymer electrolyte membrane fuel cells (PEMFCs). This thesis work focused exclusively on PEMFCs.

2.2 An overview of PEMFCs

The PEMFC is based on the principle of reverse electrolysis with hydrogen and oxygen as fuels. The redox reactions in this electrochemical cell are the hydrogen oxidation reaction and the oxygen reduction reaction (ORR), resulting in water as a product (Equation 1, Equation 2, and Equation 3) [7]. Using a proton exchange membrane is one way to allow chemical energy to be transformed into electrical energy when these two species interact instead of a combustion reaction that produces thermal energy. Hydrogen is split into protons and electrons, with the protons passing through the membrane and the electrons traveling through an external circuit where they can be used to do electrical work. On the other side of the membrane, oxygen reacts with protons and the electrons to produce water.

$$H_2 \rightarrow 2H^+ + 2e^-$$

Equation 1. Hydrogen oxidation reaction

$$\frac{1}{2}O_2 + 2H^+ + 2e^- \rightarrow H_2O$$

Equation 2. Oxygen reduction reaction

$$H_2 + \frac{1}{2}O_2 \rightarrow H_2O$$

Equation 3. Overall PEMFC reaction

A PEMFC is made up of multiple components (Figure 3). It contains two electrodes (an electrical conductor used to make contact with a non-metallic part of a circuit) labelled the anode and cathode. The anode is the negative electrode from which electrons flow out of, whereas the cathode is the positive electrode that receives electrons. Based on the reaction that takes place, hydrogen gas is directed to the anode while oxygen is directed to the cathode; hydrogen and oxygen are also referred to as the fuel and oxidant, respectively. The electrodes are made up of a gas diffusion layer (GDL), a porous material of dense carbon fibers. The GDL provides a gas diffused pathway from flow channels to the catalyst layer, helps with water management, transfers heat during cell operation, and provides mechanical strength to the membrane electrode assembly [10]. The GDL is usually topped with a microporous layer (MPL), which is a carbon black powder with a hydrophobic agent that prevents condensed water in the GDL from forming a liquid film [10]. Between the GDL and the membrane is a catalyst layer, which can either be applied directly on the MPL or on the membrane itself. The catalyst layer is a thin layer of support material with catalyst particles. The role of the catalyst layer is to catalyze the redox reactions of the PEMFC. Ideally, the catalyst layer has high electrochemical activity, high poison tolerance, corrosion stability, and mechanical and heat stability [10]. A commercial catalyst layer for a PEMFC is microscale carbon particles with nanoscale platinum. Each electrode, with its corresponding catalyst layer, is placed on opposing sides of the proton exchange membrane to form a membrane electrode assembly (MEA). If the catalyst layers are directly applied to the membrane, it is referred to as a 3-layer MEA; the addition of the GDLs forms a 5-layer MEA. The electrolyte membrane must have high ionic conductivity and selectivity, be an electronic insulator, and also have mechanical, chemical, and heat stability [7]. The thickness of the membrane is generally between 50 – 175 μm [11]. The most common membrane material is

Nafion^{TM}, a perfluorosulfonated acid polymer. A PEMFC is completed by gaskets, graphite plates with fuel canals, current collectors, and end plates.

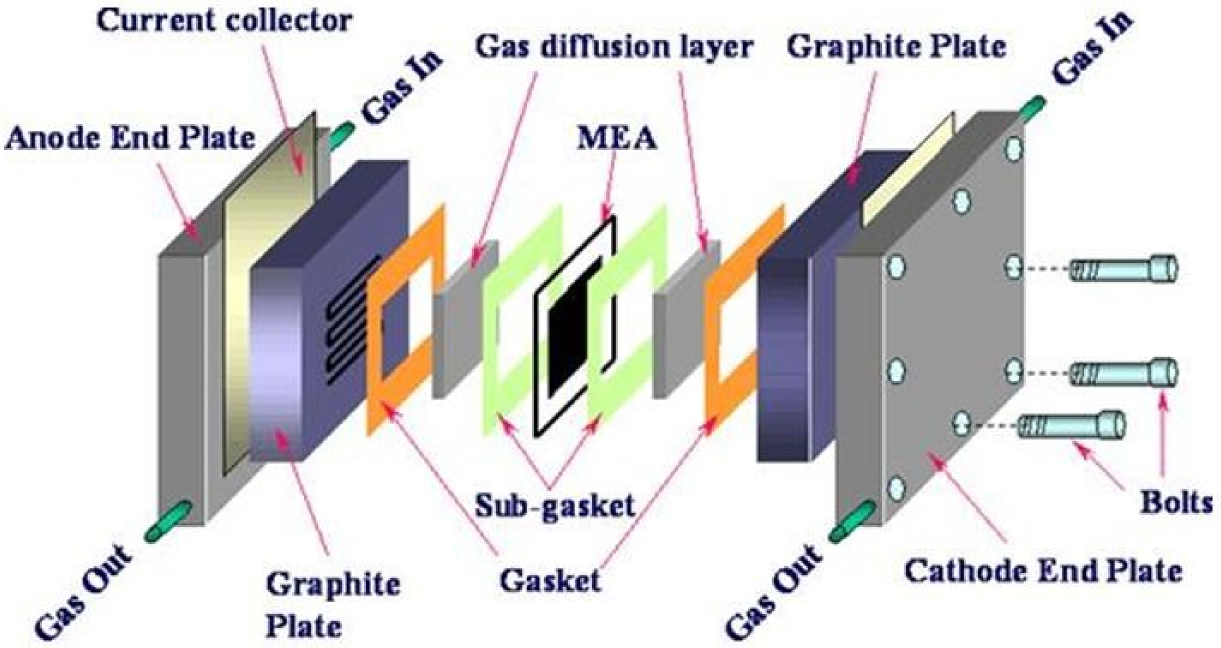

Figure 3. PEMFC diagram [12]

2.3 PEMFC applications

PEMFC applications can be divided into three fields: portable, stationary, and transport. Portable PEMFCs are designed to be compact and movable and provide power in the range of 1 W to 5 kW [13]. Their applications include auxiliary power units (APUs) and small and/or large personal electronics. Currently, there are no direct commercial computers, cordless phones, cameras, or cordless power tools with PEMFCs, but it is possible to buy external chargers for low power electronic devices [13]. These niche products, while available, are more expensive than the current industry leader, lithium-ion batteries. The prospect for PEMFCs concerning portable applications is considered the least positive of the three fields due to the current domination of the electronics market by lithium-ion batteries and the demonstrated success of DMFCs for APUs [14].

Stationary applications, as the name suggests, require PEMFCs that are not designed to be moved. Applications in this field include large and residential combined heat and power (CHP) and uninterrupted power supply (UPS). Large CHPs have been dominated by MCFCs and SOFCs because of the high electrical efficiency of these high-temperature fuel cell systems, but PEMFCs have had some success on smaller scale units in the residential sector for single-family homes. PEMFCs have also found themselves as a viable solution for UPS in backup power generation situations involving extended backup times (exceeding 15 hours); they are becoming more cost efficient than the current solution of batteries, leading to a positive outlook for this application [13].

The last field of transport is where the most positive prospects exist for PEMFC applications. Transport applications are those where the PEMFC either directly or indirectly provides the propulsive power to a vehicle. The list of applications includes forklifts, scooters, cars, buses, trucks, recreational vehicles (RVs), trains, powered bicycles, sailing yacht, and unmanned aerial vehicles (UAVs). A fuel cell powered vehicle is advantageous because of their lack of emissions and the accompanying health benefits to society. When compared to battery electric vehicles, fuel cell vehicles have a higher range and a shorter refueling time [13]. For most vehicles, the PEMFC faces no direct competition from any other fuel cell type as these cannot deliver short start-up times or handle dynamic load demands [14]. Cars relying on PEMFCs have successfully been demonstrated starting from 2004, but the high costs stemming from the use of platinum as a catalyst have hindered their wide spread use. PEMFC buses have been successfully deployed in Europe, Japan, Canada, and the USA. The direct competition for cars is other internal combustion engine-based hybrids. The most successful application and the one with the most positive future are large vehicles such as buses and RVs. The operation of a bus fleet is made easier as they are centrally located and fueled and they are also larger than cars so there is more available integration space for the PEMFC system and hydrogen tanks [13,14].

2.4 PEMFC catalysts

In a PEMFC, both redox reactions are catalyzed by a heterogeneous catalyst. Most heterogeneous catalysts are supported, meaning the catalyst is dispersed on a secondary and usually inert material. The catalyst support enhances the effectiveness of the catalyst by reducing agglomeration and exposing more surface area. As previously mentioned, the current industry leading catalyst for PEMFCs is platinum nanoparticles dispersed onto a porous carbon surface. A further classification of PEMFC catalysts is an electrocatalyst, which is specifically a catalyst that participates in electrochemical reactions.

In the field of electrochemistry, the term overpotential refers to the difference in voltage that is observed between thermodynamic calculations and experimental observations. For PEMFCs, the existence of overpotential means that less energy is recovered as it is lost as heat and thus the cell's overall voltage efficiency is decreased [10]. When comparing the respective reaction rate and overpotential of the ORR and the hydrogen oxidation reaction of the PEMFC (Equation 1 and Equation 2 in Section 2.2), the former is approximately 5 orders of magnitude slower than the latter [15]. This is because the four electron reduction of oxygen requires breaking the strong double bond of molecular oxygen. Therefore, when preparing a PEMFC

MEA, 80 – 90% of the total catalyst mass is applied to the cathode side [15]. For this reason, research efforts to improving PEMFC catalysts have been almost exclusively for the ORR.

To maximize PEMFC performance, which is to say that a higher current density can be achieved at a specific voltage, high catalyst loadings were first attempted. The problem encountered when using a platinum catalyst is that the cost becomes a major concern and a significant hurdle for scale-up and mass commercialization. Therefore, attention turned to improving efficiency and platinum catalysts were tuned with respect to nanoparticle size; the catalytic activity reaches a maximum at a particle diameter of around 2 nm [16]. Another avenue that has been explored to decrease the platinum amount while maintaining performance is by alloying them to metals such as nickel and cobalt [17,18]. Furthermore, research groups are developing nanoparticles with a platinum shell around a metal core [19,20]; these specific cores have proved to be in the same price range as the platinum shell, and cheaper metals have not been synthesized yet.

2.5 Catalyst alternatives to platinum

There are many alternatives to platinum that have been or may be investigated further as a catalyst for the ORR. To avoid the cost complications that arise by using platinum, having a platinum-free catalyst is desirable. From there, a decision must be made on whether to use a metal or rely on a catalyst composed of elements such as nitrogen, sulfur, boron, or selenium. If choosing a metal and continuing to take into account cost considerations, selecting non-noble metals is slightly more desirable. Dedicated research in the field of non-noble metal catalysts for the ORR has led to significant advances in developing various catalysts, particularly those that utilize iron or cobalt as their metal centers, to a point where they can begin to compete with the activity of platinum. It must be mentioned that although the current density is getting close to or even equivalent to platinum, the stability and durability of these catalysts is still unacceptable [15]. Figure 4 provides a logical flowchart for selecting a catalyst alternative to platinum nanoparticles immobilized onto a porous carbon surface. For the remainder of this chapter, the primary focus will be on iron-based catalysts.

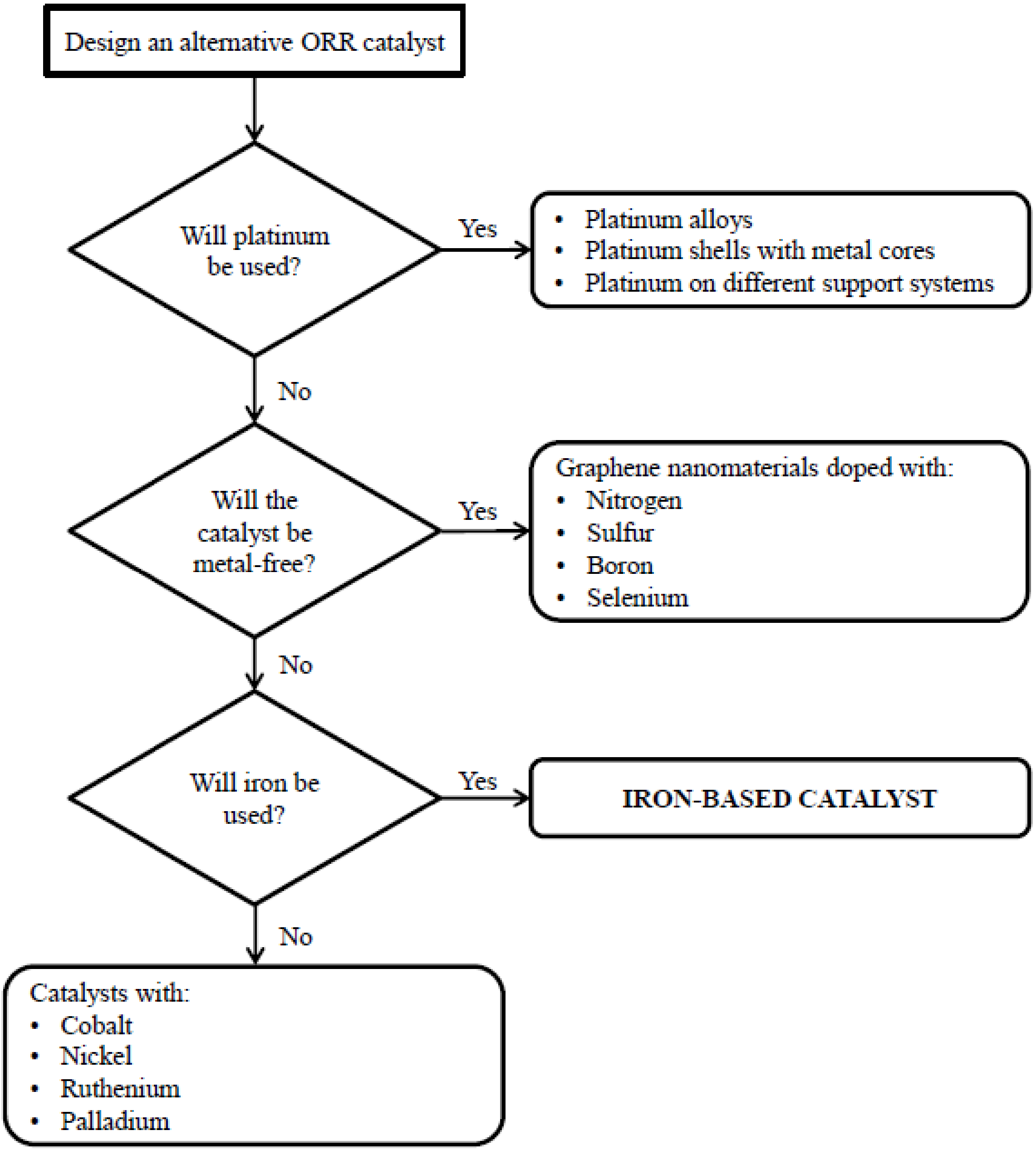

Figure 4. ORR catalysts research flowchart

The first relevant work on non-noble metal catalysts can be traced to 1964, when Jasinsky showed that cobalt phthalocyanine displays a high activity for the ORR [21]. The basic requirement to obtain this proposed catalytic site is to have the metal bonded to 4 pyridinic nitrogen atoms in aromatic carbon, similar to the phthalocyanine structure (Figure 5). The exact structure of the catalyst site is still under debate in the scientific community and there are many proposed sites that are all similar to one another. Furthermore, it is not yet known which site would be the best for the specific application of ORR. Kramm *et al.* studied potential configurations and differentiated them by Mössbauer spectroscopy [22]. They discovered that it is possible to determine oxidation state changes from the changes in the chemical environment. This information was then used to show how one could potentially predict the activity of a catalyst towards the ORR. The paper concludes that one key factor to analyze is the spin state of the iron dz^2 orbital. When the spin state is high or low, activity is possible, while an intermediate spin state means the orbital has no vacancies and thus not able to bind to oxygen, making it inactive for the ORR [22]. The configurations of three proposed catalyst sites are shown in Figure 6. From these three configurations, only the top and bottom have free dz^2 orbital sites available for possible ORR activity.

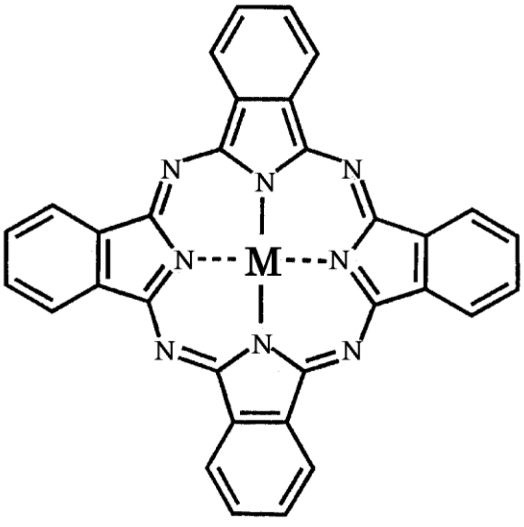

Figure 5. Metal phthalocyanines [23]

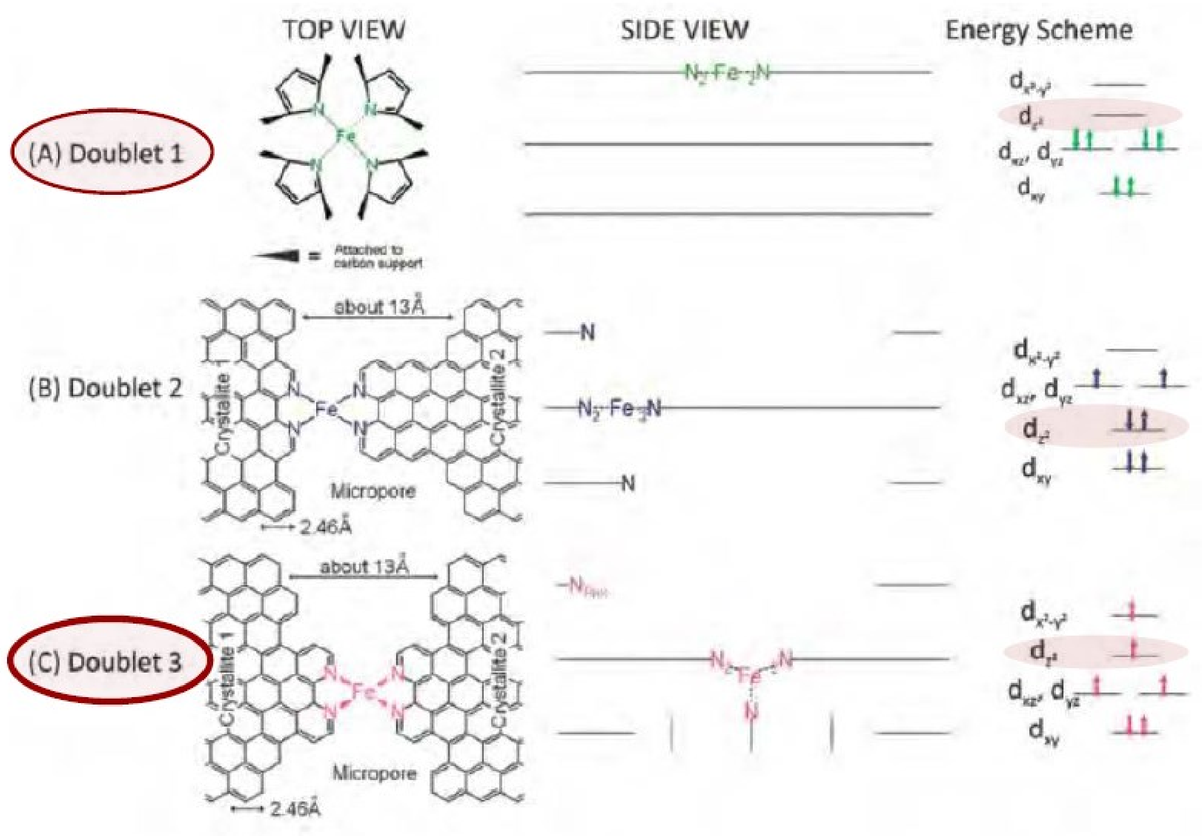

Figure 6. Proposed catalyst sites with low, intermediate, and high spin states, adapted from original publication [22]

To obtain a high activity the catalyst should ideally contain a large amount of nitrogen bonded to the carbon structure, where the nitrogen is primarily bonded to the carbon through pyridinic bonds. If the carbon support has graphitic edge structures, a multi-plane geometry can be provided for affixing nitrogen and iron atoms. Doublet 3 in Figure 6 is one such example of a complex multi-plane geometry.

A variety of metals can be used to prepare a metal/nitrogen/carbon catalyst, but in the non-noble family, iron and cobalt have distinguished themselves as being good ORR catalysts while also showing a low overpotential [24]. More specifically, most of the focus on non-noble metal catalysts research is on pyrolyzed catalysts, where a high-temperature step creates an irreversible change in the chemical composition. When compared with each other, iron is generally more active than cobalt because of its specific active sites [24]. In such a catalyst, iron should be available for catalytic activity through dispersion at the atomic level in order to promote a larger number of catalytic sites than when only available as nanoparticles. Additionally, there are a large number of iron sources, nitrogen sources, and carbon supports that can be used to create these catalysts, although to varying degrees of success. The nitrogen species is vital as it affects the overall efficiency of the catalyst through changes in morphology of the active sites [25]. Nitrogen precursors can be selected to create an amine, pyrrole, pyridines, or porphyrin-like environment. Precursors most used in PEMFC research are polyaniline (PANI), pyrrole, porphyrin, and phenanthroline [24].

2.6 Iron-based catalyst research initiatives

In the 1970s, it was discovered that pyrolysis (a heat treatment in the absence of oxygen to promote the irreversible thermochemical decomposition of an organic material) of metal-containing nitrogen-4 complexes such as iron phthalocyanine was essential to ensuring a better ORR catalyst and improved stability in acidic environments [26]. Gupta *et al.*’s work in the late 1980s found that simple metal salts could be mixed with nitrogen precursors and heat-treated to obtain comparable performance to transition metal macrocycles [1]. From this work, an innumerable amount of possibilities to create iron-based catalysts took off, which can all be summarized as taking a carbon support system, ensuring there are nitrogen and iron sources, and culminating in a heat-treatment step. Focusing on the carbon support system, desirable characteristics include a large surface area, porosity (empty space within the material), and high conductivity.

2.6.1 Carbon black

Carbon black is a term used to describe industrial products formed by the partial combustion or thermal decomposition of hydrocarbons. They are composed of carbon in spherical-like particles in either particle aggregates or agglomerates. Carbon black is different from soot, a material that is essentially impure carbon particles, because of its high surface-to-volume ratio. Different types of carbon blacks exist, each containing its own properties that are the result of its internal structure, with some having large surface areas, high porosity, and high electrical conductivity; thus they are a natural choice for a carbon support system of ORR catalysts.

2.6.1.1 Highlighted works using carbon black

Starting from the late 1990's, the team of J.-P. Dodelet (INRS, Canada) has generated iron-based catalysts with activities for the ORR that eventually matched that of platinum [5,27–38]. They begin their process with carbon black pearls with iron acetate and phenanthroline added as the iron and nitrogen sources to water and ethanol. After mixing, the mixture is heated at 95ºC for 24 hours to allow the liquid to evaporate. The sample is collected and ball milled for 3 hours to generate a micro-porous structure and imbed some iron acetate and phenanthroline into these pores. Once complete, the mixture goes through a 2-stage pyrolysis. Stage 1 takes place in argon atmosphere at 1050ºC for 1 hour. Stage 2 takes place in an ammonia atmosphere at 950ºC for 5 minutes. This procedure leads to a catalyst containing 6 and 0.92 atomic percent for nitrogen and iron, respectively. As indicated above, these catalysts showed an activity comparable to a platinum catalyst (1.25 Acm^{-2} at 0.6 V). One drawback of this work is related to the stability, which loses 15% of its current density in the first 100 hours [38]. A study from the same team showed however that the level of stability scaled well with the Raman parameters characterizing the length scales of the crystalline graphitic sheets in the structures. More and increasing lengths of the graphitic structures provided increased stability of the catalysts. Such knowledge is at the basis of the present work of enhancing the crystallinity of the carbon support material through nanocrystalline graphene sheets.

Wu *et al.* synthesized an ORR catalyst by combining a high-surface area carbon material with iron chloride and PANI (Figure 7) and then performing a heat treatment [39]. The aromatic rings of PANI, coupled with the uniform distribution of nitrogen on the surface, produce nitrogen-containing active sites. The use of this material, PANI, that resembles graphene, was attributed as the reason for the unprecedented stability measured (700 hours) with this catalyst.

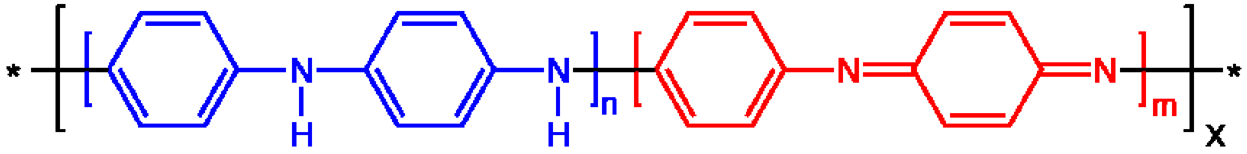

Figure 7. Polyaniline structure where n + m = 1, x = half degree of polymerization [40]

Recently, Fu *et al.* used both phenanthroline and PANI as nitrogen sources in creating an ORR catalyst with carbon black and iron acetate [41]. The role of the phenanthroline was to act as a pore-forming agent while PANI was chosen as it converts to graphene-like structures. This approach lead to an abundance of porous graphene-like structures and the final catalyst produced a max power of 1.06 W/cm^2 in a PEMFC [41].

2.6.2 Carbon nanotubes

Carbon nanotubes (CNTs) are hollow tubes made up of a rolled up graphene sheet (Figure 8). CNTs can consist of either one tube and be referred to as a single-walled nanotube (SWNT) or multiple coaxial tubes and be referred to as a multiple-walled nanotube (MWNT). The specific surface area of CNTs depend on number of walls/diameter, impurities, and surface functionalization with hydroxyl and carboxyl groups. The theoretical specific surface area of SWNTs has been estimated at 1 315 m^2/g, while the measured areas are often at 600 m^2/g or less [42]. For MWNTs, the area is a few 100 m^2/g. For the property of electrical conductivity, the chirality (the symmetry of a carbon center) of the CNTs is vital. Hexagons lined up parallel to the axis of the nanotube are referred to as an 'armchair' configuration; this configuration leads to the CNTs having metallic-like electrical properties including high electrical conductivity. 'Zigzag' configurations leads to the CNTs behaving like semiconductors. These two configurations are shown in Figure 9.

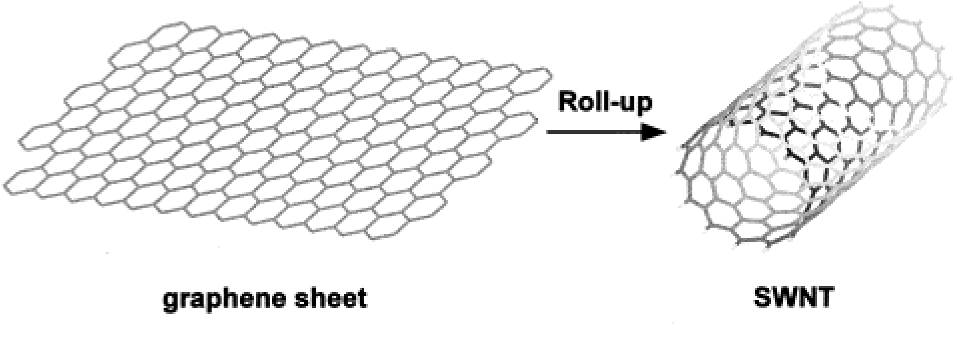

Figure 8. Formation of SWNT by rolling up of a graphene sheet [43]

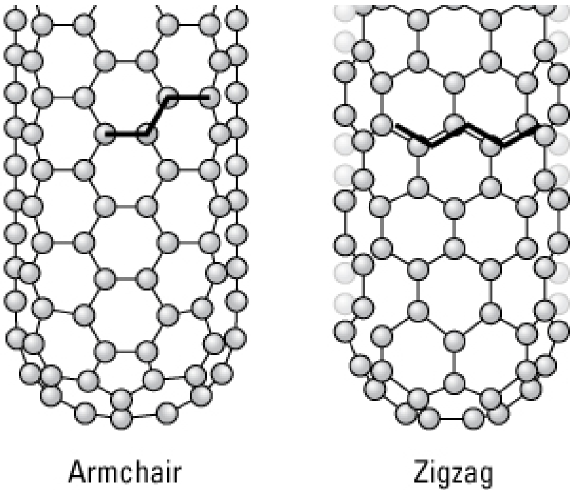

Figure 9. Configurations of CNTs [44]

2.6.2.1 Highlighted works using carbon nanotubes

In research performed by Merzougui *et al.* MWNTs with a surface area of 170 m^2/g were coated with PANI and then mixed with iron chloride hexahydrate and heated to obtain a non-noble metal catalyst for the ORR [45]. The study focused on electrochemical studies and showed comparable activities to other novel catalysts. Their work involved long-term stability experiments and they found a small 15% decrease in activity after 15 000 cycles in acidic media in which they attributed the stability of the catalyst to the high nitrogen content [45]. No PEMFC results were mentioned, but a stability test in methanol showed no noticeable change after 20 000 cycles. They finally conclude that the produced catalyst is an excellent ORR catalyst, but probably better suited for DMFCs or AFCs.

Yasuda *et al.* utilized what they refer to as vertically aligned carbon nanotubes (VA-CNT) as their carbon support system to create an ORR catalyst [46]. VA-CNTs have a large specific surface area in the range of 1 000 m^2/g, which increases the potential for catalytic sites along the surface. Iron phthalocyanine is used as both an iron and nitrogen source and pyrolyzed to the VA-CNTs to produce the final catalyst (Figure 10). Electrochemical studies showed a highly active catalyst in acidic media and long-term stability which was the best reported performance of a CNT-based catalyst at the time of publishing in 2016 [46]. This work was complemented by a characterization of the catalyst that indicates an abundance of active sites. The attention now turns to testing the catalyst in an actual PEMFC.

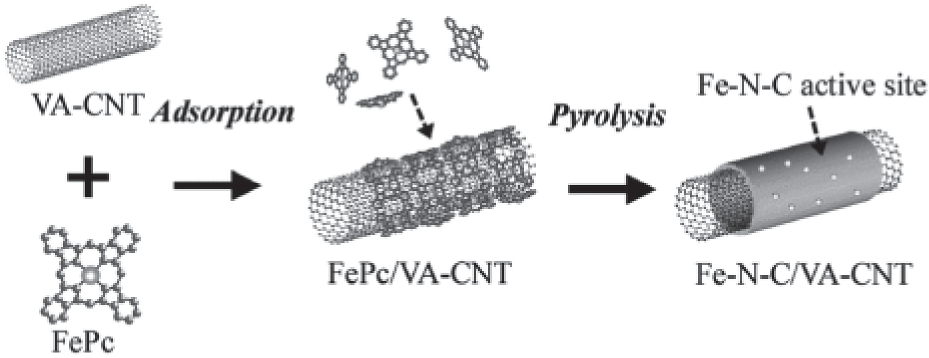

Figure 10. Synthesis procedure for Fe-N-C/VA-CNT catalyst [46]

2.6.3 Graphene oxide and reduced graphene oxide

Graphene oxide (GO), as the name implies, is made from the oxidation of graphite to exfoliate graphitic layers and form the oxidized form of graphene. It is considered a cost-effective substitute for graphene, which is expensive and much more difficult to produce, as graphite is a cheap and abundant material. Furthermore, GO can be reduced to resemble graphene even more and make a product called reduced graphene oxide (rGO). This is an essential step to creating a carbon support system for ORR catalysts as the reduction process enhances the low electrical conductivity of GO. The specific surface area of GO is in the 200 – 300 m^2/g range.

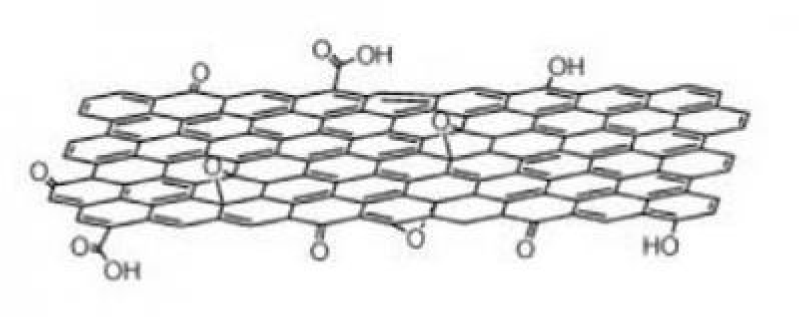

Figure 11. Graphene oxide [47]

2.6.3.1 Highlighted works using graphene oxide

Researchers at the Massachusetts Institute of Technology in Cambridge (USA) have synthesized an iron ORR catalyst from the heat treatment of a mixture of iron chloride, thermally polymerized dicyandiamide, and rGO [48]. The final catalyst has a surface containing 5 atomic percent of nitrogen and 0.4 atomic percent of iron, which was present as nanoparticles. Activity approached that of state-of-the-art non-noble metal catalysts in acidic media with stability experiments showing a 30% drop in the first three hours. No PEMFC tests were mentioned or reported and they conclude that more work must be done [48].

This next catalyst is difficult to classify as strictly an iron-based catalyst as it contains iron, cobalt, nitrogen, and either boron or phosphorous, however its carbon support system is rGO. Choi *et al.* synthesized their own GO and then reduced it with hydrazine to make rGO. The rGO was then mixed with graphene-dicyandiamide, cobalt chloride hexahydrate, and ferrous chloride tetrahydrate and then put through two pyrolysis steps in an argon environment [49]. The catalyst is then doped by introducing either boric or phosphoric acid. The full characterization of the catalyst gave importance to the nitrogen, boron, and phosphorous contents, but the performance of the catalyst in electrochemical studies in acidic media was comparable to other research leaders using graphene derived-materials [49]. As is the case for most novel catalysts, PEMFC tests were not mentioned or reported.

2.7 Alternative carbon support systems

This section will present different carbon nanomaterials not presented in section 2.6.

Graphene

Graphene is a hexagonal matrix of carbon atoms as a single layer with a thickness of one atom. It has the highest tensile strength of any material at roughly 130 gigapascals and has very high electrical and heat conductivity [50]. The theoretical specific surface area of graphene is 2 630 m^2/g, far superior to carbon black and CNTs [42].

Graphite

Graphite is a naturally occurring allotrope (different physical form) of carbon. It is composed of many thousands of layers of graphene sheets (Figure 12). Although composed of graphene sheets, the properties of graphite are incredibly different. For example, the specific surface area of graphite is between 2 – 20 m^2/g.

Stacked graphene/Few-Layer Graphene/Multilayer Graphene/Graphene nanoflakes

Between the extremes of graphene and graphite lies a material referred to as either stacked graphene, few-layer graphene (FLG), or multilayer graphene. This is a material that is not a single layer of carbon atoms, and as such cannot be labeled as graphene, yet the 2-dimensional properties of the material more closely resemble graphene than graphite [33]. There is no definitive threshold value for the number of layers as most reports of FLG deal within the range of 2 – 20 planes. This material corresponds to the carbon support system used in the present thesis and is referred to throughout the thesis as graphene nanoflakes (GNFs), first generated by Pristavita *et al.* [3] at McGill University (Figure 13). Important characteristics of this material are the extreme crystallinity (low defect concentration) and purity of the powders in comparison to regular GO and rGO materials. The purity is characterized by a strong graphitic peak as measured by Raman spectroscopy (Figure 14). The GNFs generate typically have between 5 and 15 planes (Figure 15). The next chapter covers the fabrication method of these graphene nanoflakes.

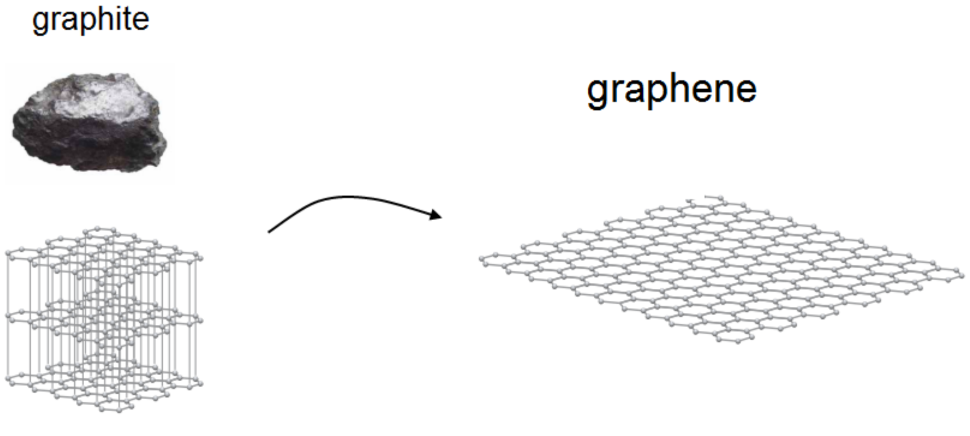

Figure 12. Graphite vs graphene as planes of carbon atoms [49]

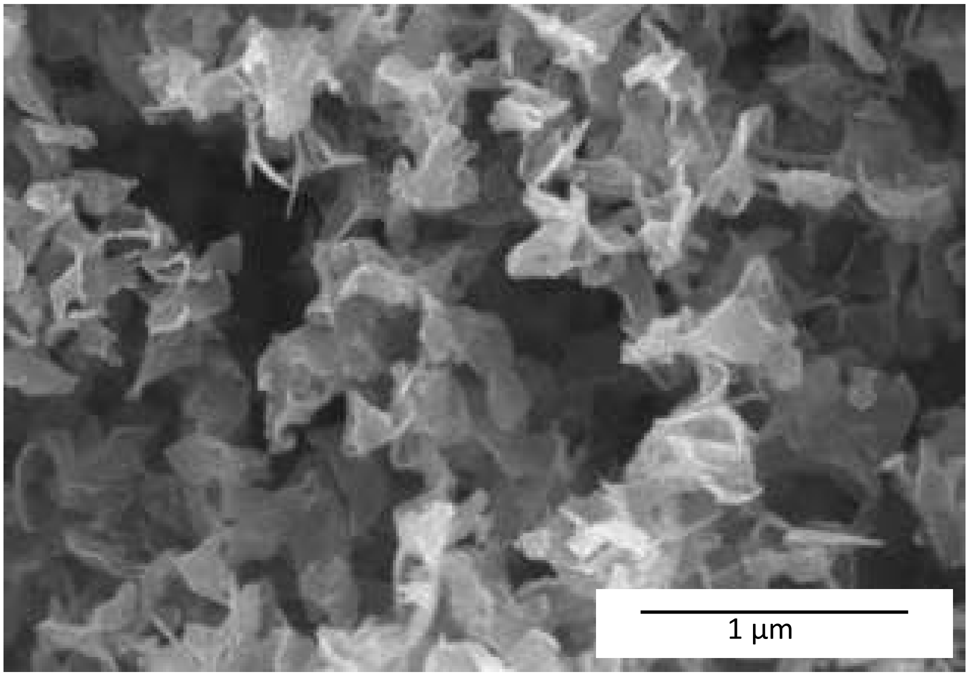

Figure 13. Scanning electron microscope micrograph of graphene nanoflakes [51]

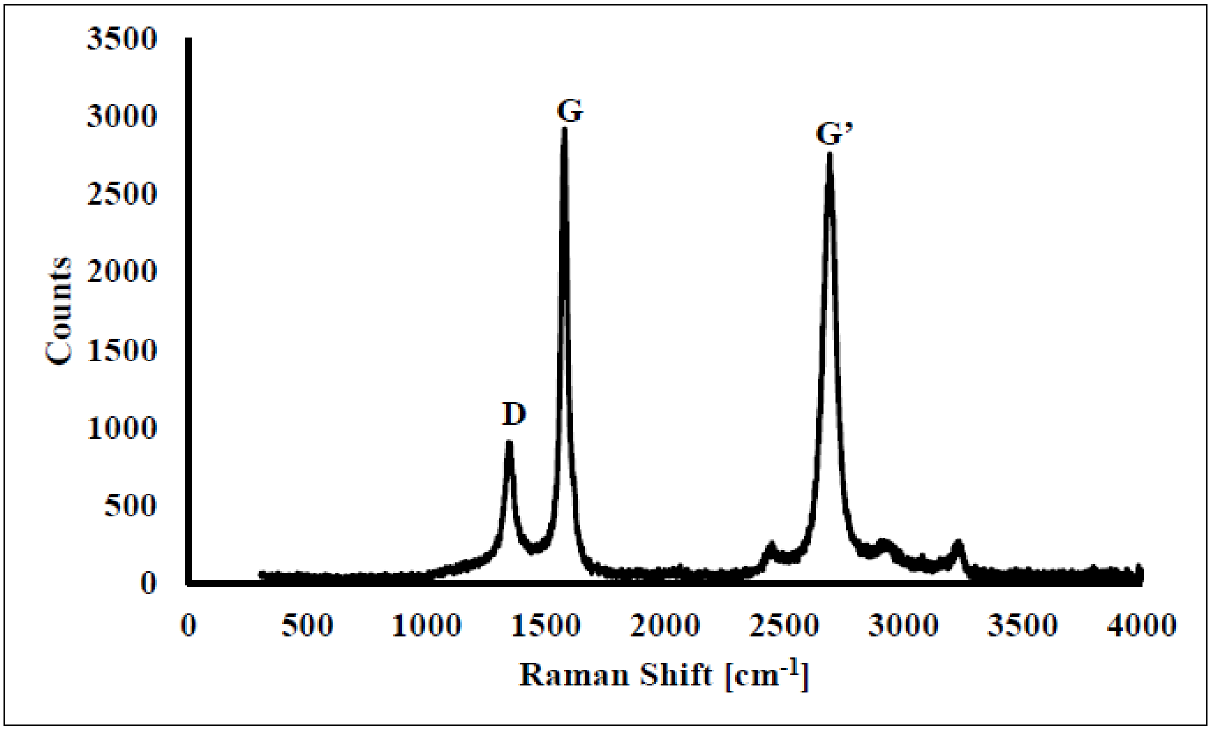

Figure 14. Raman spectroscopy of graphene nanoflakes

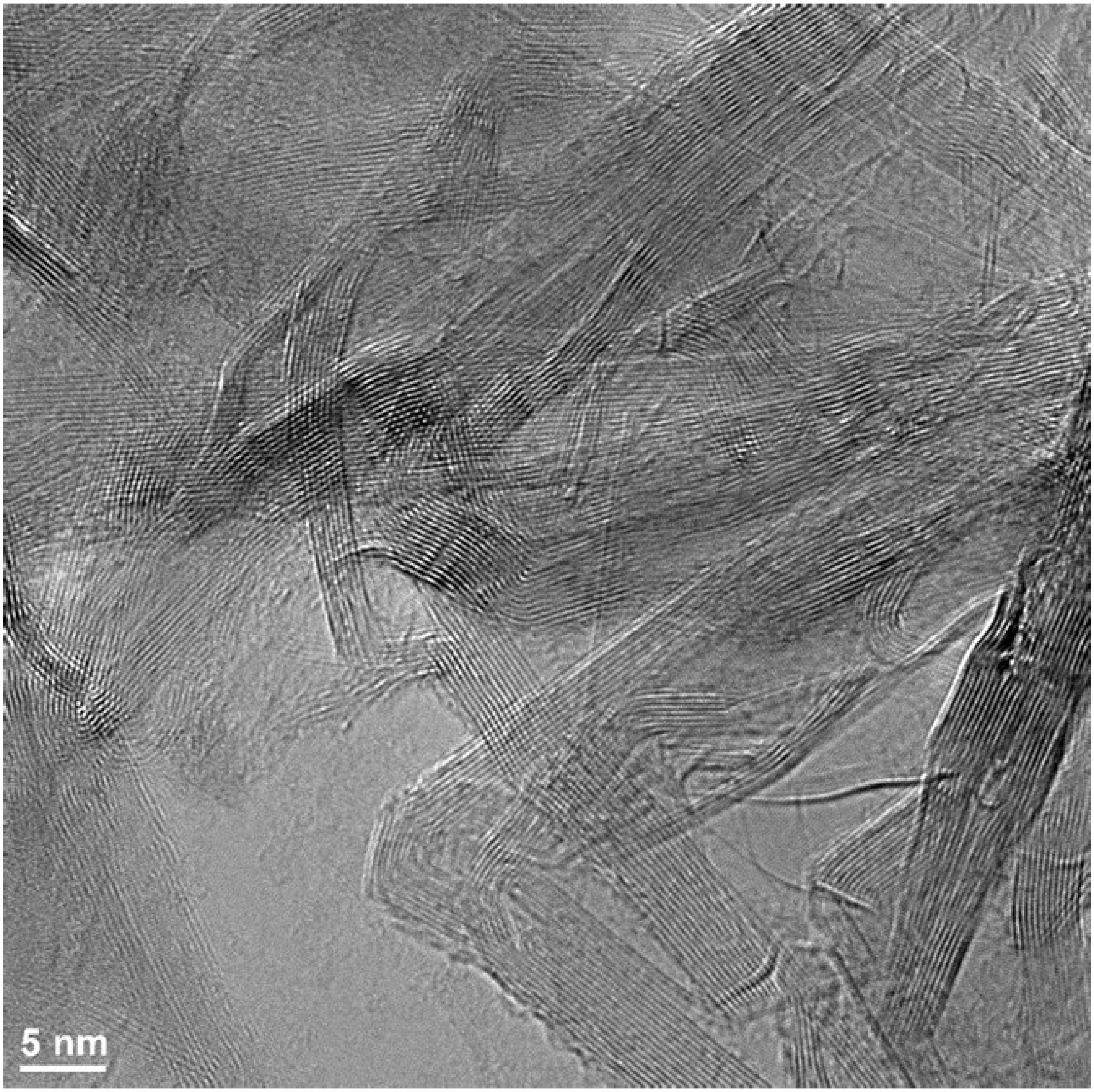

Figure 15. Transmission electron microscope micrograph of graphene nanoflakes [51]

Chapter 3: Experimental Methods and Materials

3.1 Catalyst synthesis

3.1.1 GNF growth

In this work, the procedure developed by Pristavita *et al.* [51] was used to grow GNFs and to first functionalize these with low amounts of nitrogen. The procedure developed by Binny *et al.* [52] was then used as a second step to increase the level of functionalization to much higher levels of nitrogen. The synthesis of this material relies on the thermal plasma decomposition of methane and nitrogen, with the use of an inductively coupled plasma (ICP) system. It is to be noted here that methane is the only carbon precursor involved in the present homogeneous nucleation scheme occurring in the gas phase from the completely dissociated molecules. This produces carbon powders with extreme purity, which is a strong advantage as impurities generate problems and inconsistencies in experimental results and fuel cell operation.

The ICP system is composed of an ICP thermal plasma torch (TEKNA PL-35 model; 35kW power) and a radio frequency (RF) generator (Lepel; maximum of 60 kW of power with a nominal operating frequency in the range of 2-5 MHz); the control console and all other piping and instrumentation was also provided by Tekna. A thermal plasma is characterized by an equilibrium of the electron temperature with the heavy species (atoms, ions, molecules) temperature. In the present scheme of operation, the thermal plasma generated within the ICP torch typically has a temperature in the order of 1 eV (~10,000 K). Figure 16 shows the diagram of the plasma torch body that includes a ceramic plasma confinement tube, the induction coil, gas entrances, and the water cooling system. The gas distributor head produces a uniform axial flow parallel to the wall of the plasma confinement tube (sheath gas) and a swirl flow to the central gas. The torch head supports a ceramic tube that separates the sheath and central gas flows and an injection probe (powder and carrier gas). An exit nozzle is found at the end of the torch body. The control console is responsible for all the operating parameters such as gas flows, pressure, power, and water cooling.

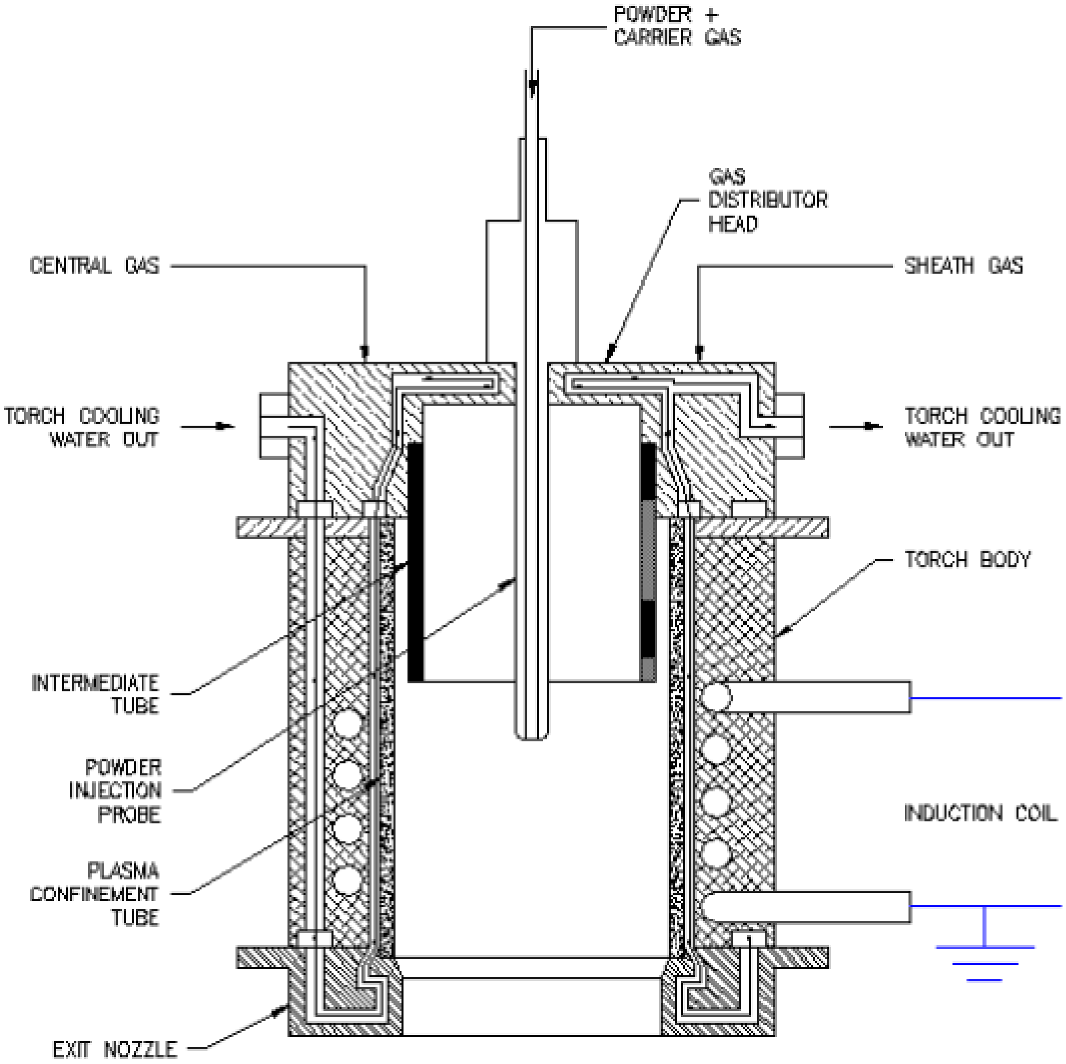

Figure 16. Diagram of the plasma torch body [53]

The ICP torch relies on the principle of inductance to generate plasma. A ceramic confinement tube with an internal diameter of 35 mm is wrapped on the inside of three to four turns of water-cooled copper coil. The generator delivers a RF current to the torch coil and induces an alternative magnetic field that heats up a gas and creates a thermal plasma in the temperature range of 5,000 K to 12,000 K [54]. A continuous flow of gas maintains the plasma within the torch body and forms the high-temperature/high velocity jet at the outlet of the torch.

The torch is attached to a custom built conical water-cooled reactor. The conical water-cooled reactor has a length of 50 cm and a full angle expansion of 14° (Figure 17). The geometry of the conical reactor allows a gradual gas expansion and minimizes recirculation areas while also providing a symmetrical flow pattern within the reactor chamber.

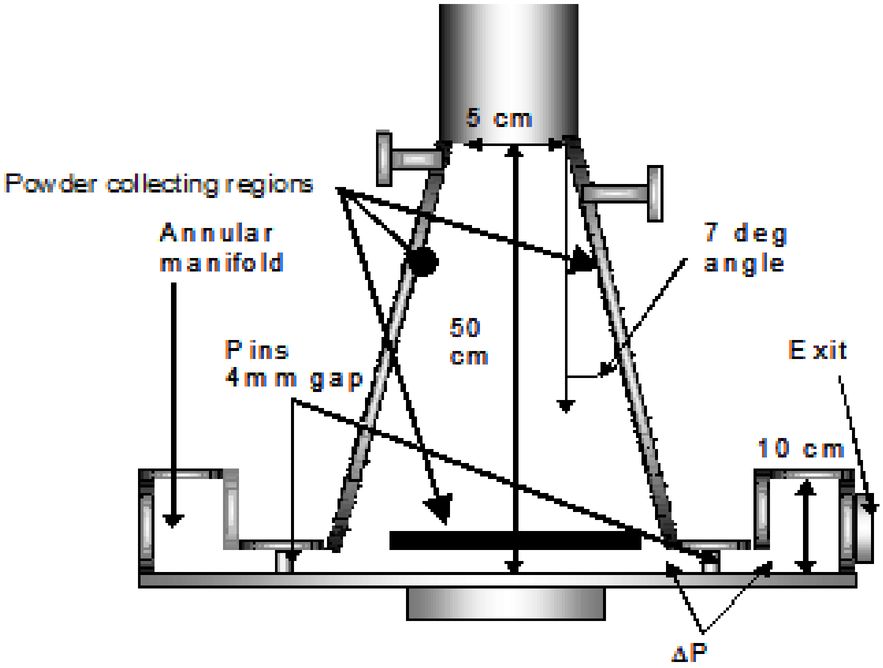

Figure 17. Schematic of conical water-cooled reactor [51]

GNFs are formed through the homogenous nucleation of atomic carbon in a very specific temperature/flow field within the reactor. Once formed, the presence of nitrogen ions and exited nitrogen species enable nitrogen functionalization to occur on the GNF structures during their transport to the collection sites. The plasma expansion design enables a control of the residence time distribution of the carbon precursor in the homogeneous nucleation field, and provides a means for generating a crystalline critical cluster that grows from condensation in the 2-dimensional (2-D) direction of the graphene sheet. The temperature, flow, species density, and nanoparticle nucleation fields, as well as the thickness and the 2-D evolution of the GNF nucleation, have been modeled by Mendoza-Gonzalez *et al.* [55]. This provided an understanding of the physics involved and, more importantly in the present work, of the homogeneity of the particle nucleation and growth fields for essentially all stream lines. This means that besides the purity of the GNF product, narrow 2-D particle size and number of atomic planes distributions are obtained for this graphene material. The temperature window of the GNF nucleation and growth is calculated to be between 4900 K down to 4200 K. Such high temperatures and the gradual downstream cooling enables a very good organization of the graphene structure and the low defect concentration, as discussed in Section 2.7.

The growth of GNF can be separated into three steps. In the preparation step, a 20 kW argon plasma is produced at a pressure of 55.16 kPa with argon gas being directed to the sheath and central gas ports at a flow rate of 45 and 13 slpm respectively. In the growth step, the pressure is decreased to 13.79 kPa. Once the plasma is stable, methane and nitrogen are delivered to the injection gas port at a flow rate of 1 and 0.1 slpm respectively for 10 minutes; stopping the plasma after this step results in GNFs with low levels of nitrogen. Additionally, if the nitrogen flow is omitted, GNFs with no nitrogen are generated. The third step is a functionalization step used to attain high levels of nitrogen. Directly following the 10 minutes of the growth step, the sheath flow gas is changed from argon to nitrogen gas, while the values of the flow rate to the sheath and central gas ports are maintained. The flow of methane is stopped and the amount of nitrogen directed to the injection gas port is increased to 5 slpm. Additionally, the pressure is decreased to 13.79 kPa and the power is increased to 25 kW. These conditions are maintained for 30 minutes after which the plasma system is shut down. After cooling, the reactor can be opened and the GNFs can be collected from the reactor walls. A full standard operating procedure for the growth of functionalized GNFs can be found in Appendix A.

3.1.2 Iron incorporation

A modified version of the iron inclusion method established by Jaouen *et al.* [31] for carbon soot materials was used in this work with ferric acetate chosen as the iron source. In a glass beaker, iron acetate is added to a mixture containing equal parts ethanol and water and GNFs; the amount of iron being added depends on what is desired as an overall iron mass content and how big a batch of GNF is being prepared (Equation 4). In another scheme, phenanthroline was also added in a 1 to 1 mass ratio to the GNFs. The solution is mixed in an ultrasonic cleaner for 1 hour and then heated in an oven at around 100°C to evaporate the liquid. The sample is then collected from the beaker walls and pyrolyzed with argon gas at a temperature of 700°C and a flow rate of 600 sccm.

$$Iron\ Acetate\ mass = \frac{mass\ percent * (GNF\ mass + Phenanthroline\ mass)}{\frac{55.845}{173.93} - mass\ percent}$$

Equation 4. Iron acetate mass calculation

3.2 Structural characterization techniques

3.2.1 X-ray photoelectron spectroscopy

X-ray photoelectron spectroscopy (XPS) is a characterization technique that can analyze a sample’s surface up to 2 - 5 nm in depth. It detects which elements (except hydrogen and helium) exist on a sample and the type of chemical bonds between elements [56–58]. The surface of the sample is exposed to a monochromatic X-ray under ultra-high vacuum (better than 10^{-9} kPa), which is needed to ensure the sample doesn’t degrade through interactions with the ambient gas atmosphere. Enough energy needs to be provided by the X-ray for the photoelectric effect to occur, where the photoelectrons can overcome the nuclear attraction force of the element and be emitted [59]. Electrons leaving the sample are collected by an electron analyzer and their kinetic energy is measured. These measurements are used to produce an energy spectrum in the form of intensity (electrons per time) versus binding energy (the starting energy of the electrons in the atom).

The binding energy indicates the specific element and bond type; binding energy values can be found in the literature or from the National Institute of Standards and Technology (NIST) database [60]. Each element is associated with an energy range on the spectrum. The intensity of the peaks is also essential as peak areas are proportional to the number of atoms present in each element. With the correct sensitivity factors, the analysis of the XPS intensities enables the evaluation of atomic percentage of a given element on the surface. For information about the specific bond types present, a de-convolution of the elemental signals must also be done.

The protocol for collecting XPS data is to begin with a general ‘survey spectrum’, where a large energy value (200 eV) is used to scan the entire energy range of the photoelectrons (0-

1200 eV); this scan enables a survey of the elements present on the sample. Once the elements are determined, scans are performed at a lower energy value (50 eV) in the specific elemental energy range. These are 'high resolution' profiles used for the determination of the elemental composition and bond types. The number of scans needed for a specific element is reduced with stronger signals as the signal to noise ratio is higher. Detection limits exist where the ratio is less than 2, which corresponds to an atomic percent value of around 0.1%.

All the XPS data in this thesis was performed on a Scientific K-Alpha XPS system from Thermo Scientific with aluminium X-ray source energy of 1486.6 eV and 300 μm spot size. Avantage 5.932 software was used to analyze and de-convolute all data.

3.2.2 Raman spectroscopy

Raman spectroscopy refers to the phenomenon of inelastic scattering of light and the existence of scattered radiation, which was first observed by Raman and Krishnan in 1928 [61]. Photons that make up light can either be absorbed, scattered, or not interact with a material. Absorption occurs when the energy of the photon matches the energy gap between the ground and excited states of a molecule. In the case of scattering, the energy level does not need to be matched and the photons can be perceived by collecting the light at an angle to the incoming light source. Since energy matching is not needed, Raman spectroscopy only requires a single frequency of radiation, thus making it simpler than other spectroscopy techniques that rely on the principle of absorption.

Most photons are scattered elastically, this being called Rayleigh scattering. Inelastic scattering, called Raman scattering, is a weak process that only occurs in one in every 10^6 to 10^8

photons when nuclear motion is induced and energy is transferred so that the scattered photon is one vibrational unit different than the striking photon [62]; to compensate, high power densities are delivered to small sample sizes through the use of lasers. Inelastic scattering is classified as either Stokes (molecule goes to a higher energy excited vibrational state) or anti-Stokes (molecule goes from excited state to a ground state). For Raman spectroscopy, the Stokes spectrum is used and is expressed as the amount of light absorbed with respect to the shift in energy between the ground and excited states.

Raman spectroscopy provides valuable insight for graphene materials. It can be used to determine the number and orientation of graphene layers, the quality and type of edges, and the effects of doping and functional groups [63]. Figure 18 shows the typical spectrum of single layer graphene; the set of peaks for multilayer graphene is very similar. The 2D peak is closely linked to the electronic band structure and its shape and intensity provide information on the number of layers in stacked graphene [64,65]. Figure 19 shows the Raman shift when moving from single layer graphene to graphite. A traditional parameter used with graphene is the average in-plane length (L_a), given as the ratio of the intensities in the G and D peaks and multiplied by a coefficient with respect to the laser wavelength [66]; for a 514.5 nm laser, the coefficient is 4.4 nm. However, this ratio is not precise for disordered carbon or graphene layers with demonstrated curvature [67]. A study conducted on novel graphitic indices aimed at incorporating the curvature that is often present in graphene layers made slight adjustments to the L_a parameter and found a better match when the peak areas were used instead of the peak intensities [33]. Additionally, a tortuosity ratio (twice the ratio of the areas of the 2D and G peaks) was multiplied to the new L_a parameter to create a parameter for the average continuous graphene length (L_{eq}). The L_{eq} parameter provides complementary information to the L_a parameter for graphene layers with high crystalline quality and curvature (Figure 20).

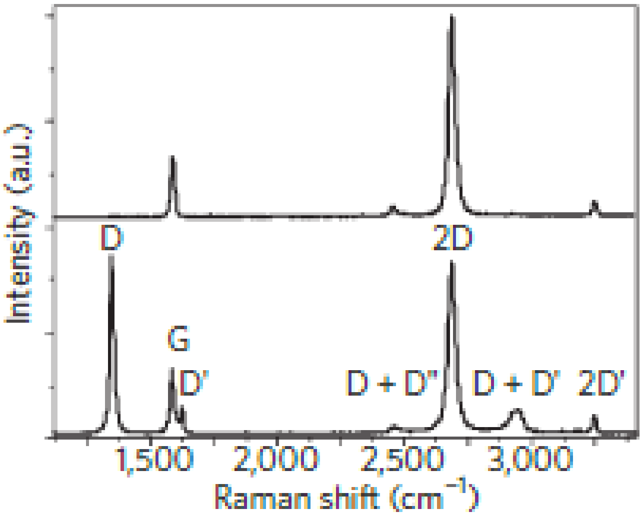

Figure 18. Raman spectra of pristine (top) and defected (bottom) graphene [63]

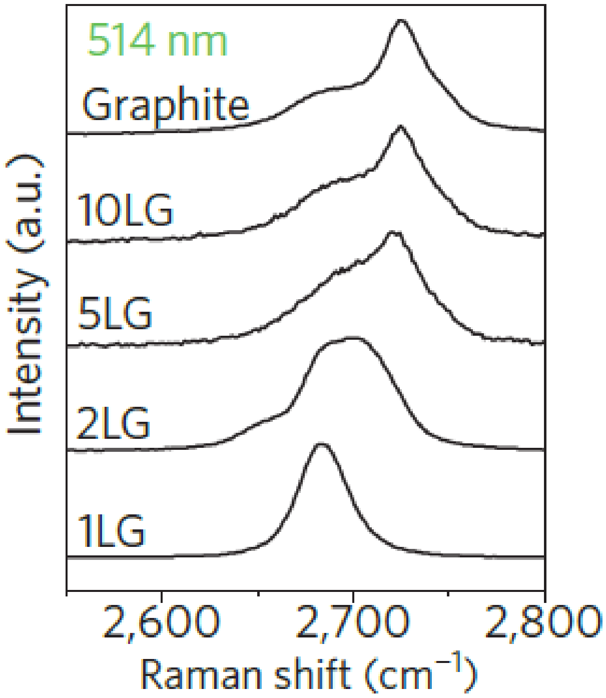

Figure 19. 2D peak as a function of N layers of graphene for 514 nm excitation [63]

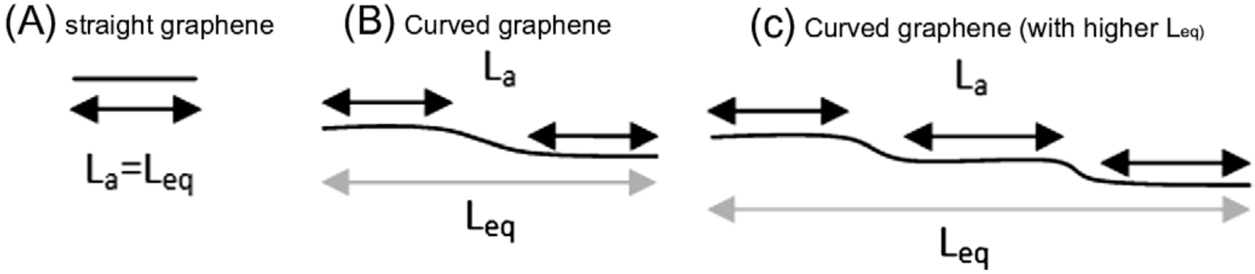

Figure 20. Comparison of L_a and L_{eq} for straight and curved graphene layers [33]

The Raman instrument used in the present project was an inVia Reflex confocal micro-Raman (Renishaw) with a laser emitting at a wavelength of 514.5 nm. All peak intensities and areas were measured using the Wire 2.0 software and an average of points was used to represent each sample.

3.2.3 Microscopy

Scanning electron microscopy (SEM) uses a high-energy beam of electrons to raster-scan (scanning one line from left to right, and then jumping to the next scan line, similar to reading text) the surface of a sample to provide high-resolution images [68]. The emitted electrons from the sample are collected to form an image, with the secondary electrons being attributed to the resolution and the backscattered electrons providing contrast. SEM is used to gain information on the morphology and particle size of the sample. Transmission electron microscopy (TEM) also used a high-energy beam, but here the transmitted electrons are of interest [68]. TEM works on very thin samples in the nm range of thickness and allows imaging at the atomic level; this can provide information on dislocations, grain boundaries, sub-nanoscale morphologies, nanoparticle shapes and sizes, and the counting of graphene layers for stacked graphene samples.

All SEM images were captured on a Hitachi S-4700 Field Emission Scanning Electron Microscope. The conditions used for all images were 5 kV accelerating voltage, 10 μA beam current, and a 6 mm working distance. All TEM images were captured on a Philips CM200 equipped with a field emission gun (FEG-TEM).

3.2.4 Brunauer-Emmet-Teller (BET) surface area analysis

In 1916, future Nobel Prize winner Irving Langmuir developed a model to quantify the amount of adsorption as a function of partial pressure at a given temperature. By treating the adsorption process as a reaction, gas molecules are said to react with an empty site on an adsorbent to yield adsorbed complexes. The Langmuir Theory is still used today to describe monolayer molecular adsorption. In 1938, scientists Brunauer, Emmett, and Teller (BET) extended the Langmuir Theory to describe multilayer adsorption [69]. There are 3 assumptions needed to extend the theory:

Assumption 1: Multilayer adsorption is possible with the forces of adsorption higher for the first layer and then constant for all other layers.

Assumption 2: The surface is homogeneous

Assumption 3: The Langmuir Theory can be applied to each adsorption layer (no lateral interactions)

The BET method is used to determine the surface area of a solid through the physical adsorption of gases. The calculation of the area is dependent on the total volume and molar volume of the adsorbate gas, the adsorption cross section of the adsorbing species, Avogadro's number, and the mass of the adsorbent.

For BET area measurements, an Autosorb iQ Gas Sorption machine from Quantachrome Instruments. Nitrogen was used as the analysis gas with a bath temperature of 77.35 Kelvin. The BET area of each sample was calculated by generating a multi-point BET plot and focusing on the relative pressures in the range of 0.05 to 0.3.

3.2.5 Neutron activation analysis (NAA)

Neutron activation analysis (NAA) relies on the collection of emitted gamma-rays of a sample as it is excited by neutrons. The bombardment of neutrons causes elements to form radioactive isotopes and as the radioactive emissions and decay paths of elements are known, NAA can be used to determine the mass concentration of the elements. Nuclei can have different cross sections and half-lives so the gamma-ray intensity can vary, making detection limits variable, but NAA is overall a very responsive technique with the ability to analyze trace elements. Overall, seventy-four elements can be detected with minimum detection limits in the range of 10^{-5} to 10^{-13} mass percent [70].

NAA was used in this work to evaluate the amount of iron in prepared samples. All NAA was performed with the SLOWPOKE nuclear reactor at École Polytechnique de Montréal, an Ortec GEM30185-P germanium semiconductor gamma-ray detector, an Ortec DSPEC Pro^{TM} multichannel analyzer, a Sartorius precision balance, and the EPAA analysis software.

3.3 Catalytic performance

3.3.1 Electrochemical studies

One indicator of a catalyst's ability to aid a reaction is to study the electrochemistry (interaction between electrical energy and chemical change) of oxidation/reduction reactions. As detailed in section 2.2, a PEMFC works off the principle of the hydrogen oxidation and oxygen reduction reactions. Using an electrochemical cell, a device that produces electric current from the energy released by a reaction, one can measure and quantify the chemical changes of reactions.

All electrochemical cells are composed of electrodes. An electrode is a conductive solid that interfaces with an electrolyte solution. Electrodes are labeled as either reference, counter, or working. A reference electrode acts as an experimental reference point for potential measurements and holds a constant potential during experiments. A counter electrode completes the current path in the cell and is mostly used as the current source/sink, so they are typically made of inert material. The working electrode is the material being studied. Experiments can use 2, 3, or 4 electrodes. In a 2-electrode setup, the reference and counter electrodes are connected, whereas in the very rare case of the 4-electrode setup, the working electrode is divided into a working electrode and a 'working sense' electrode [71]. The most common setup is the 3-electrode system, where the potential changes of the working electrode are measured independently of the changes that may occur at the counter electrode and thus allow the reaction to be accurately studied.

Working electrodes made of solid materials come with a host of complications and problems including intermediates forming on the surface, the forming of oxides and films, and the maintaining of electrode geometry during cleaning. These disadvantages make it difficult to obtain reproducible results. Using a working electrode with a disk-shaped surface facilitates cleaning without geometric changes. Furthermore, rotating the working electrode removes the dependence that exists between the distance of the point on the disc to the axis of rotation; this means that the current density measurement is more accurate as the same value can now be obtained on the entire surface area of the disk [72].

Electrochemistry can be used to study mass transport caused by diffusion, convection, or migration due to a potential gradient. A rotating disk electrode (RDE) can be used to create a flow pattern within the solution so that only convection occurs (Figure 21). The rotation pulls the solution up towards the center of the electrode and then outwards. RDE can thus be used to calculate a number of parameters related to mass transport, including the double layer capacitance, onset potential, and electrocatalyst specific/mass activity.

RDE studies were used primarily to quickly evaluate the ability of catalysts to reduce oxygen. The 3-electrode system consisted of a saturated silver/silver chloride reference electrode and a platinum wire counter electrode. The working electrode was the different prepared catalysts in this work, mixed in an ink and dried onto the disk of the RDE tip (Pine Instruments, AFE3T050GC, glassy carbon 5 mm disk diameter, 12 mm PTFE shroud diameter). The RDE tip is inserted into the electrode rotator (Pine Instruments, AFMSRCE), where the rotation rate is controlled. Nitrogen and oxygen gas delivery lines were also installed for the cell and all electrochemical measurements were done by an EZ-Stat potentiostat (NuVant System Inc.).

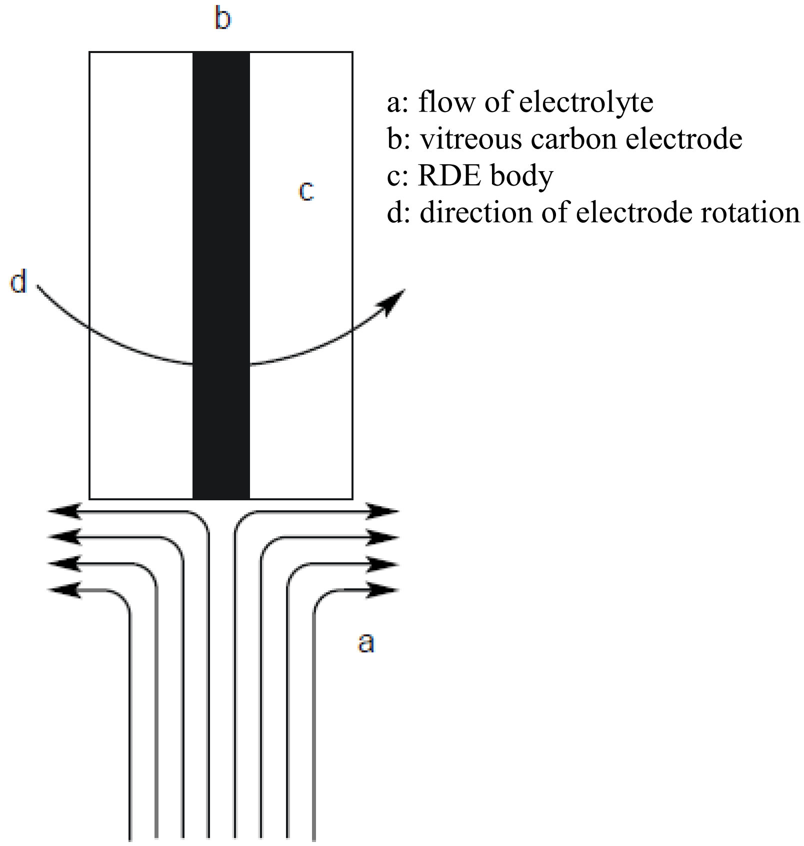

a: flow of electrolyte
b: vitreous carbon electrode
c: RDE body
d: direction of electrode rotation

Figure 21. Solution movement caused by rotation of a RDE [73]

Catalyst inks were prepared as a mixture of 80% water and 20% alcohol by volume with the GNFs introduced to obtain a concentration of 2 mg per ml of solution. A 5 wt% Nafion^{TM} solution was introduced at 2 μL per mg of graphene material. The ink was deposited on the glassy carbon RDE tip at a concentration of 0.1 mg per cm^2 of electrode and dried in a humid environment until a uniform film was obtained.

RDE experiments are composed of 3 tests. The first test is called the conditioning or ‘break-in’. In this experiment, cyclic voltammetry is performed in the positive voltage range at a scan rate of 100 mV/s with nitrogen gas being introduced into the cell until the results become invariant with time. The second test is a background current correction to remove the capacitive current contributions. Cyclic voltammetry is again performed, but now at a scan rate of 20 mV/s. The third test is to obtain the experimental ORR current. Oxygen is now introduced into the electrolyte solution and cyclic voltammetry is performed at a scan rate of 20 mV/s. The rotation rate should be consistent in the second and third tests for an accurate correction value. The controllable parameters in RDE experiments are the electrolyte solution, temperature, pH, rotation rate, and oxygen amount. Various values were used and are always quoted when reporting results.

3.3.2 Polymer electrolyte membrane fuel cell (PEMFC) testing

3.3.2.1 Preparation of catalyst inks

The catalyst layer is where the chemical reaction takes place within the fuel cell. An ideal catalyst layer allows the catalyst particles to be in contact with each other, the electrolyte membrane, and the GDL [74]. As well, reactant gas must be able to reach the reaction sites and the reaction product (water) must be able to exit. The liquid precursor of the catalyst layer is the catalyst ink. There are three general categories for catalyst inks: hydrophobic ink, hydrophilic solution & colloid ink, and platinum ion solution ink & platinum foil. In this work, the hydrophilic solution was used for all catalyst ink preparations.

To prepare a hydrophilic solution, the catalyst is mixed with a solvent such as alcohol and a hydrophilic perfluorosulfonate ionomer; the ionomer solution chosen was Nafion^{TM} as it matched the membrane being used. This solution is stirred and dispersed in an ultrasonic cleaner to create a uniform ink. Water was also added to the ink solution to slightly increase the viscosity. A very important consideration for the solution is the Nafion^{TM} content and an entire study can be done to find the weight percent that maximizes performance for individual catalysts.

3.3.2.2 Fabrication of the MEA

The MEAs used in this work were all of the 5-layer variety and fabricated using the catalyst-coated substrate (CCS) method. The CCS method, as opposed to the catalyst-coated membrane (CCM) method was chosen here for its simplicity and the availability of required equipment. CCM is known to give better results as a stronger ionomer network is formed [75], which is considered when discussing the results obtained.

In the CCS method, the catalyst ink is deposited and dried onto a GDL (Toray carbon paper with 20% wet proofing and a micro-porous layer, TGP 090 20%, MPL) to achieve the desired catalyst loading, thus forming the GDE. Before being used, the Nafion^{TM} membrane is cleaned. Cleaning involves exposing the membrane to one hour of each of the following solutions at their boiling temperatures: 3 wt% peroxide solution, 1.2 M H_2SO_4 solution, and finally water.

The MEA is made by hot-pressing a Nafion^{TM} membrane in between two GDEs that contained their respective catalyst layers. For hot-pressing, the MEA was placed in between two sheets of Kapton and copper plates and pressed at 5 860 kPa for 2 minutes at a temperature of 120°C, around its glass transition temperature. Similar to the Nafion^{TM} content, the hot-pressing conditions have an effect on the catalyst performance and an entire study can be done to find the conditions that maximize performance for individual catalysts.

3.3.2.3 Loading the MEA

When loading the MEA into the actual fuel cell, special care must first be taken with the gasket. The gasket material in this work is Teflon coated fiberglass tape. Gaskets are employed to compress the MEA and they need to be a certain shape and have the perfect opening to ensure that the guiding pins fit and that the GDE sits snuggly within the gasket and that none of the active area is being covered (Figure 22). The thickness of the gasket determines the compression experienced by the MEA. By assuming the membrane is incompressible, the compression is calculated as the difference between the overall thickness of the 2 GDEs and the overall thickness of the gaskets with respect to the overall thickness of the 2 GDEs; ideally, a thickness of 15 – 25% is desirable. When the MEA is finally loaded, the bolts that hold the fuel cell components together must be tightened in a diagonally opposite pattern with small increments to a desired torque of 10.5 to 13.5 Newton meters. This is easily achieved with the use of an adjustable torque wrench. Tightening is important to avoid leaks, but overtightening may lead to extra compression and damage to the MEA.

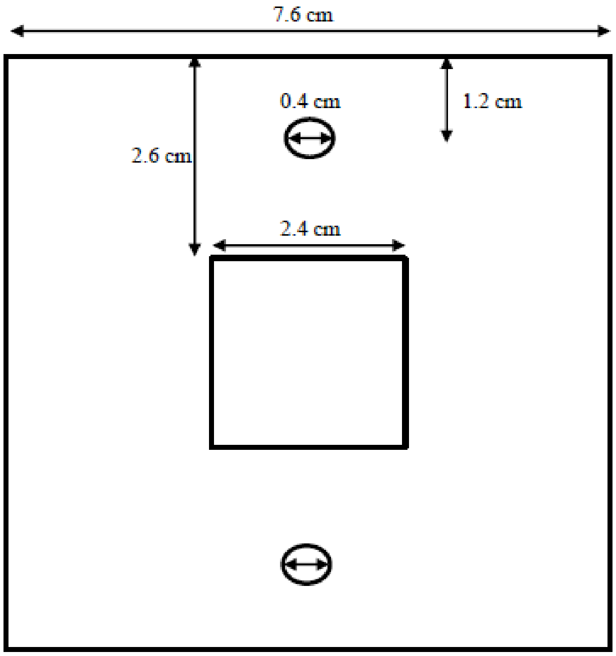

Figure 22. Gasket shape

3.3.2.4 PEMFC testing station

A PEMFC testing station (university model, Fuel Cell Technologies, Inc.) is composed of a gas delivery control system, a temperature control system, a direct current (15 V / 60 amps) electronic load, humidity bottles, back pressure regulators, and a computer with control and measurement software and a peripheral component interconnect general purpose interface bus (Figure 23). Appropriate gas cylinders must be provided to the station and the fuel cell must be connected to the gas ports, cartridge heaters, and sense leads. All gas lines are quarter inch tubing that is rated properly for the operating pressure. For safety reasons, hydrogen gas is first directed to a flash arrestor before entering the anode inlet; oxygen gas is directed to the cathode inlet. Both gases are sent to their individual mass flow controller to set the flow rate. Nitrogen is also connected to the station for such cases when nitrogen gas is desired (start-up, cool down, and emergency shutdown). The station is equipped with a 3-way solenoid valve which acts in conjunction with programmed alarms within the computer software for emergency shutdowns. Each gas line is directed towards a manual 3-way valve where the user can control if the gas is stopped, sent to the humidity bottle, or sent directly to the fuel cell. If sent to the humidity bottle, the gas will first pass through a water trap. The humidity bottle is a stainless steel water vessel that is wrapped with a heater pad and insulation. The temperature is controlled with a type T thermocouple and a proportional-integral-derivative (PID) controller and the water level within the bottle is controlled with a float switch and an automatic-fill pump; a reservoir of deionized water is provided by a connection to the rear panel of the station. Humidified gases then proceed to the fuel cell and exit the station and travel through a section of tubing lined with a heater, referred to as the preheater, where the temperature is also controlled. The exits of the preheaters are the inlets to the fuel cell.

A single cell fuel cell with a working area of 5 cm^2 was used in this work. The fuel cell includes gold plated copper current collectors with high current connectors and sense leads with banana plugs, aluminum alloy end plates, and 115 V cartridge heaters to heat the cell with an accompanying thermocouple measuring the cell temperature on the cathode side; the cartridge heater is dipped in a heat-conducting coating, such as Milk of Magnesia, to improve thermal conductivity. The cell is held together by 8 bolts and internal gas paths are sealed with O-rings. The gases enter the top of the Poco graphite blocks (grade AXF-5Q) that have machined serpentine grooves with a quarter cm depth. On the fuel cell, a 'sense' and 'load' connection must be made on both the anode and cathode side to complete the circuit with the electronic load. Gas leaving the fuel cell is then redirected back into the station to back pressure regulators that are controlled by the user. From there, the anode gas line is sent to an exhaust and the cathode vents to a condensing bottle.

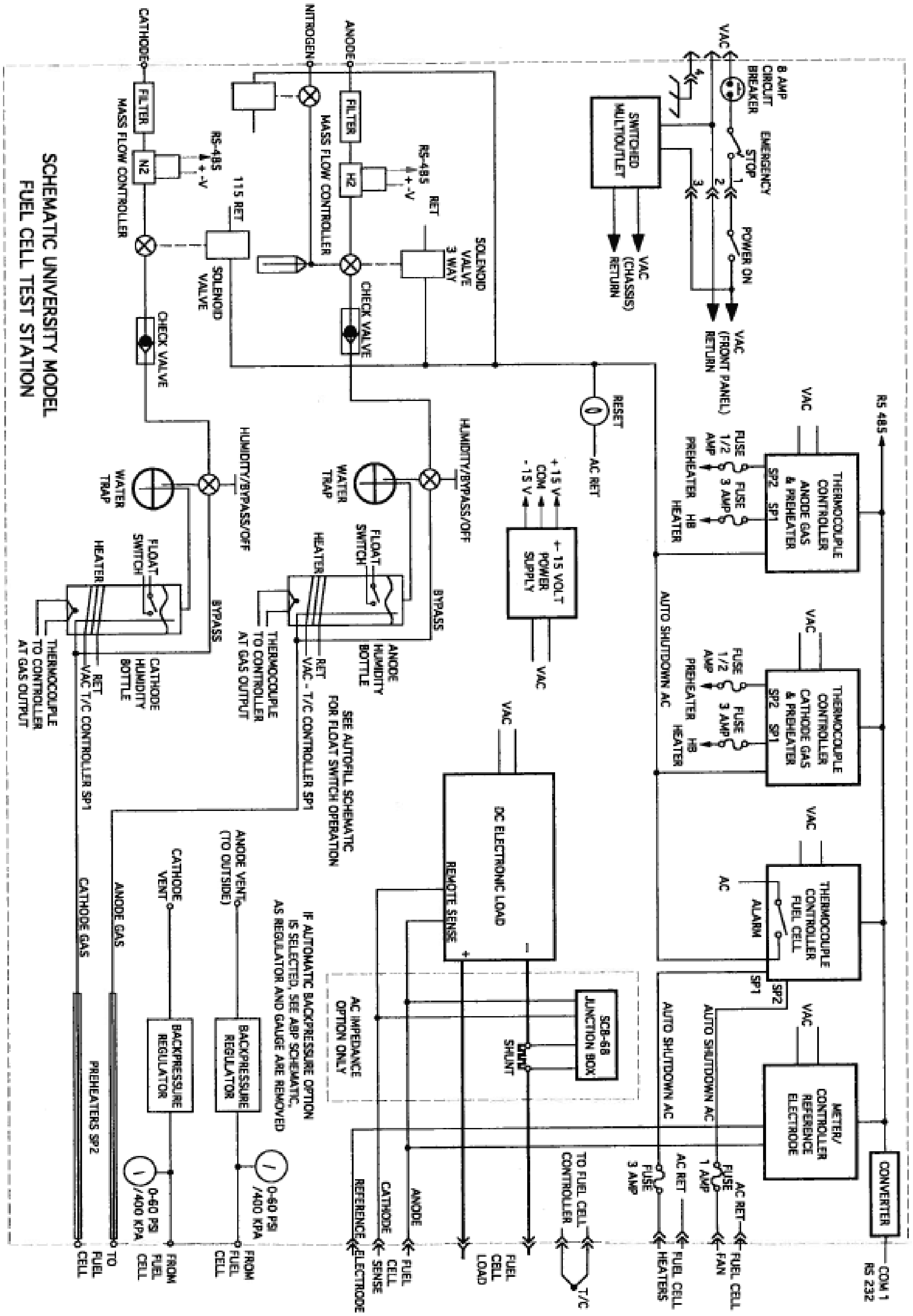

Figure 23. Control scheme of fuel cell testing station

3.3.2.5 PEMFC testing parameters

A PEMFC has a large number of parameters that can be controlled by the user. When connecting the fuel cell to the gas outlets of the testing station, the direction of the incoming gas on the anode and cathode gas can be set to flow in the same direction (co-current) or in opposite directions (counter-current). Co-current flow has been associated to better overall performance, but counter-current has been recommended by the US department of energy for any automotive application because it leads to a more uniform current density across the working area [76]; it was not possible to install the fuel cell with a counter-current flow on the testing station in this work, so a co-current flow was used. The flow rate of the hydrogen and oxygen gases must also be set with either a fixed-stoichiometry condition or a fixed-flow-rate condition [10]. In the fixed-stoichiometry condition, the parameter λ is used to define the ratio between the reactant feed into the fuel cell and the reactant consumption inside the fuel cell and is always set to a value greater than 1; this is also colloquially referred to as ‘stoich flow’. Using Faraday’s laws, the flow rate of each gas can be calculated with respect to the cell’s current (I_{cell}), the working area ($Area_{MEA}$), the stoichiometric parameter, Faraday’s constant ($F = 96485.33289\ C\ mol^{-1}$), and the amount of electrons transferred in the electrochemical reaction (Equation 5 and Equation 6). In the case of fixed-flow-rate, the flow is held at a sufficiently high rate for even the largest current densities. This control method ensures that there are no mass transport issues from gas not being available at high currents and is generally the method used at the lab scale, but comes with the drawback that excess gas is used and there is more gas to humidity. The fixed-flow-rate condition was used in all fuel cell experiments in this work.

$$M_{Hydrogen}^{controlled} = \frac{I_{cell} * Area_{MEA} * \lambda_{H_2}}{2F}$$

Equation 5. Controlled flow rate of hydrogen

$$M_{Oxygen}^{controlled} = \frac{I_{cell} * Area_{MEA} * \lambda_{O_2}}{4F}$$

Equation 6. Controlled flow rate of oxygen

Another parameter that can be set on the fuel cell is the back pressure on each electrode side. It is recommended to operate at a back pressure between 100 and 500 kPa [10], where higher pressure has been linked to improved performance, but a value between 200 and 300 kPa is more realistic. The humidity temperature of each of the incoming gases can also be controlled depending on what the user wants to study. It is possible to run ‘dry’, but a host of performances issues arise at low humidity, namely major current fluctuations. It has been shown that cell performance increases with respect to relative humidity, therefore most users operate as close to 100% relative humidity as possible. The cell temperature is also controlled and it is recommended to operate within the temperature range of 40 and 90°C, but it is possible to explore higher temperatures for specific research goals towards designing new materials. For catalysts on Nafion^{TM} membranes, an operating temperature of 80°C is commonly used to prevent membrane drying. Finally, the temperature of the preheaters is also controlled and is usually set to a few degrees Celsius higher (5 to 10) than the cell temperature in order to prevent condensation.

Concerning the electronic load, it is possible to operate in either a ‘current mode’ or a ‘voltage mode’, where the user controls one variable and measures/records the other. When controlling the current of the cell, the gas requirement remains constant over time, but there is the possibility that as cell performance decreases over time, in which case the desired current is no longer obtainable and the cell fails. When controlling the voltage of the cell, the current may vary, but the worst case scenario of the cell failing leads to no current being drawn at an applied voltage.

3.3.2.6 PEMFC experiments

To perform a fuel cell experiment, one must first attain whichever cell temperature, humidity, gas flows, and back pressure that is desired. At this point, a repeatable break-in procedure must be done to bring the cell materials to a stable level of performance before further testing. Many different break-in protocols exist and can be as short as 10 minutes or as long and exhaustive as 27 hours. In this work, the cell was considered broken-in when subsequent polarization curves taken 1 hour apart showed a deviation of less than 5 mV. Once broken-in, two types of experiments were performed. To obtain the performance of the catalyst at all possible values, a polarization curve is performed in which the voltage is varied from the open circuit voltage down to 0.25 V and the current is measured. To monitor the stability of the catalyst, the current is measured as a voltage is applied over a time period.

Chapter 4: Iron Incorporation on Graphene Nanoflakes for the Synthesis of a Non-noble Metal Fuel Cell Catalyst

4.1 Preface

This chapter presents a published article with the following citation:

P.-A. Pascone, J. de Campos, J.-L. Meunier, and D. Berk, *Iron Incorporation on Graphene Nanoflakes for the Synthesis of a Non-noble Metal Fuel Cell Catalyst*, Applied Catalysis B: Environmental **193** (2016), 9–15.

P.-A. Pascone (the Ph.D. candidate) was responsible for the planning of experiments, the complete synthesis of the catalyst, performing the experimental work (catalytic testing), characterizing the material through XPS and Raman with the accompanying analysis, and writing the article. J. de Campos worked as a summer intern under the supervision of P.-A. Pascone and performed some experimental runs of the catalytic testing. J.-L. Meunier and D. Berk supervised the work and reviewed the manuscript.

The article investigates the level and chemical composition of nitrogen functionalization on the GNFs as a precursor to the wet-chemical method of iron incorporation. In addition, the role of iron acetate, phenanthroline, and pyrolysis are investigated. It is shown that the best catalytic performance occurs when GNFs with a high level of nitrogen functionalization (HN-GNFs) are mixed with iron acetate and pyrolyzed. This study simplified the catalyst synthesis procedure and indicated that further work on the catalyst should be dedicated to HN-GNFs.

Iron Incorporation on Graphene Nanoflakes for the Synthesis of a Non-noble Metal Fuel Cell Catalyst

Author names: Pierre-Alexandre Pascone[a], Jasmin de Campos[a], Jean-Luc Meunier[a], Dimitrios Berk[a]

Affiliations: a: Plasma Processing Laboratory (PPL), McGill University, Chemical Engineering, 3610 University Street, Montreal, Québec, H3A 0C5, Canada

Abstract: In the present work, graphene nanoflakes (GNFs) were grown at both low and high levels of nitrogen functionalization and subsequently put through a wet-chemical method to add iron functionalities to the surface and create active catalyst centers. No mechanical treatments are used in order to minimize the formation of defects on the GNFs and evaluate if iron-nitrogen-GNF edges or surface sites can generate catalytic activity rather than the macropore structures holding these functionalities on porous carbon black. The catalysts produced under various synthesis routes were characterized and screened for their performance as an oxygen reduction reaction (ORR) catalyst. Characterization included an electrochemical study, an examination of the carbon and nitrogen content and bonding structure, in addition to Raman analysis and the calculation of the BET surface areas. It was found that samples that were both treated with iron acetate and put through pyrolysis produced the most active samples. These samples were composed of graphitic carbon and contained a large amount of pyridinic nitrogen. Additionally, when working with GNFs generated with high levels of nitrogen, no extra nitrogen source was

needed during the iron incorporation step. This study further develops the GNF-based catalyst already seen to be a suitable ORR catalyst for the polymer electrolyte membrane fuel cell.

Keywords: Graphene; Nanomaterial; Catalyst; Oxygen Reduction Reaction; Nitrogen functionalization

4.2 Introduction

Graphene, an atomic layer of carbon atoms in a two-dimensional aromatic ring matrix, has attracted much attention as a material due to its large surface area and high electrical conductivity [77]. This material has potential applications in varying fields, such as nanofluids [78], supercapacitors [79], and fuel cells [80]. Producing high quality and purity graphene was shown to be possible by Prisitavita *et al.* by the thermal decomposition of a carbon feedstock in a thermal plasma [54]. The produced graphene, called graphene nanoflakes (GNFs) powder, has a structure that is characterized by a stacking of roughly 5 to 15 graphene planes of typical planar dimensions of 100 by 100 nm. The GNFs are considered graphene rather than graphite because the properties of single-layer graphene, such as the length scale of the stacked crystalline planes, persist within this material [33]. The resulting powder is extremely pure and contains little to no amorphous carbon, in addition to having a very high degree of crystallinity and being chemically resistant to acidic and basic environments.

Depending on the plasma conditions during GNF growth, nitrogen can be attached at various levels reaching up to above 30 atomic percent on the surface with a fraction of around 25 percent of this nitrogen being in pyridinic sites of the graphene structure [81]. By introducing iron into the nitrogen functionalized GNFs through a wet-chemical method outside the plasma reactor, a catalyst for the oxygen reduction reaction (ORR) can be crafted. For the catalyst to be effective, the iron should be bound to nitrogen atoms which are part of the graphitic structure. The key to obtaining a high catalytic activity for ORR is in the nature of the iron-nitrogen-carbon bond, and whether there is pyridinic or pyrrolic nitrogen. The evaluation of the iron active site is still under investigation in the research community with pyrrolic nitrogen being associated with higher activity, but pyridinic nitrogen being associated with decreased peroxide formation and increased energy efficiency [82].

For the specific applications of alkaline fuel cells (AFCs) and polymer electrolyte membrane fuel cells (PEMFCs), platinum, an expensive precious metal, is typically used as a catalyst for the ORR. Non-noble metals, particularly cobalt and iron, atomically dispersed on carbon nanomaterials show promise as platinum cathode catalyst replacements for both PEMFCs [21,27,37,39,83–94] and AFCs [95–103].

In this work, GNFs were produced with varying amounts of nitrogen functionalization and used as the carbon base onto which iron could be atomically dispersed. The synthesis parameters were varied and the resulting catalysts were fully characterized by their elemental composition, crystallinity, in addition to being tested for their ability to reduce oxygen in neutral media.

The iron-incorporation method used in this work has been adapted for the GNFs from an existing process developed by Dodelet *et al.*. Their work used carbon black particles as the carbon precursor, and iron acetate and phenanthroline were then added as their iron and nitrogen sources respectively [5,30,31,34–36,38]. They then tuned the porosity of carbon black particles and filled the pores using a ball milling step and a two-stage pyrolysis. The catalytic activities of these structures were very close to matching those of platinum while the amount of defects and specific porosity of the carbon black particles seem to play a major role in attaining the high level of catalytic activity. A microscale porosity was induced on the carbon black structures used by Lefèvre *et al.* for creating the porphyrin-like catalytic sites through mechanical/thermal treatments [5,34–36]. The catalytic stability of these structures over time, however, remains problematic, and the increased crystallinity of the carbon structures was observed to correlate with stability improvement of the catalyst [38]. The requirement of defects and porous sites on the carbon black support proved to be necessary for the formation the iron-nitrogen-carbon catalytic sites, while such defects are not involved at the same level on the highly crystalline graphene structures for the generation of such sites.

We may thus hypothesize that further increasing the crystallinity level through the use of graphene-based materials hosting the iron-nitrogen-carbon catalytic sites would present a promising avenue for providing both activity and stability. The ball milling treatment and pyrolysis procedure presented by Jaouen *et al.* [30] was first used unchanged on our GNFs in a preliminary study [104]. Although the low iron content yielded the expected relatively low activity levels, the catalyst produced did show catalytic stability during a 100-hour PEMFC test [104]. Optimization of iron incorporation levels onto our GNFs is now required to enhance their catalytic performance while maintaining the integrity of the graphene structure.

In using the mechanical/thermal treatments of Lefèvre *et al.* on the GNFs for the synthesis of the catalyst, we noted from Raman spectroscopy that the graphene structures showed a significant reduction of the crystallinity parameters [104]. Instead of forming the macropore structures holding the functionalities on porous carbon black, one objective here is to prevent the formation of defects on the pure GNFs and form the catalytic sites on the GNF edges; thus the ball milling step that follows the addition of iron acetate and phenanthroline has been omitted in the new set of experiments presented here. Additionally, since the GNFs already contain nitrogen, the ammonia pyrolysis stage is removed, and the temperature of the argon pyrolysis is lowered to minimize damage to the GNFs. The main objective of this work is to investigate the role of iron acetate, phenanthroline, and pyrolysis as synthesis steps and determine their effect on the catalyst structure and activity towards reducing oxygen.

4.3 Experimental materials and methods

4.3.1 Graphene nanoflakes growth

The GNF powders are produced by the plasma decomposition of methane and their surface is functionalized with nitrogen [54,81]. The plasma parameters used to grow the different GNFs are shown in Table 1. In this work, two distinct levels of nitrogen functionalization are used: low (0.5 to 3 atomic percent of nitrogen on the surface) and high (15 to 25 atomic percent of nitrogen on the surface).

Table 1. GNF growing parameters

Sample #	Low Nitrogen (LN-GNFs)		High Nitrogen (HN-GNFs)	
Preparation Stage	Power	20 kW	Power	20 kW
	Pressure	13.79 kPa	Pressure	13.79 kPa
	Argon	64.5 slpm	Argon	64.5 slpm
	Time	5 minutes	Time	5 minutes
1st Stage	Power	20 kW	Power	20 kW
	Pressure	55.16 kPa	Pressure	55.16 kPa
	Argon	64.5 slpm	Argon	64.5 slpm
	Methane	1 slpm	Methane	1 slpm
	Nitrogen	0.1 slpm	Nitrogen	0.1 slpm
	Time	20 minutes	Time	10 minutes
2nd Stage			Power	25 kW
			Pressure	13.79 kPa
			Argon	15 slpm
			Nitrogen	50 slpm
			Time	30 minutes

4.3.2 Catalyst synthesis

The low nitrogen (LN) and high nitrogen (HN) GNFs are further treated outside the plasma reactor to form the catalyst by adding iron using iron acetate and/or nitrogen using phenanthroline. The GNFs are mixed in a 1 to 1 volume ratio of ethanol and water in an ultrasonic cleaner for 1 hour. In cases where phenanthroline is added, a 1 to 1 mass ratio is used with GNFs. Iron acetate is added to the solution to obtain 1 percent mass of iron within the solid mixture. After mixing, the solution is transferred to an oven and heated to 105°C until all the liquid evaporates and the dried sample is then collected. At this stage, the sample is pyrolyzed to promote the incorporation of atomically dispersed iron. Pyrolysis is carried out using argon gas at a flow rate of 600 sccm and a temperature of 700°C for 1 hour. Following pyrolysis, no further treatments are performed. A series of 14 samples were prepared under various precursor and process combinations in order to evaluate the possible effects of the synthesis procedure. Table 2 illustrates the different conditions used to produce the samples in this work. The sample numbers presented in this table will be used for identification purposes.

Table 2. Conditions for samples produced

Sample #	Nitrogen Amount	Iron Acetate	Phenanthroline	Pyrolysis
HN-0	High			
HN-1	High	✓		
HN-2	High	✓		✓
HN-3	High		✓	
HN-4	High		✓	✓
HN-5	High	✓	✓	
HN-6	High	✓	✓	✓
LN-0	Low			
LN-1	Low	✓		
LN-2	Low	✓		✓
LN-3	Low		✓	
LN-4	Low		✓	✓
LN-5	Low	✓	✓	
LN-6	Low	✓	✓	✓

4.3.3 Characterization techniques

An electrochemical study using a rotating disk electrode (RDE) was conducted as a screening technique to determine which samples stood out as suitable catalyst candidates for reducing oxygen. For these tests we have chosen a neutral solution to follow the work done by Amirfakhri *et al.* on the catalytic ORR [105]. If the synthesized catalysts are to be used in PEMFCs and AFCs, experiments in acidic and alkaline solutions will have to be performed to assess their activities and stabilities under those conditions. However, it is already known from previous work that the GNF-based catalysts are suitable for the acidic environments of PEMFCs [104].

The GNF samples are dispersed in an ink made up of Nafion^{TM}, water, and ethanol. To prepare the ink, the GNFs are mixed in a 4 to 1 volume ratio of water and ethanol at a concentration of 1 mg per mL, and a 5 weight percent Nafion^{TM} solution is added at 4 µL per mg of GNF. The ink is sonicated in an ice bath for 1 hour, deposited on a glassy carbon RDE tip to obtain a concentration of 0.1 mg of GNFs per cm^2 of electrode, and dried in a humid environment at 65°C until the liquid evaporates. After drying, the tips are examined under a microscope to confirm uniform coverage. The tip is used as the working electrode in a 0.1M sodium sulfate neutral solution, with an oxygen and argon gas mixture being bubbled into solution in order to obtain a concentration near 32 mg of oxygen per litre. A rotation rate of 2500 rpm and a scan rate of 10 mV/sec were used in the RDE experiments.

All the GNF samples are characterized using X-ray photoelectron spectroscopy (XPS) to determine the elemental composition on their surface. XPS is performed on a Scientific K-Alpha XPS system from Thermo Scientific with an aluminium x-ray source, 300 µm spot size, and Avantage 5.932 software. Additionally, Raman spectroscopy is performed to study the graphitic content of the samples. The Raman instrument used in the present project is an inVia Reflex confocal micro-Raman (Renishaw) with a laser emitting at a wavelength of 514.5 nm. All peak intensities and areas are measured using the Wire 2.0 software. Finally, the Brunauer-Emmett-Teller (BET) area is calculated by an Autosorb iQ Gas Sorption machine from Quantachrome Instruments. Nitrogen is used as the analysis gas with a bath temperature of 77.35 Kelvin. The BET area of each sample is calculated by generating a multi-point BET plot and focusing on the relative pressures in the range of 0.05 to 0.3.

4.4 Results and discussion

4.4.1 Catalytic activity

The best method to determine the performance of a catalyst for fuel cell applications is through tests in a real fuel cell environment; however, these tests are costly, time consuming, and require a great use of resources. Instead of testing all the samples produced in this study in a fuel cell, an electrochemical study with RDE is performed as a screening technique to determine which candidates merit a more vigorous investigation. The RDE study may also provide information on the reaction mechanism and kinetics. The ORR occurring at the cathode of the cell is the slowest and limiting reaction and requires the highest load of catalyst; attention is thus given primarily to this ORR reaction. The GNF samples were studied here using RDE focussing on the range from 0.15 V to -0.15V vs RHE, which corresponds to the region right before the 2-electron electrochemical reduction of oxygen with the superoxide anion as the intermediate, and the current density was measured with respect to the applied voltage (Figure 24) [92].

The electrocatalytic activity is equivalent to the rate of reduction of oxygen in this case which is proportional to the current. The cathodic nature of the reaction shows here the currents as negative values. Therefore the lowest curves in Figure 24 a) and b) represent the samples with the strongest catalytic performance. To better illustrate the performance of the samples, the values at 0 volts for each sample were gathered over many runs (Figure 25).

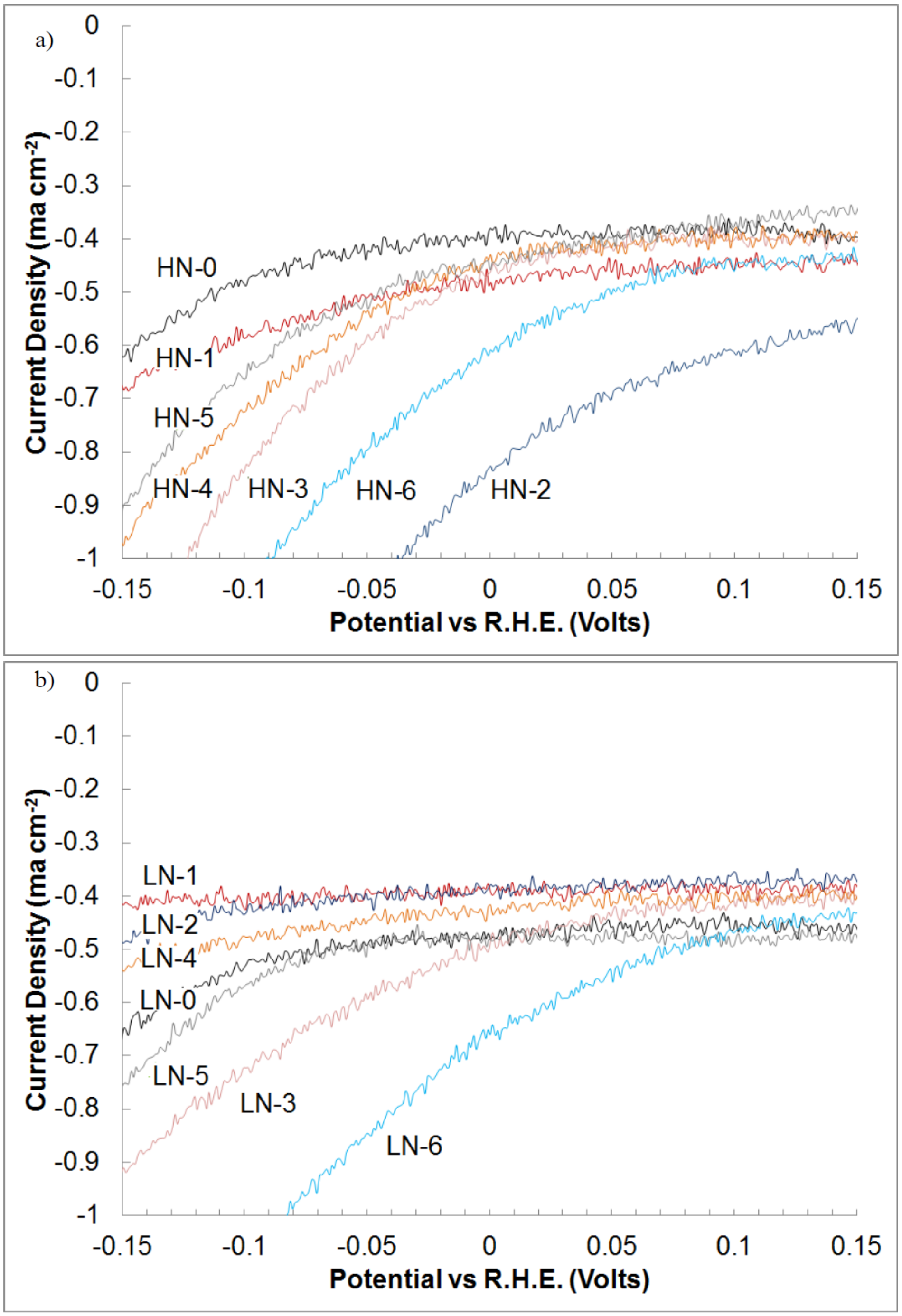

Figure 24. Current density vs R.H.E. for a) low nitrogen samples and b) high nitrogen samples

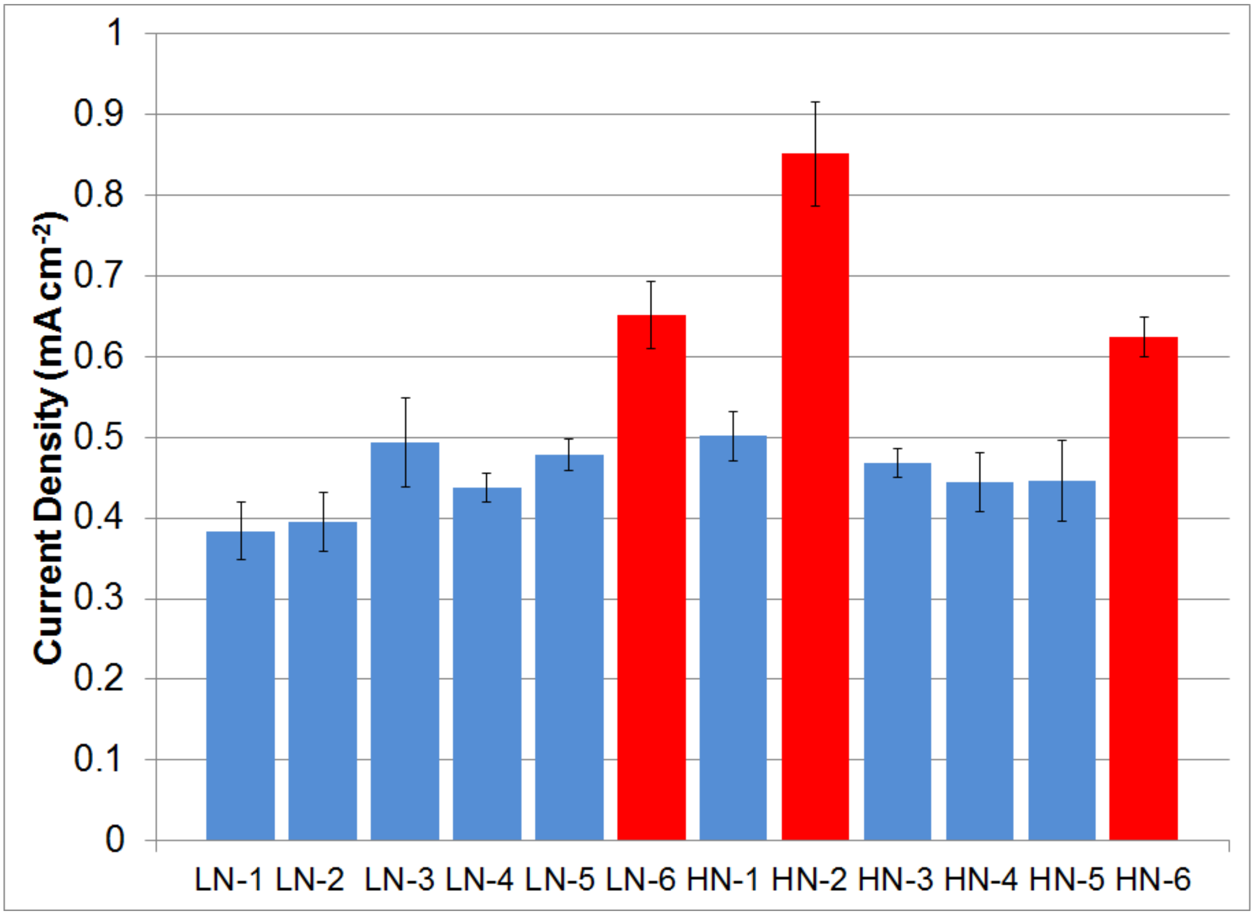

Figure 25. Absolute value of current density at 0 V vs R.H.E.

All samples demonstrate some level of activity, including the untreated samples (LN-0 and HN-0), with the activity of the LN-0 sample towards the reduction of hydrogen peroxide already having been demonstrated in previous work [105]. The GNFs have a catalytic effect on the reduction reaction, but the aim is to improve the activity of the untreated samples by incorporating iron, phenanthroline, and performing pyrolysis. In Figure 25, most of the samples were at the level between 0.4 and 0.5 mA cm^{-2}, making them statistically similar to one another and not significantly greater than untreated GNFs. Three samples stood out with higher activities, namely sample numbers HN-2, HN-6, and LN-6. The best performance was that of the

HN-2 at a value of 0.851 mA cm^{-2}. The activity value of HN-2 compares favorably with other non-platinum catalysts, such as carbon supported manganese oxide nanoparticles [87] and beanpod-shaped Fe-C-N composites [93], which fall in the range of 0.2 to 2.8 mA cm^{-2}; however, these studies do not clearly report the amount of catalyst material used during experiments, making a normalized comparison on the basis of mass hard to do. The HN-2 catalyst was able to achieve a high activity in a neutral solution with a relatively small loading. In a study by Wu *et al.* that investigated the electrochemical reduction of oxygen catalyzed by reduced graphene sheets in neutral media, they report a value of around 0.75 mA cm^{-2}, but their experiments used double the catalyst loading than in our experiments [92]. The fact that HN-2`s performance already surpasses other non-platinum catalysts in the literature is a good sign for its future as an ORR catalyst.

Figure 25 also provides information on the effect of using iron acetate, phenanthroline, and the use of a pyrolysis step. As expected none of the four iron-free samples (LN-3, LN-4, HN-3, HN-4) stand out in terms of activity, because iron is the active component of this catalyst. These results further exemplify the importance of iron acetate to the catalyst synthesis procedure. When comparing all the iron-containing samples, the pyrolyzed samples (LN-2, LN-6, HN-2, HN-6) produced a higher current density than their respective un-pyrolyzed counterparts (LN-1, LN-5, HN-1, HN-5). In fact, the iron-containing samples that have not experienced pyrolysis are statistically equivalent to the iron-free samples and the untreated GNFs. The three most active samples in this study (red columns in Figure 25: LN-6, HN-2, HN-6) went through a pyrolysis process. This result shows the importance of the pyrolysis step for proper iron incorporation. The chemical composition and physical phase of the GNFs can be irreversibly changed to incorporate the atomically dispersed iron on the surface of the graphene sheets.

Focusing on the iron-containing samples and comparing the phenanthroline-free samples (LN-1, LN-2, HN-1, HN-2) to the phenanthroline-containing samples (LN-5, LN-6, HN-5, HN-6), one sees the presence of phenanthroline increases the current density of the LN-GNF samples whereas it is decreasing it for HN-GNFs. It appears that the LN-GNFs do not have enough nitrogen present initially, phenanthroline acting as an extra nitrogen source for them. However, for HN-GNFs, the nitrogen is already at a very high loading on the GNF surface following the plasma process; the addition of phenanthroline is not seen to improve the catalyst activity. Contrary to the carbon black material and catalyst preparation technique used by the team of Dodelet *et al,* phenanthroline can be omitted from the iron incorporation step altogether because the carbon nanomaterial precursor already has the proper nitrogen content to form an active catalyst.

The surface area of the untreated GNFs and the three most active samples were measured by the BET method to further validate the RDE results. The results presented in Figure 24 and Figure 25 are normalized with respect to the area of the RDE disc, but since each sample is prepared at the same concentration and the same volume is deposited, it is equivalent to normalization with respect to mass. By determining the surface area, this mass can be converted into a ‘GNF surface area’ and the results can be re-evaluated to determine if they still are statistically different from the control case of untreated GNFs. The area calculation will vary depending on whether the sample is in powder form or dispersed in an ink, but it is assumed that the differences between the samples are relatively similar for either condition. In the present work, the area was measured in powder form for comparison reasons. All the samples produced a fairly similar BET surface area, which is shown in Table 3. These results were then used to re-normalize the RDE values, also presented in Table 3. When these new values are considered, the active samples still stand out among the rest, further confirming the RDE results.

Table 3. Current density normalized with 'GNF surface area'

Sample Name	Current Density w/ 'geometric area' [mA cm^{-2}]	BET Surface Area [m^2 g^{-1}]	Current Density w/ 'GNF surface area' [mA m^{-2}]
HN-0	0.454	211	21.51
HN-2	0.851	209	40.62
HN-6	0.625	174	35.97
LN-0	0.448	182	24.62
LN-6	0.651	178	36.56

The BET surface area is also useful for comparing this material to similar materials being used by other research groups where values can range from 400 to 1800 m^2 per g [32,106–108]. The BET results obtained in this study may seem to be low especially when compared to the 'perfect case' of graphene. By assuming a unit cell of one benzene ring with a bond length of 0.142 nm, one-sixth of a carbon atom at each vertex (or one atom per ring), and a mass of 2x10^{-23} g per atom, one obtains a surface area of 2619 m^2 per g, which matches the literature quite well [109]. The GNFs produced in this work had a surface area less than one-tenth of the calculated value, but the GNFs contain nitrogen, iron, oxygen, and may not be perfect aromatic rings; each of these defects adds mass to the structure and decreases the surface area value. Defects are sought in our catalyst structure as we want iron-nitrogen-GNF edges to be potential active sites. A relatively low BET surface area is a good sign for our catalyst.

4.4.2 Elemental composition

All produced samples were characterized by XPS to evaluate the overall content of nitrogen; in addition, a deconvolution of the peaks was performed to attribute the elemental signals to bond types. The results of the two primary peaks, carbon and nitrogen, are shown in Table 4 with the three most active samples from the RDE study (HN-2, HN-6, and LN-6) shown in bold. The other elemental signals in the samples were iron, when applicable, in small amounts (less than 0.5 atomic percent) and oxygen (1.5 to 5 atomic percent).

Table 4. Elemental atomic percent from surface analysis

Sample Name	Carbon [atomic percent]	Nitrogen [atomic percent]
HN-0	74.16	20.60
HN-1	78.62	17.41
HN-2	**93.03**	**4.28**
HN-3	76.27	19.90
HN-4	89.83	8.54
HN-5	80.04	14.24
HN-6	**90.23**	**6.02**
LN-0	97.92	0.74
LN-1	95.88	1.15
LN-2	98.81	0.38
LN-3	97.59	1.26
LN-4	95.60	2.96
LN-5	92.85	3.95
LN-6	**94.13**	**3.84**

The HN-GNFs produced in this work had a nitrogen content of about 20 atomic percent on the surface before being treated. There is a noticeable difference between the pyrolyzed (HN-2, HN-4, and HN-6) and non-pyrolyzed samples (HN-1, HN-3, and HN-5). Pyrolysis always resulted in at least a 58 percent decrease of the nitrogen content; for the case in which only iron acetate was added (HN-1 and HN-2), a 75 percent decrease was observed. This result indicates that, with the untreated HN-GNFs, a large amount of nitrogen might be attached to amorphous carbon and the pyrolysis procedure breaks these bonds, leading to the sharp decrease in nitrogen content. For the LN-GNFs, the original nitrogen content was very low (less than 1 atomic percent), but in all the cases where phenanthroline was added (LN-3, LN-4, LN-5, and LN-6), the nitrogen content increased significantly, even by more than 400 percent for the lone active low nitrogen sample (LN-6 compared to LN-0).

When examining the carbon and nitrogen signals of all the samples, the three most active samples from the RDE study (HN-2, HN-6, LN-6) produced similar signals to one another, exhibiting the same overall shape and relative bond types, although with differing amounts of total nitrogen and carbon for both the low and high nitrogen cases. All other samples produced the same XPS spectra for carbon and nitrogen as untreated GNFs (HN-0 and LN-0). Figure 26 shows the carbon signal of the most active sample (HN-2) compared to the untreated HN-GNFs (HN-0). The main carbon peak is at a binding energy of 284.6 eV and the peak of HN-2 is slightly less broad than that of HN-0, best illustrated in the binding energy of 285 to 287 eV, indicating slightly less amorphous carbon [60]. At the binding energies of 287 to 291 eV are the signals for functional group attachments. HN-2 and HN-0 both give a signal in this range, but that of HN-2’s is at a lower intensity, symbolizing that the functional groups are attaching to graphitic carbon and not amorphous carbon. This decrease in amorphous carbon content for the three most active samples means that they contain an overall higher graphitic content and are therefore a purer material, which increases their catalytic activity towards the ORR.

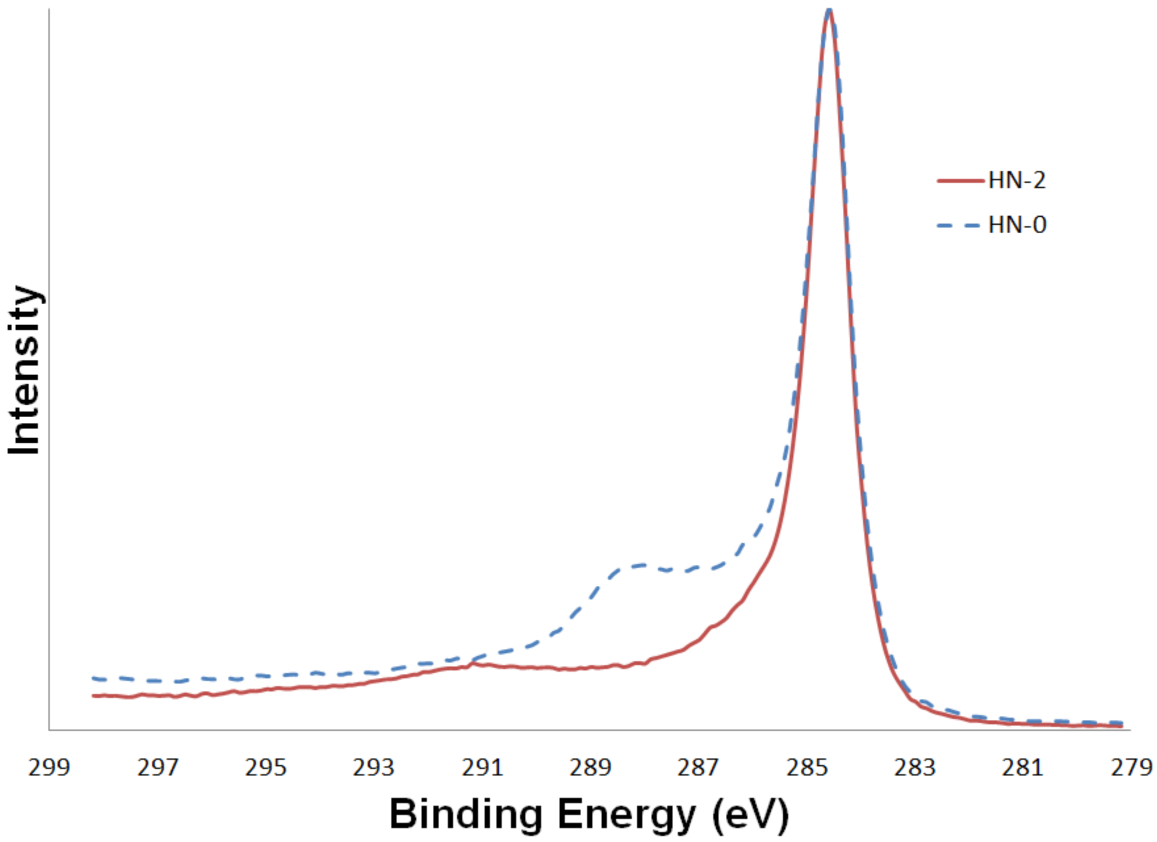

Figure 26. XPS of carbon peak for HN-0 and HN-2

Figure 27 shows the nitrogen signals for HN-0 and HN-2. The two cases have noticeably different shapes. HN-0 produces a symmetrical nitrogen signal, with 32 percent being attributed to the pyridinic peak (binding energy of approximately 398.7 eV), while HN-2 has a noticeable slant to a lower binding energy and 70 percent of the signal coming from the pyridinic peak. The high pyridinic content is desirable for the specific application of PEMFCs, but the lack of pyrrolic nitrogen (binding energy of approximately 400.3 eV) likely indicates a low overall activity.

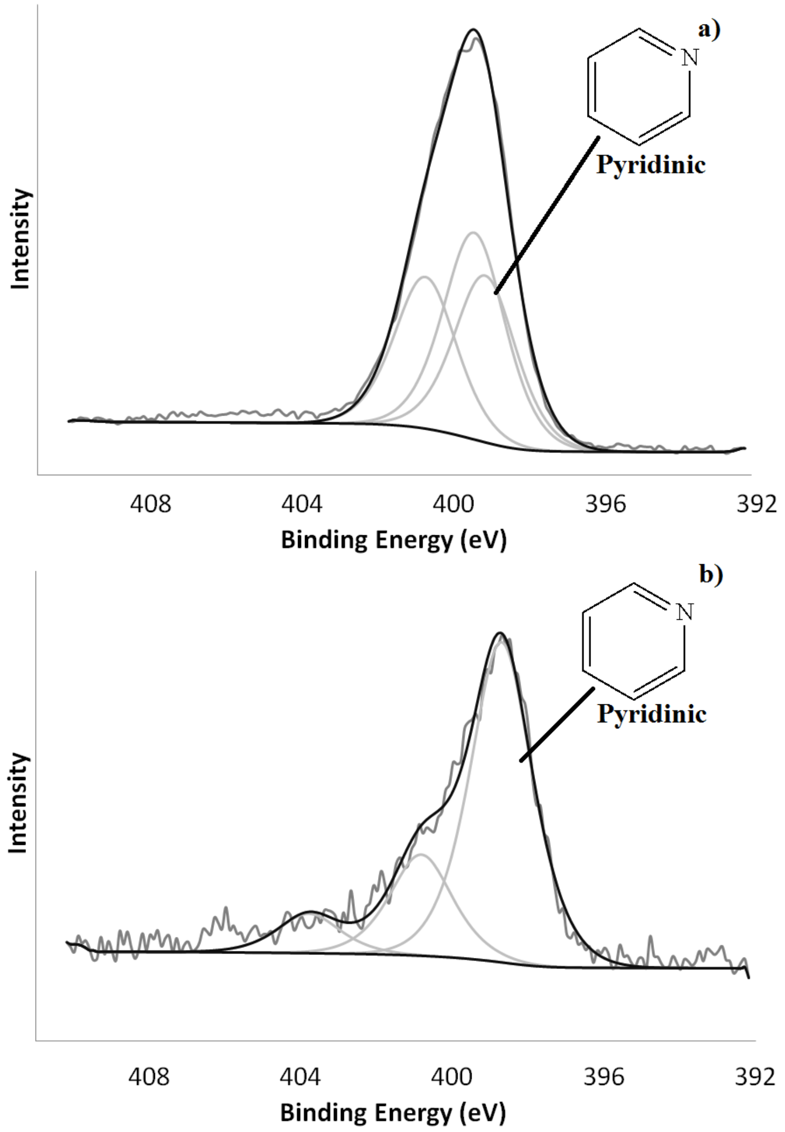

Figure 27. XPS of nitrogen peak for a) HN-0 and b) HN-2

4.4.3 Crystallinity

The Raman spectra for each of the samples in this study were obtained and analyzed. Indices for the purity, the crystallite size, and the average length of graphene planes provide a better understanding of the nature of the graphitic content through examination of the three main peaks [67,110–112]. The calculated values for these factors for the three most active samples are presented in Table 5. It can be observed again here that sample HN-2 stands out. The addition of iron acetate to the HN-GNFs still maintains a high purity factor, with an average length of graphene plane that almost doubles the two other samples. In comparison, when the unmodified incorporation method of Jaouen *et al.*is used on GNFs, the average length of the graphene planes is around 10 nm by the end of the second pyrolysis step [104]. By using HN-GNFs and eliminating phenanthroline, ball milling, and one pyrolysis stage from the iron incorporation method, the damaging of the graphene sheets is minimized.

Table 5. Crystallinity parameters

Sample Name	Purity	Crystallite Size [nm]	Average Length of Graphene Plane [nm]
HN-2	2.37 ± 0.06	6.86 ± 0.15	18.51 ± 0.92
HN-6	1.82 ± 0.10	5.76 ± 0.54	8.87 ± 0.21
LN-6	2.11 ± 0.07	7.37 ± 0.48	9.72 ± 1.43

Raman performed on the samples demonstrated an interesting property that further helps reinforce the importance of pyrolysis for the iron incorporation step. When the HN-GNF samples are treated with iron, phenanthroline, or both, they all give off a fluorescent signal in their Raman spectra. However, the fluorescence is eliminated by performing pyrolysis. Figure 28 shows this result for the HN-GNF with iron. This seems to show that poly-aromatic hydrocarbons are formed by the iron incorporation steps and then removed by pyrolysis, yielding a cleaner material.

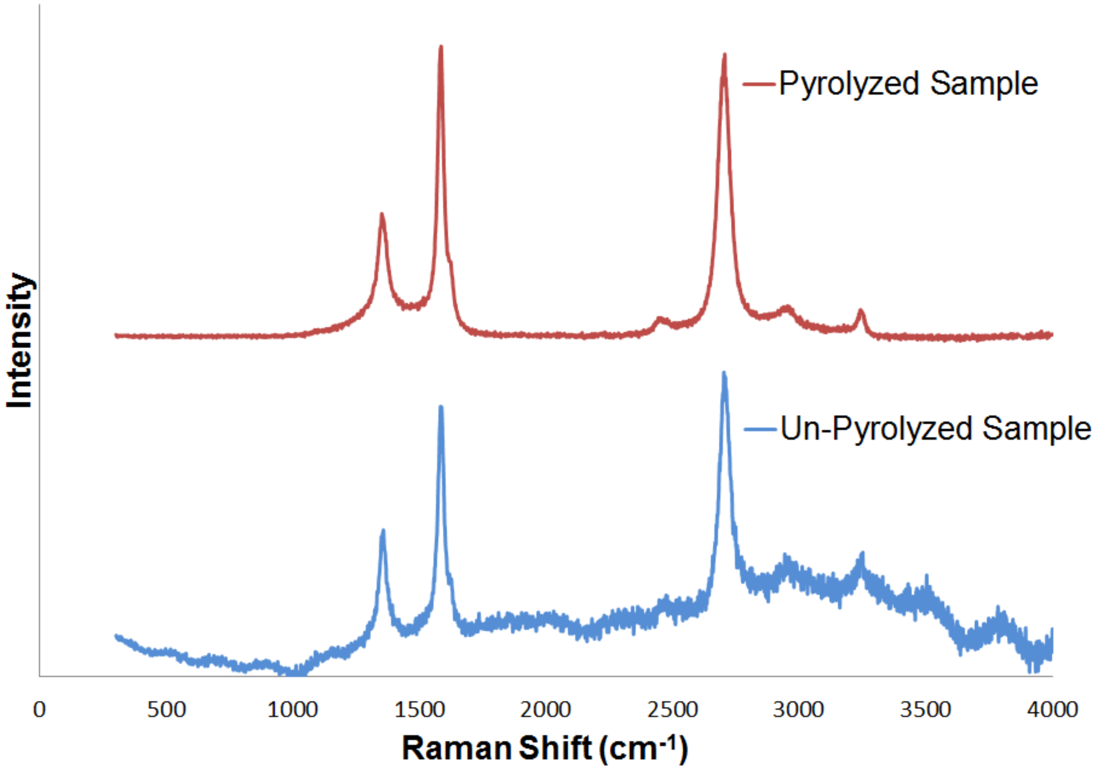

Figure 28. Raman spectra of HN-GNFs with iron before (HN-1) and after (HN-2) pyrolysis

4.5 Conclusions

GNFs grown in a thermal plasma reactor at two nitrogen levels were treated with iron acetate, phenanthroline, and a pyrolysis step in order to optimize their catalytic activity. It was found through RDE, XPS, Raman, and BET analysis that iron acetate and pyrolysis were essential components for the incorporation of iron onto the GNFs. Additionally, pyrolysis is required as a final step for iron incorporation as it improves the activity while removing the fluorescence of the samples. By altering the nitrogen levels of the nanomaterial, it was found that phenanthroline was not needed for GNF samples containing a high level of nitrogen by plasma functionalization, but helped the GNF samples generated with a low level of nitrogen to obtain a higher activity. The carbon and nitrogen signals also showed that the catalyst having the highest activity also have the highest level of graphitization and the majority of their nitrogen in pyridinic states. This study provides results towards optimizing the iron incorporation process for GNFs and eventually developing a suitable non-noble metal ORR catalyst. With the untreated GNFs already providing some activity for ORR, a relatively small amount of atomically dispersed iron added onto the GNFs is shown here to double this initial activity level. Studies on the active site and the position of the atomically dispersed iron within the catalysts are currently underway, in addition to actual fuel cell testing.

Acknowledgments

The authors would like to acknowledge the funding contributions of the *Fonds de Recherche Nature et Technologie du Québec* (FRNTQ) and the *Natural Science and Engineering Research Council* (NSERC) of Canada. Additionally, Pierre-Alexandre Pascone would like to thank David Morris for his help with the BET machine and Ulrich Legrand for useful discussions.

Chapter 5: Influence of Iron on Structure and Catalyst Activity of Nitrogen-functionalized Graphene Nanoflakes

5.1 Preface

This chapter presents a published article with the following citation:

P.-A. Pascone, J.-L. Meunier, and D. Berk, *Influence of iron on structure and catalyst activity of nitrogen-functionalized graphene nanoflake*, Materials Today Communications **9** (2016), 54–59.

P.-A. Pascone (the Ph.D. candidate) was responsible for the planning of experiments, the complete synthesis of the catalyst, performing the experimental work (catalytic testing) and accompanying analysis, characterizing the material through XPS and SEM with the accompanying analysis, and writing the article. J.-L. Meunier and D. Berk supervised the work and reviewed the manuscript.

The article investigates the effect of the iron weight percent on the catalyst for acidic, basic, and neutral electrolyte solutions. In addition, the shape, location, and bonding of the iron nanoparticles are explored. Of the three samples prepared, the one labeled Fe-Medium, (which contains 3.77 weight percent iron), is the best performing catalyst. It is shown that the presence of iron is vital for the catalyst in acidic media and that the iron nanoparticles are covered with graphene sheets, which is believed to be associated to stability in fuel cells. This study was paramount as it provided knowledge on the placement of iron within the HN-GNFs and also indicated that a PEMFC study should proceed.

Influence of Iron on Structure and Catalyst Activity of Nitrogen-functionalized Graphene Nanoflakes

Authors: Pierre-Alexandre Pascone[a], Jean-Luc Meunier[a], Dimitrios Berk[a]

Affiliations: a: Plasma Processing Laboratory (PPL), McGill University, Chemical Engineering, 3610 University Street, Montréal, Québec, H3A 0C5, Canada

Abstract: A cost effective alternative catalyst to platinum for the oxygen reduction reaction (ORR) in polymer electrolyte membrane fuel cells is iron nanoparticles deposited into nitrogen-rich stacked graphene sheets. In this work graphene nanoflakes with high levels of nitrogen (HN-GNFs) are grown from the plasma phase and iron functionalities are added by a wet-chemical method. The amount of iron is varied to study the structural and electrochemical effects on the catalyst. The amount of iron in the sample and on the surface is measured and proven to have no effect on the qualitative surface conditions of HN-GNFs, as the iron is imbedded into the HN-GNFs. Electrochemical studies with a rotating disk electrode reveal that the addition of iron is beneficial in acid and neutral environments, with improvements of over 0.3 V to the onset potential and 1.85 mA cm^{-2} to the current density at 0 V versus a reversible hydrogen electrode when the iron catalysts are compared to untreated HN-GNFs. The iron did not improve the

catalytic performance in alkaline environments, with untreated HN-GNFs already showing good activity towards the ORR.

Keywords: catalyst; iron; nitrogen; graphene; oxygen reduction reaction

5.2 Introduction

The oxygen reduction reaction (ORR) is an essential and often rate-limiting reaction in energy conversion devices such as fuel cells [113]. For polymer electrolyte membrane fuel cells (PEMFCs), the ORR occurs at the cathode side with slow kinetics, requiring a catalyst showing good performance at low cost. The leading catalysts currently used, in particular for transport industry applications, are based on platinum. Economic evaluations made for this noble metal yield a catalyst cost corresponding to close to half of the total fuel cell stack price when reaching a high production rate of 500 000 systems per year [114]. A cost effective alternative must be developed to achieve commercially viable PEMFCs with one promising avenue being non-noble metal catalysts using, for example, cobalt or iron active centers [115–123].

The non-noble metal catalyst produced in this work consists of iron nanoparticles deposited into nitrogen-rich stacked graphene sheets. Using the method developed by Pristavita *et al.*, graphene powders in the form of stacked sheets with an extremely high level of purity are produced by the thermal decomposition of methane in a thermal plasma [54]. The graphene, hereafter called graphene nanoflakes (GNFs), have typical planar dimensions of 100 by 100 nm, and contain roughly 5 to 20 atomic planes. The GNFs display an exceptionally high degree of crystallinity from the nucleation and growth processes occurring in a temperature window between 3 700 and 4 900 K, and are generated with essentially no amorphous carbon present in the powders [55]. Following their nucleation from the gas phase and deposition, the GNFs can be functionalized in the same reactor using a second plasma step to generate high amounts of nitrogen (15 to 25 atomic percent) on their surface and create a novel starting material for catalysis applications [81]. These high nitrogen-containing graphene nanoflakes (HN-GNFs) are collected and mixed with an iron coordination complex through a wet-chemical method in order to produce the final iron-containing catalysts [124].

A previous study has already shown the viability of HN-GNFs as a support structure for synthesizing non-noble metal catalysts [104,124]. Here, iron is added at different proportions to HN-GNFs with all other synthesis parameters fixed in order to study the effect of the iron content on catalyst structure and activity towards the ORR. The prepared catalysts are analyzed to determine the amount of iron in the bulk sample, their elemental surface composition, and detect any changes to the structure of graphene stacking. An electrochemical study is also performed in different electrolyte solutions to monitor increases in performance of the HN-GNFs stemming from the addition of iron.

5.3 Experimental materials and methods

5.3.1 Catalyst synthesis

HN-GNFs are grown by a 2-stage plasma process using an inductively coupled thermal plasma torch (TEKNA PL-35 model), a radio frequency generator (Lepel; 60 kW power/2-5 MHz frequencies), and a conical water-cooled reactor [3,54,81]. Once collected from the reactor, the HN-GNFs are mixed in an equal part ethanol/water mixture at a concentration in the range of

2 to 4 g L^{-1} with iron acetate added afterwards. In this set of experiments, the amount of iron acetate introduced was controlled to obtain different iron contents in the catalyst. Three samples are prepared to obtain a ‘low’, ‘medium’, and ‘high’ amount of iron; the iron weight used in the wet-chemical method is 1% (Fe-Low), 3% (Fe-Medium), and 15% (Fe-High). The final mixture is ultrasonically dispersed for 1 hour and then transferred to an oven and heated until drying of the sample. The dried sample then goes through argon pyrolysis at a temperature of 700°C for 1 hour.

5.3.2 Characterization techniques

The elemental composition on the surface of the catalysts is evaluated by X-ray photoelectron spectroscopy (XPS) performed using a Scientific K-Alpha XPS system from Thermo Scientific with an aluminium x-ray source, a 300 μm spot size, and the Avantage 5.932 software. Neutron activation analysis (NAA) is utilized to determine precisely the amount of iron in the bulk catalyst material. NAA is achieved at the SLOWPOKE Laboratory of the Institute of Nuclear Engineering (École Polytechnique de Montréal) with a SLOWPOKE nuclear reactor, an Ortec GEM30185-P germanium semiconductor gamma-ray detector, an Ortec DSPEC Pro^{TM} multichannel analyzer, a Sartorius precision balance, and the EPAA analysis software [125]. For qualitative information about the catalysts, scanning electron microscopy (SEM) is accomplished with a FEI Inspect F50 FE-SEM at a 5 kV accelerating voltage and 10 μA beam current in addition to transmission electron microscopy (TEM) with a FEI Tecnai G2 F20 200 kV Cryo-STEM.

Electrochemical studies by rotating disk electrode (RDE) are performed at room temperature in 3 distinct electrolyte solutions: acidic, neutral, and alkaline. The acidic electrolyte is a 0.1 M H_2SO_4 solution prepared from reagent grade sulfuric acid and diluted with deionized water and having a measured pH of 0.70. The neutral electrolyte is a 0.1 M Na_2SO_4 solution prepared in-house by mixing the salt in deionized water and has a measured pH of 7.8. The alkaline electrolyte is a 1 M NaOH solution with a measured pH of 13.3. The catalysts are prepared in an ink composed of Nafion^{TM}, water, and ethanol and dried in a humid environment onto a glassy carbon RDE tip at a concentration of 0.2 mg of catalyst per cm^2 of electrode. A saturated silver/silver chloride (Ag/AgCl) electrode and a platinum wire are used as the reference and counter electrodes respectively. RDE conditioning (break-in) with nitrogen is performed on each sample until the cyclic voltammogram becomes invariant with time and cycles [126]. Oxygen reduction reaction (ORR) curves are then obtained from the cathodic scans of a linear voltage profile from 1 to -1 V at a scan rate of 20 mV/s and a rotation rate of 2500 rpm. A background correction to account for the capacitive current contributions is conducted and removed from all data curves [126]. For comparison with the literature, results are displayed with respect to a reversible hydrogen electrode (RHE) as a reference electrode. The Nernst equation is used to adjust the reference electrode potentials and also account for the pH of the electrolyte solution (Equation 7); the standard potential is taken as 0.1976 V at 25°C [127].

$$E_{RHE} = E_{Ag/AgCl} + E^{\circ}_{Ag/AgCl} + 0.059 * pH$$

Equation 7. Nernst equation for conversion of Ag/AgCl to RHE

5.4 Results and discussion

5.4.1 Iron content

Iron acetate is mixed with HN-GNFs at different ratios with the express purpose of producing samples with increasing iron content. The range of values chosen for this study (1 to 15 weight percent) are on the low end of ranges that are found in industrial platinum catalysts, where loadings on a mass basis as high as 80% exist on carbon supports. The three catalysts in this study were prepared and NAA was used to verify the weight percent of iron (Table 6). The samples are labeled Fe-Low, Fe-Medium, and Fe-High to represent their relative amount of iron used in the catalyst synthesis. NAA reveals that the iron content of all samples is slightly higher than the desired value, with the difference attributed to carbon material losses in the synthesis procedure. The iron weight percent achieved in this study demonstrates that it is indeed possible to add more iron to the HN-GNFs structures through the wet-chemical iron incorporation technique, as this study marks the first attempt to go above 1% with GNFs [104,124].

Table 6. Iron content of samples based on NAA

Sample Name	Iron Weight Percent
Fe-Low	1.25
Fe-Medium	3.77
Fe-High	18.03

XPS is performed to determine the elemental composition of the catalyst surfaces (Table 7). HN-GNFs have typical nitrogen amounts of 15 to 25 atomic percent, but the wet-chemical method, and especially the pyrolysis treatment, removes much of the pyrrolic and quaternary nitrogen on the surface and leaves a final nitrogen signal that is in the 1 to 4 atomic percent range and primarily composed of pyridinic nitrogen [124]. This phenomenon is again observed in this study with more iron content leading to a sharper decrease in surface nitrogen. If the XPS results, which represent surface conditions on an atomic basis, are translated into weight percentages, the iron content roughly translates into 2.08, 2.36, and 1.77 for Fe-Low, Fe-Medium, and Fe-High respectively. When comparing the iron results from XPS to NAA, no correlation is observed between the bulk and surface contents of iron, implying that XPS alone should not be used on these types of catalysts as an indicator of overall iron content or catalyst suitability. The surface content is however a confirmation of iron incorporation and is still an excellent analysis technique for determining the iron state and the relative amounts of carbon, nitrogen, and oxygen.

Table 7. Elemental atomic percent from surface analysis

Sample Name	Carbon [Atomic Percent]	Nitrogen [Atomic Percent]	Oxygen [Atomic Percent]	Iron [Atomic Percent]
Fe-Low	94.71	3.80	1.03	0.46
Fe-Medium	96.34	1.72	1.42	0.52
Fe-High	96.45	1.30	1.86	0.39

Further XPS analysis on the iron signals in the 700-740 eV binding energy range show differences in the iron species on the surface (Figure 29). Signals are detected for Fe, Fe^{2+}, Fe^{3+} at binding energies of 707 eV, 713 eV, and 710 eV respectively [60]. XPS shows the different iron species, however it does not allow infallible assignment of iron signals to specific bonds. The Fe signal is attributed to metallic iron. Fe^{2+} is generally favored when considering $Fe-N_x$ active centers, but it could also signal oxide formation, whereas the Fe^{3+} signal is generally assigned to iron oxides and/or hydroxides [117]. Using the sample names indicated in Table 6, Fe-High has a dominant Fe signal and a weaker Fe^{3+} signal, whereas Fe-Low has a strong Fe^{3+} signal and noticeable Fe^{2+}. Fe-Medium, on the other hand, has a fairly even distribution of all three iron signals. It is difficult to gain the full information about the entire iron content in the samples due to the fact that most of the iron is in the bulk and thus undetectable using XPS.

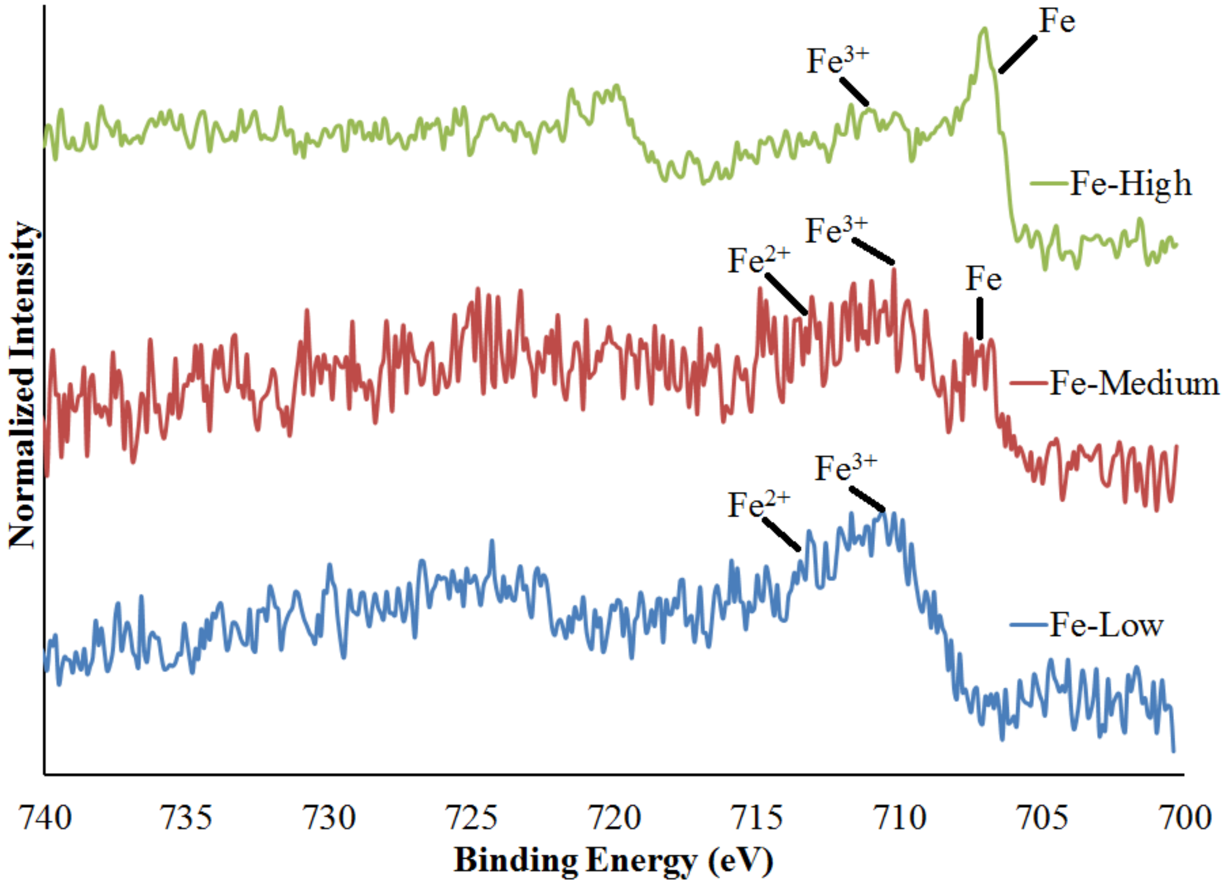

Figure 29. High resolution of iron XPS peak of Fe-High, Fe-Medium, and Fe-Low

SEM was performed to see if any structural differences could be noticed at the micrometer level between samples having different iron contents (Figure 30). The samples proved to be indistinguishable from one another, with all displaying the same ‘nanoflake’ structure of the untreated HN-GNFs. Absent from these images are iron structures or macroparticles, thus confirming the XPS results which show little iron on the surface. TEM was performed on the Fe-High catalyst to see iron particles within the structure (Figure 31). At the 500 nm scale (Figure 31a and b), iron nanoparticles are clearly visible throughout the HN-GNFs structure; these nanoparticles have diameters ranging from 10 to 35 nm. The iron however is not uniformly dispersed throughout the structure, with a mixture of low and high density areas. At the 20 nm scale (Figure 31c and d), it can be seen that the iron nanoparticles are coated with graphene-like structures encapsulating the nanoparticle into a core-shell structure and having high crystallinity similar to the GNFs. The spacing between graphene-like encapsulation layers is approximately half the lattice parameter of graphite (~0.3 nm) and these layers are composed of 5 to 20 single graphene sheets. The iron nanoparticles are thus surrounded by 5 or more nm of crystalline carbon material. The XPS measurement relying primarily on the information gathered from the first few nanometers of the surface, such encapsulation further questions its accuracy on the amount of iron in the sample. Furthermore, Figure 31d also shows the graphene nanoflake structure to be untouched or damaged, which confirms that the process for iron incorporation does not affect the structural integrity of the GNF structures. Finally it is to be noted that none of the XPS, NAA and TEM diagnostics used are able to reveal possible catalytic sites based on the nitrogen coordination of atomic iron in a way similar to the porphyrin organic ring.

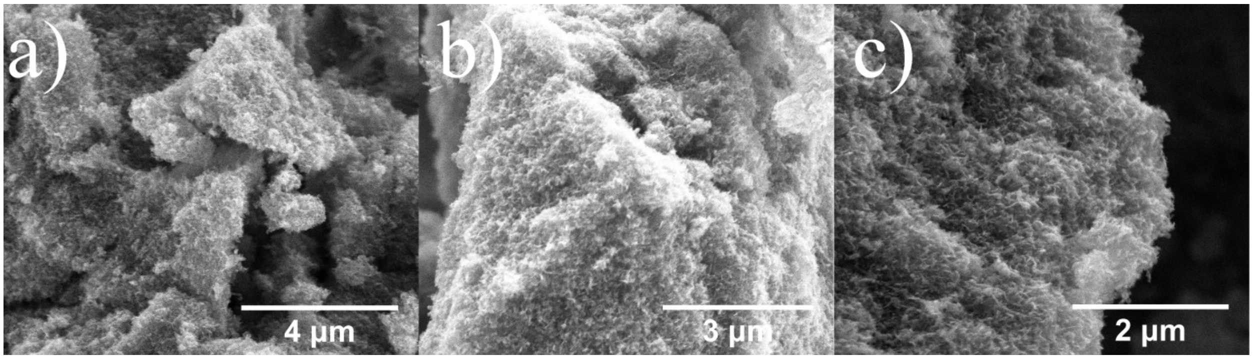

Figure 30. SEM micrograph of a) Fe-Low, b) Fe-Medium, and c) Fe-High

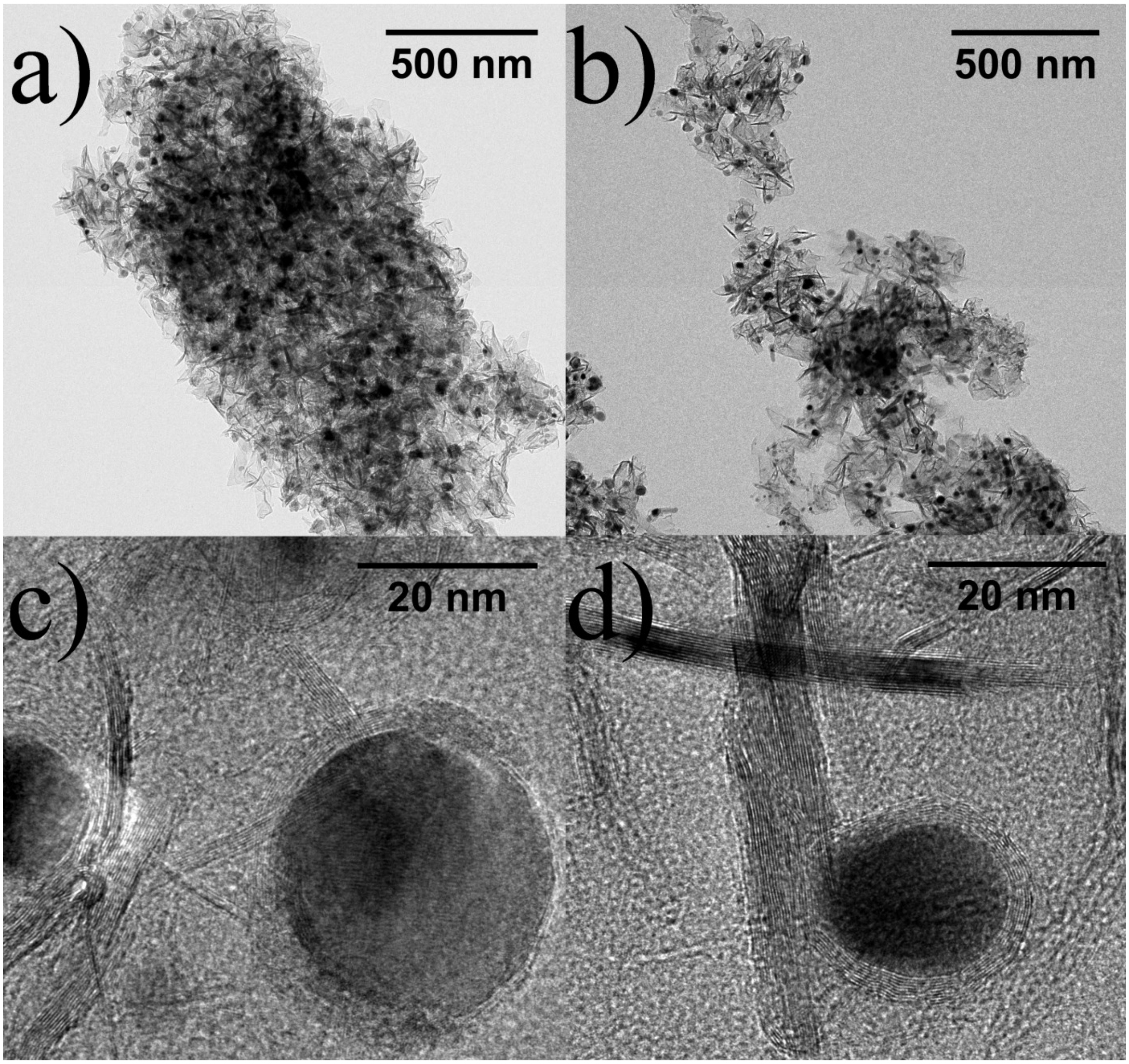

Figure 31. TEM micrograph of Fe-High at different magnification, a) & b) scale bar of 500 nm and c) & d) scale bar of 20 nm

5.4.2 Catalytic activity

An electrochemical study using RDE is done to gain information on the performance of the iron catalysts for the ORR. In fuel cell applications, the cathode requires a higher catalyst loading than the anode, so the focus at this stage is solely on the ORR. The performance of the iron catalysts, along with the untreated HN-GNFs, is shown in Figure 32, Figure 33, and Figure 34 for acidic, neutral, and alkaline electrolyte environments respectively.

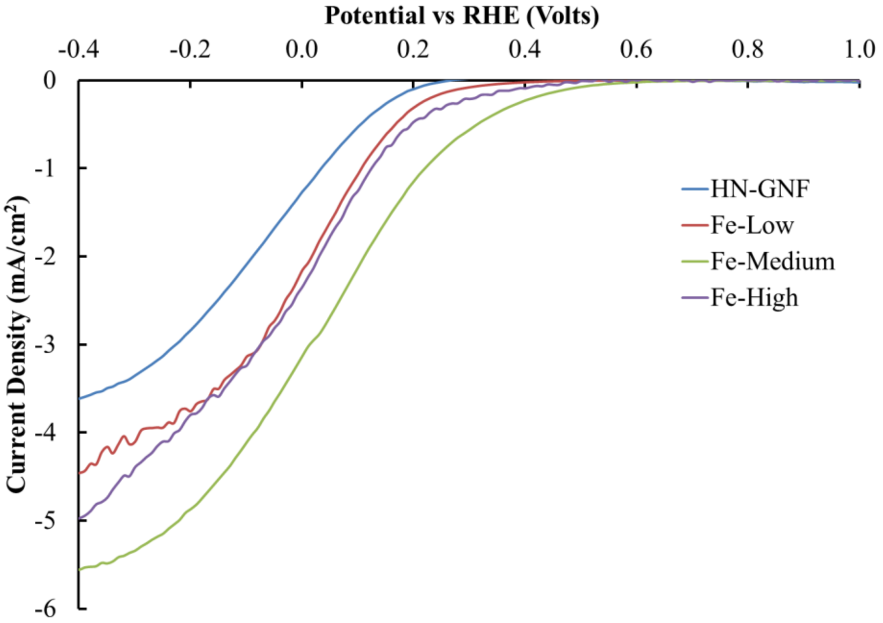

Figure 32. Current density vs RHE for HN-GNFs and iron catalysts in acidic electrolyte

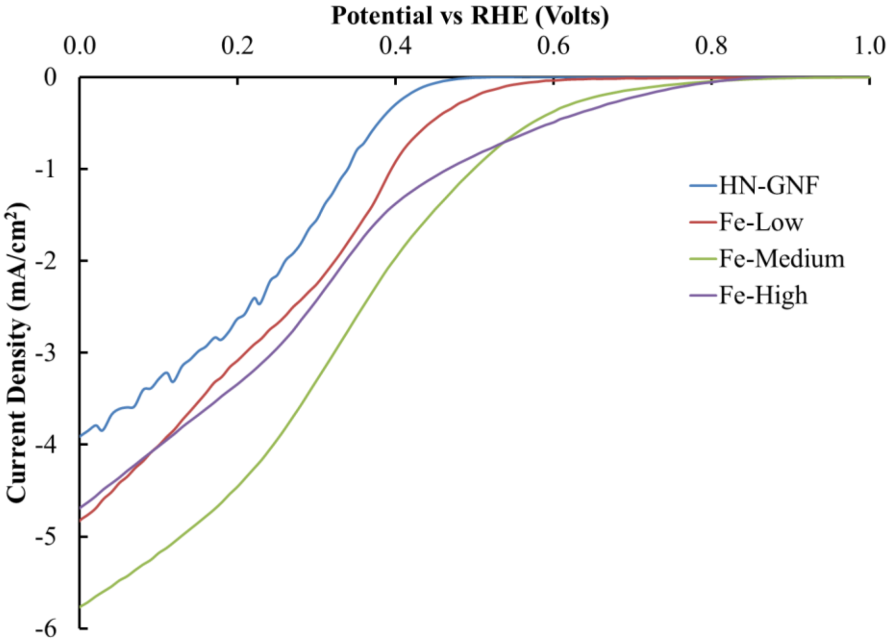

Figure 33. Current density vs RHE for HN-GNFs and iron catalysts in neutral electrolyte

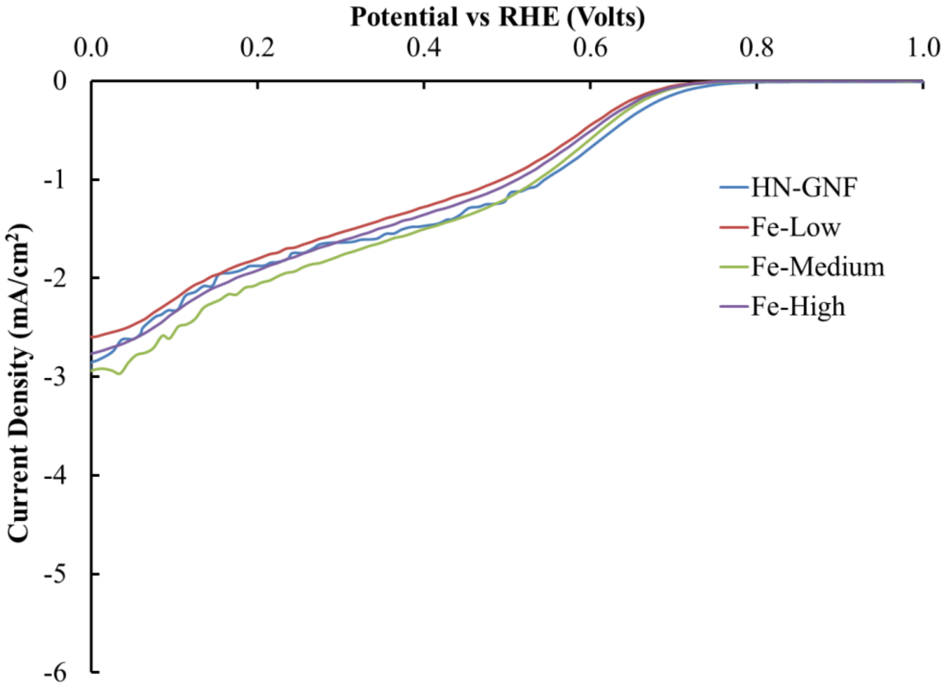

Figure 34. Current density vs RHE for HN-GNFs and iron catalysts in alkaline electrolyte

All samples displayed activity towards the ORR, but different parameters can be evaluated from these results to better illustrate the performance of the samples. Table 8 displays the onset potential, half-wave potential, and the max current density achieved for the catalyst in each of the electrolyte solutions. The onset potential for cathodic reactions such as the ORR is the highest potential at which reaction products can form and is useful for the evaluation of the catalytic activity and in comparing different catalyst materials. The current used to determine the onset potential is set to -0.05 mA cm^{-2}, where the curve can be differentiated from a zero value. The half-wave potential is the potential where the current is equal to one-half of the limiting current (the maximum current achieved). Ideally, a high half-wave potential is desired, which symbolizes a sharp decrease and thus a faster reaction. For the alkaline results, the half-wave potential of the first drop is taken. The current density reported in Table 8 is the current at a potential of 0 V vs RHE, reported as a density by taking into account the geometric surface area of the RDE. The current densities are negative since they represent the cathodic reaction but are reported as positive numbers where large values are indicators of better catalytic activity.

Table 8. Electrochemical performance of HN-GNFs and iron catalysts

Sample Name	Onset Potential (V)			Half-wave Potential (V)			Current Density @ 0 V (mA cm^{-2})		
	Acid	Neutral	Alkaline	Acid	Neutral	Alkaline	Acid	Neutral	Alkaline
HN-GNFs	0.22	0.46	0.74	-0.07	0.26	0.59	1.26	3.91	2.83
Fe-Low	0.33	0.58	0.70	-0.01	0.28	0.57	2.15	4.82	2.57
Fe-Medium	0.53	0.79	0.71	0.04	0.32	0.58	3.13	5.76	2.92
Fe-High	0.46	0.80	0.70	-0.02	0.30	0.58	2.35	4.69	2.73

When examining the electrochemical performance, certain trends are noticeable. In looking solely at the iron catalysts, Fe-Medium consistently stands out as the best overall catalyst in both the acidic and neutral environments; Fe-Medium has the highest onset potential, half-wave potential, and current density in these environments. Samples Fe-High and Fe-Low produced similar results for all parameters, with the exception of Fe-High showing a higher onset potential in the acidic and neutral environments. HN-GNFs are tested along with the iron catalysts to provide a baseline used to determine what the direct effect of the addition of iron is towards the catalyst's performance. In an alkaline environment, no great improvement is seen with respect to the HN-GNFs as all the samples produce statistically similar results. This is not the case for acidic and neutral environments; in these two environments, HN-GNFs are consistently the catalyst showing the smallest activity. In the acidic environment, the addition of iron in the Fe-Medium catalyst lead to a shift of 0.31 V in the onset potential and an increase of 148% in the current density of the HN-GNFs. This RDE study shows that adding iron to the HN-

GNFs greatly improves the catalytic performance if the desired application is for acidic or neutral environments.

There are two hypothesis on the role of transition metals in nitrogen-carbon catalysts: the first is that the transition metal participates as a metal/nitrogen species on pyridinic edge sites and the four-electron electroreduction of oxygen to water [128], while the second is that the presence of the metal creates a promotion effect on the formation of carbon-nitrogen moieties that have intrinsic active sites [38]. Additional experiments are needed to better understand and tune the desired level of the iron as the RDE results indicate that iron does increase activity, but there is a limiting concentration above which performance will start to decrease [129]. The iron content of around 4 weight percent seems to be near an optimal point for the HN-GNFs, but further investigation is needed to find the exact concentration.

For comparison purposes, a platinum catalyst (40 weight percent platinum on Vulcan XC 72) tested in-house produced an onset potential of 0.80 V and a current density of 7.81 mA cm^{-2} in the same acidic environment. The Fe-Medium catalyst achieves half the current density of this platinum catalyst with only one tenth the loading. Additionally, when considering only the cost of the active metal component, the cost of platinum is more than 450 times the cost of iron. Fe-Medium is clearly the most active of the produced iron catalysts in this study and is a viable catalyst for the ORR in PEMFC applications when considering cost effective alternatives to platinum, but its overall activity still needs to be improved in order to completely replace a platinum catalyst.

5.5 Conclusions

The wet-chemical iron incorporation method is modified to control the iron weight percent in HN-GNFs and non-noble catalysts with varying iron contents are synthesized for the ORR. Iron in the form of nanoparticles is observed to be encapsulated by graphene sheets. This results in having only a small fraction of the iron detectable on the surface using XPS techniques. A bulk analysis technique such as NAA is therefore critical in differentiating samples based on their iron content. TEM proves to be beneficial in visualizing the iron nanoparticles deposition, whereas SEM shows no structural difference between untreated and iron-containing HN-GNFs. The addition of iron improves the catalytic activity of HN-GNFs towards the ORR in the cases of acidic and neutral environments, seen primarily as an increase in the onset potential, half-wave potential, and current density. This study shows that the amount of iron that should be added to the catalyst during the synthesis process to maximize catalytic activity is around 4 weight percent. Untreated HN-GNFs, already having very good activity in alkaline environments, do not display any noticeable improvement with the addition of iron. This result indicates that the main application of iron and HN-GNFs based catalysts should be towards PEMFCs and not alkaline fuel cells. Studies moving away from RDE electrochemical tests and towards the PEMFC with the iron HN-GNFs catalysts are ongoing.

Acknowledgments

The authors would like to acknowledge the funding contributions of the *Fonds de Recherche Nature et Technologie du Québec* (FRNTQ) and the *Natural Science and Engineering Research Council* (NSERC) of Canada. Additionally, the authors acknowledge Dr. Cornelia

Chilian at École Polytechnique de Montréal for her help with NAA, Dr. David Liu for TEM services, and Jasmin de Campos and Ulrich Legrand for useful discussions.

Chapter 6: Performance of Iron Catalyst Supported on Nitrogen Functionalized Graphene Nanoflakes for the Oxygen Reduction Reaction in Polymer Electrolyte Membrane Fuel Cells

6.1 Preface

This chapter presents a submitted article that has the current citation:

> P.-A. Pascone, J.-L. Meunier, and D. Berk, *Performance of iron catalyst supported on nitrogen functionalized graphene nanoflakes for the oxygen reduction reaction in polymer electrolyte membrane fuel cells*, submitted to Applied Catalysis B: Environmental, (2018).

P.-A. Pascone (the Ph.D. candidate) was responsible for the planning of experiments, the preparation of catalyst inks and MEAs, the commissioning of the fuel cell testing station, performing the experimental work, and writing the article. J.-L. Meunier and D. Berk supervised the work and reviewed the manuscript.

Testing catalysts in a polymer electrolyte membrane fuel cell (PEMFC) is a more involved and advanced experiment than a study in an electrochemical cell and provides the true catalytic performance for this application. Membrane electrode assemblies (MEAs) were prepared with the catalysts presented in Chapter 5 on the cathode side and a commercial platinum catalyst on the anode side. The article contains the PEMFC results of these MEAs and comments on the current density and power density at varying voltages. A primary concern for novel iron-containing catalysts is the stability within the PEMFC environment. To study this and demonstrate the stability of the catalysts in this work, a 200-hour stability test (where the current density at an applied voltage is measured over time) was performed.

Performance of Iron Catalyst Supported on Nitrogen Functionalized Graphene Nanoflakes for the Oxygen Reduction Reaction in Polymer Electrolyte Membrane Fuel Cells

Authors: Pierre-Alexandre Pascone[a], Jean-Luc Meunier[a], Dimitrios Berk[a]

Affiliations: a: Plasma Processing Laboratory (PPL), McGill University, Chemical Engineering, 3610 University Street, Montréal, Québec, H3A 0C5, Canada

Abstract: A non-noble metal catalyst for the oxygen reduction reaction of a polymer electrolyte membrane fuel cell (PEMFC) was synthesized by the heat treatment of a mixture of iron acetate and a nitrogen functionalized carbon support system as a cost-effective alternative to platinum. The carbon nanomaterial used in this work is classified as stacked graphene and is produced through homogeneous nucleation from the gas phase using a thermal plasma system with a nitrogen source introduced during the plasma process. The amount of iron introduced is varied to produce three different samples that are all tested in a hydrogen/oxygen PEMFC. Membrane electrode assemblies (MEAs) with platinum on the anode side and the novel catalysts on the cathode side were fabricated and the activity (current density at an applied voltage) and power density values obtained were about 10% that of the MEAs fabricated with platinum on both sides. When the results are normalized with respect to the mass of metal present in the catalysts, the performance is about 37% that of platinum. The catalyst stability over time at an applied voltage of 0.3 V was very high, showing only a small drop of 3% of beginning-of-life activity after 200 hours of PEMFC operation.

Keywords: catalyst; iron; graphene; oxygen reduction reaction; PEMFC

6.2 Introduction

The polymer electrolyte membrane fuel cell (PEMFC) is a leading candidate as an alternative energy source to the internal combustion engine. These are highly efficient in converting chemical energy to electrical energy and are environmentally friendly as their by-product being water. The basic principle of the PEMFC is the reverse hydrolysis of water, where hydrogen is oxidized at the anode and oxygen is reduced at the cathode. For each electrode, a catalyst is employed to accelerate each reaction. When comparing the two reactions of the PEMFC, the oxygen reduction reaction (ORR) is approximately 5 orders of magnitude slower than the hydrogen oxidation reaction [15]. For this reason, the primary focus of recent research for the PEMFC catalyst is towards the ORR.

Chemically, the best catalyst is platinum typically deposited as nanoparticles on a carbon support [130]. Platinum is a commodity as it experiences diseconomies of scale, meaning that scale-up to mass production quantities would not decrease its cost [131]; this absence of a reasonably priced catalyst is one of the most significant reasons why PEMFCs have not yet reached worldwide commercialization. For this reason, there has been a major drive at the research level to develop a replacement for platinum; these catalysts are referred to as non-noble or non-precious metal catalysts. There are numerous catalysts being developed with some of the most promising catalysts having their active site formed of a transition metal such as cobalt or iron on carbon containing nitrogen [116,121,122]. Recent research showed non-precious metal catalysts performing very comparably to commercial platinum catalysts in terms of the current density that can be achieved, but with inadequate stability [38].

In this work, an iron salt is incorporated to stacked graphene nanostructures (GNFs) with added nitrogen functionalized groups in order to produce a non-precious metal catalyst. These catalysts previously characterized and studied for catalytic activity with a rotating disk electrode [132], are now used in a PEMFC environment to determine their level of activity and stability. Activity here refers to the current density drawn at a given applied voltage whereas stability refers to the ability to maintain a current density at an applied voltage over a length of time. Catalysts are compared to one another, to platinum, and to other non-precious metal catalysts in the literature.

The iron content of these samples was previously analyzed and characterized in a previous study [132]. The aim of incorporating iron into the GNF structure is to form active sites on the surface of the catalyst, but surface analysis showed that even at elevated iron incorporation levels the surface functionalization is effectively the same. It was also shown that the iron, present as nanoparticles, was primarily not on the surface of the catalyst, but instead encapsulated by the graphene sheets (Figure 35). Additionally, the overall weight percent of each sample was determined through the use of neutron activation analysis (NAA), providing a very accurate knowledge of the encapsulated iron loading decorating the GNF, particularly in comparison with surface analysis tools such as x-ray photoelectron spectroscopy (XPS). Added to these results are the GNF characteristics providing an exceptional crystallinity when compared to typical graphene oxide or reduced graphene oxide. Higher levels of carbon support crystallinity typically results in improved stability of the ORR catalyst layer [32,104]. The GNF structure is also providing a powder-like morphology with the 2-dimensional sheets having typically 100 nm scale lengths which tend to open the catalyst layer for good mass transfer to the catalytic sites. Following the above and the apparent advantages of these iron/nitrogen/GNF catalyst structures, the objective of the present paper is to effectively test the activity and stability of this catalyst in an actual PEMFC environment, and compare with a platinum-based ORR catalyst tested under similar conditions.

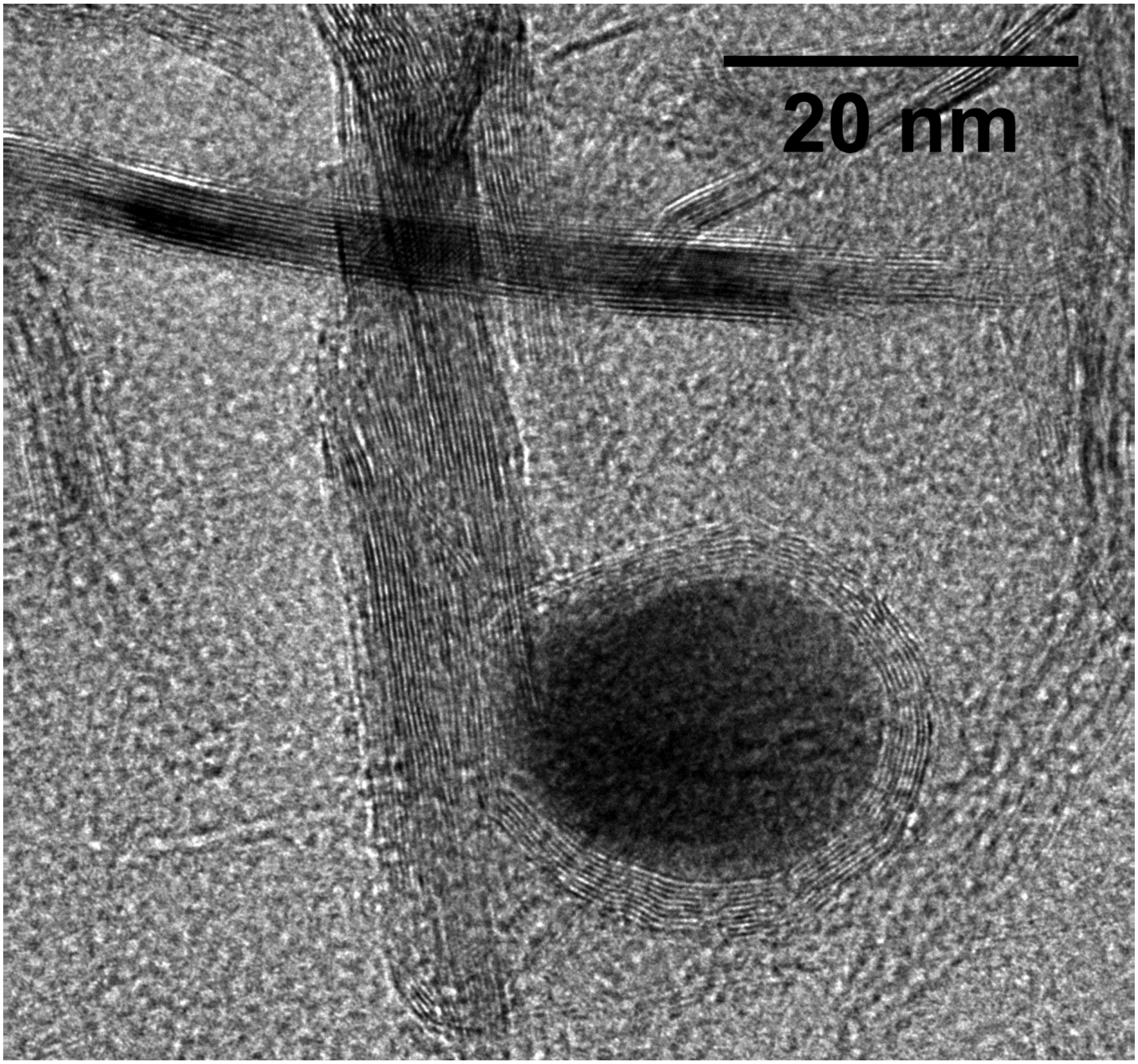

Figure 35. Transmission electron microscope micrograph of an iron nanoparticle encapsulated with stacked graphene sheets and decorating a graphene nano-flake support. Image adapted from [132]**.**

6.3 Experimental materials and methods

6.3.1 Catalyst synthesis

The iron-based catalysts in this study were produced by synthesizing graphene nanoflakes with a high amount of nitrogen functionalized to the surface (15 to 25 atomic percent) and then introducing an iron salt. Graphene nanoflakes (GNFs) were grown by high temperature gas phase homogeneous nucleation following the thermal plasma decomposition of a carbon-containing feedstock, methane in this case [54]. The plasma setup was composed of an inductively coupled thermal plasma torch (ICP-TP; TEKNA PL-35 model), a radio frequency generator (Lepel; 60 kW power/2-5 MHz frequencies), and a custom built conical water-cooled reactor with a length of 50 cm and a full angle expansion of 14°. The geometry of the conical reactor allows a gradual gas expansion that minimizes recirculation areas, provides a 2-dimensional (2D) symmetrical flow pattern within the reactor chamber, and sets the temperature, flow, and particle nucleation fields for a control of the 2D evolution of the nucleated crystalline carbon nanoparticles [55]. A confinement tube in which the plasma is generated is inserted on the inside of a three to four turns water-cooled copper induction coil. The RF magnetic field generated in the central gas induces currents heating up the gas and creating a thermal plasma in a typical temperature range around 10,000 K (~1eV). There are three gas ports to the ICP-TP torch system: central, sheath, and injection. The injection probe is inserted into the torch so that the tip of the probe is just below the first copper coil turn; this ensures that injection occurs in the core of the plasma.

The very pure and highly crystalline graphene-based powders having mean sizes of 100 nm lateral lengths and 10 atomic layer thicknesses are generated by a 3-step process. In the first step, an argon thermal plasma is produced. Following plasma ignition, the pressure is increased and methane and nitrogen are directed to the gas injection port; this is the step where the GNFs are grown, the nitrogen providing a relatively low amount of functionalities to levels of around 2 atomic percent of nitrogen as measured on the surface of the GNF structures [54], forming low nitrogen GNFs (LN-GNFs). The last step corresponds to a substantial increase in the amount of nitrogen functionalities taking place at a lower pressure and a higher power of the downstream recombining plasma environment. In this step the sheath flow gas is changed from argon to nitrogen gas, the flow of methane is stopped, and the amount of nitrogen directed to the injection gas port is increased. This leads to high nitrogen levels on the surface of the GNFs (HN-GNFs) reaching between 15 and 25 atomic percent. The entire procedure with specific operating parameters is described in detail in Pascone *et al.* [124].

Iron incorporation occurs in a separate step by introducing iron acetate salt (Sigma-Aldrich; Iron (II) acetate, 95%) in various amounts to the HN-GNF powders and mixing in an equal parts ethanol/water solution; the amount of iron salt was varied to produce samples with different iron contents. The mixture is ultrasonically dispersed for 1 hour, and then dried in an oven before finally being pyrolyzed in argon at a temperature of 700°C for 1 hour. The three samples in this study are labelled with respect to their iron weight percent, as analyzed by NAA, and are presented in Table 9. The atomic percent of iron on the surface of the catalysts, as measured by XPS, is also presented in Table 9.

Table 9. Sample identification with respect to iron composition

Sample Name	Iron Bulk Content [Weight Percent]	Iron Surface Content [Atomic Percent]
Fe-Low	1.25	0.46
Fe-Medium	3.77	0.52
Fe-High	18.03	0.39

6.3.2 Preparation of catalyst inks

For the preparation of the anode catalyst inks, 40% platinum on Vulcan carbon black powder (FuelCellsEtc) was used with a Nafion^{TM}-to-platinum ratio of 0.8 (which leads to a Nafion^{TM} mass content of 24.24%). The cathode catalyst inks used in this work were prepared with the iron containing HN-GNFs and the same Nafion^{TM} mass content of 24.24%. The source of Nafion^{TM} was from a 5 wt% Nafion^{TM} perfluorinated resin solution in lower aliphatic alcohols and water containing 15-20% water (Sigma-Aldrich), with a density of 0.874 g mL^{-1} at room temperature. All inks had a concentration of 1 mg of HN-GNFs per 150 μL with an ethanol content of 92% by volume, the rest of the volume coming from deionized water and the Nafion^{TM} solution. A normalized batch of this ink would be 20 mg of catalyst, 2 760 μL of ethanol, 146.45 μL of Nafion^{TM} 5 wt% solution, and 93.55 μL of deionized water; this batch size fitting nicely in a 1 US fluid dram vial (~3.7 ml). All inks were ultrasonically dispersed for 2 hours before being used on the electrodes.

6.3.3 Preparation of membrane electrode assemblies

The catalyst-coated substrate (CCS) method was used to fabricate the membrane electrode assemblies (MEAs) [10]. Gas diffusion electrodes (GDEs) were prepared by depositing the catalyst ink onto a 5 cm^2 square piece of the gas diffusion layer (Toray carbon paper with 20% wet proofing and a micro-porous layer, TGP 090 20%, MPL). The GDEs were dried in an oven at 80°C and weighed afterwards to verify deposition amounts. All cathodes containing the catalysts had a concentration of 4 mg catalyst per cm^2 of active area, whereas the platinum-containing anode GDEs had a concentration of 1.25 mg of catalyst in order to achieve a platinum concentration of 0.5 mg per cm^2 of active area; this platinum amount was chosen to guarantee a non-limiting anode reaction and eliminate any effect on the kinetics of the electrochemical reaction [133,134].

The final MEAs were prepared by hot-pressing GDEs on both sides of a Nafion^{TM} membrane (Nafion^{TM} 115 with a thickness of 127 µm) at a temperature of 120°C, around its glass transition temperature [135]. The MEA was placed in between two sheets of Kapton and copper plates and pressed at approximately 5 860 kPa for 2 minutes. Before being used, all membranes were pretreated. Membranes were purchased from an external supplier (Fuel Cell Store) and may contain impurities or may not be fully protonated, which can hinder the fuel cell's performance. All membranes were exposed to a boiling solution of 3 weight percent hydrogen peroxide for an hour to remove impurities, followed by a boiling solution of 1.2 M sulfuric acid solution to protonate the membrane, and finally one hour of boiling water to rinse the membrane [7].

6.3.4 Fuel cell testing

All PEMFC experiments were carried out in a University Test Station (Fuel Cell Technologies) with a DC electronic load module (0-60 V, 60A, 300 W, Agilent Technologies). The fuel cell has a 5 cm^2 active area and includes gold plated copper current collectors and Poco graphite blocks with machined serpentine grooves. All gas flows, temperatures, voltage and current readings were controlled/monitored by a custom-built Labview software (Fuel Cell

Technologies), while the back pressures were controlled by a manual back-pressure regulator. Teflon coated fiberglass tape gaskets were used to achieve a compression of 11.4% on the MEA.

For gas compositions, the purity of the hydrogen gas was of quality 4.0, the oxidant gas was oxygen and the fuel cell had a co-flow configuration. A fixed-flow-rate condition [136] was used, where the flow rates were held constant during the entire test at a flow rate that was sufficiently high so that even at the largest current densities there was a sufficient supply of both gases, instead of fixed-stoichiometry flows. For activity studies, the flow rates were 56 and 42 sccm for hydrogen and oxygen, respectively. For stability tests, a flow rate of 200 sccm was used for both gases. For the fuel inlet pressures, the back pressure was controlled to maintain a constant pressure and minimize pressure changes related to fluctuations caused by the gas flow and pressure drop. The anode had an absolute pressure of 200 kPa, a typical value in automotive applications that ensures a high power density, while the cathode had an absolute pressure of 190 kPa to facilitate mass transfer and have proper water management [76]. The cell temperature was 80°C and measured at the centre point of the cathode monopolar plate of the cell, with the temperature maintained by 2 cartridge heaters covered with a heat-conducting coating (Milk of Magnesia). Both fuel gas inlet temperatures were kept 5°C above the operating temperature of the cell to prevent water condensation at the cell inlet. A nominal value of relative humidity corresponding to 100% with respect to the cell temperature was used for both gases. Temperatures for the humidity vessels were calculated by Antoine's empirical equation (Equation 8, Equation 9, and Equation 10) where the temperature variables are in Celsius and pressure variables are in Pascals [137]. Therefore, at a cell temperature of 80°C, the temperature for both humidity vessels was also set at 80°C.

$$Log\ (p_{vap\ sat}) = 10.196213 - \frac{1732.7549}{T_{cell} + 233.426}$$

Equation 8. Vapour pressure of water in saturated gas

$$Log\ (p_{vap}) = 10.196213 - \frac{1732.7549}{T_{dew} + 233.426}$$

Equation 9. Vapour pressure of water in gas

$$Relative\ Humidity = 100 * \frac{p_{vap}}{p_{vap\ sat}}$$

Equation 10. Relative humidity of gas

All MEAs were humidified and then “broken-in” for three hours to obtain steady state behaviour. For activity tests, polarization curves were obtained by scanning the cell voltage from the open circuit voltage down to 0.25 volts; tests continued until no change was detected between subsequent runs. For stability tests, the cell voltage was held for 200 hours and the current was recorded.

6.4 Results and discussion

6.4.1 Catalyst activity

The polarization curves of the three iron samples are shown in Figure 36 and their corresponding power densities in Figure 37. The activities of the three iron samples are very similar and within the same margin of error, with Fe-Medium showing slightly higher current density values for voltages lower than 0.4V. This result is expected as the current density is linked to the amount of active sites on the surface. It is not possible to quantify the exact amount of sites being active in the PEMFC environment. This number is however related to the total amount of iron available on the surface as reported in Table 9, with the three samples showing very similar levels of iron functionalization but Fe-Medium having slightly more iron than Fe-Low and Fe-High. The max power density of the catalysts occurs in the 0.25 – 0.3 V range, which is lower than the typical value of 0.5 V that is common for platinum based catalysts. This difference comes from the lower overall activity and open circuit voltage of these catalysts. In terms of peak power density Fe-Medium has a value of 48.32 mA cm^{-2}, which is 5.5% and 13% better than Fe-High and Fe-Low respectively. The slightly better performance of Fe-Medium compared to the other prepared catalysts matches perfectly with our previously reported work on rotating disk electrodes in acidic media [132].

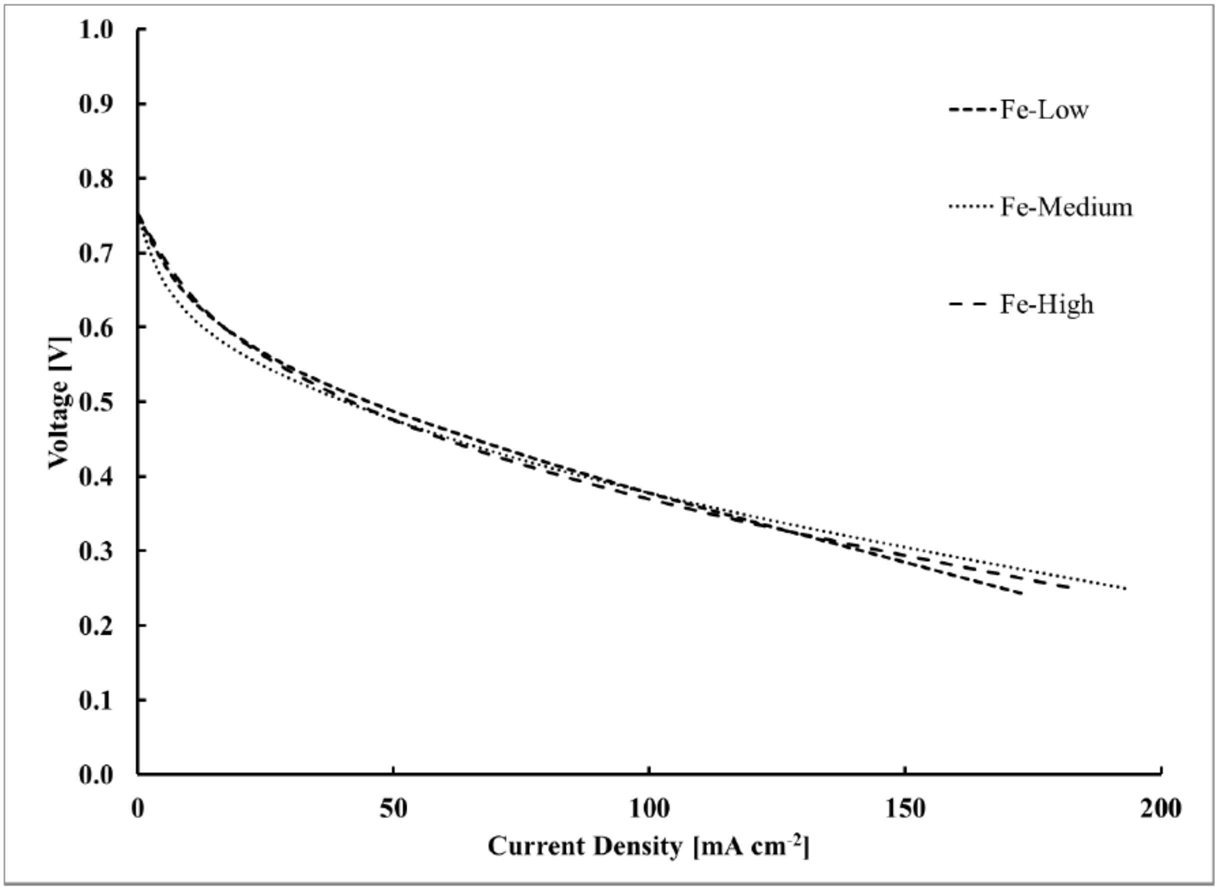

Figure 36. Polarization curves of MEAs produced with iron-containing HN-GNF catalysts on the cathode and platinum on the anode

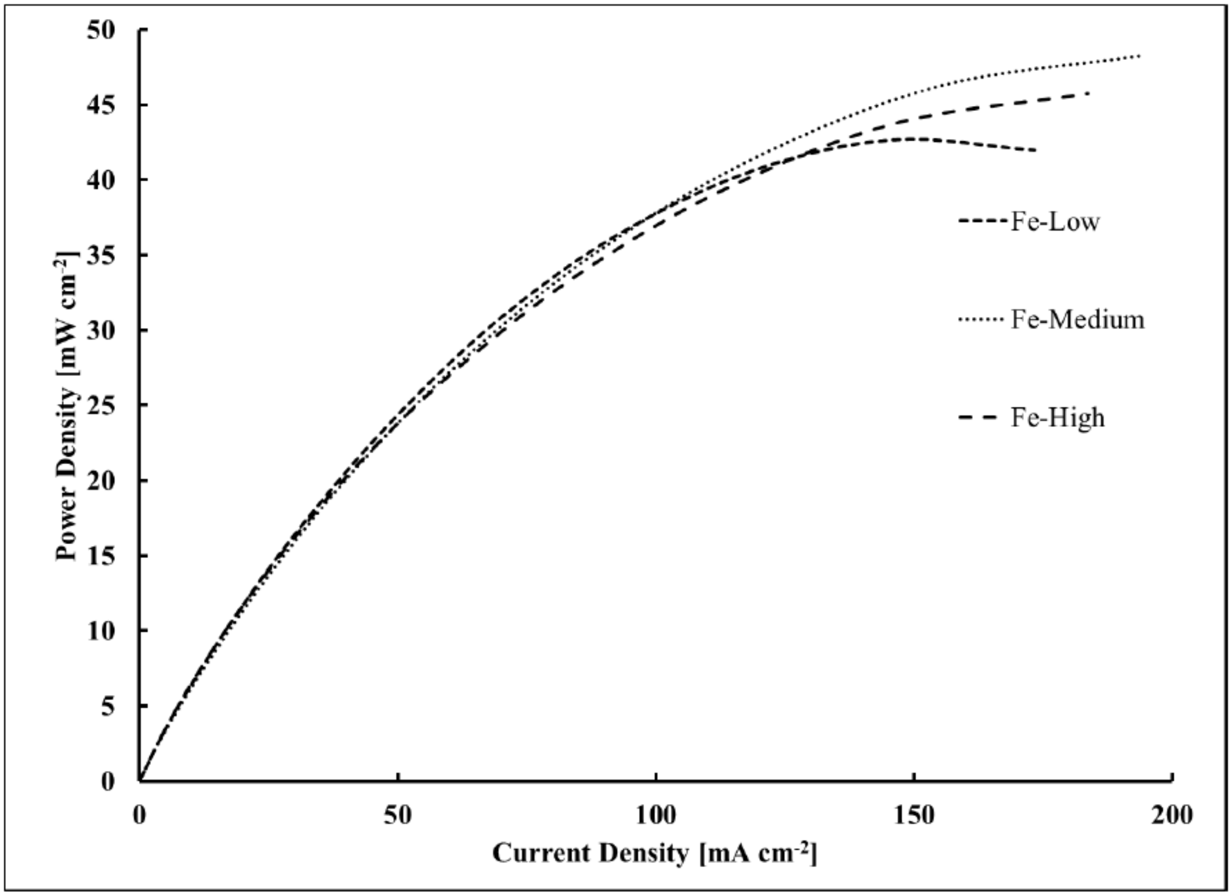

Figure 37. Power density curves of produced MEAs

The low activity of the catalysts is mostly attributed to the low concentration of active sites on the surface as the iron in the catalysts is predominantly coated within the graphene sheets. The cell performance was relatively low compared to what can be found in the literature for the most active non-noble metal catalysts where current densities of 1 000 mA cm^{-2} and greater at a voltage of 0.5 V is regularly being obtained [138–140]. This was expected from some of the inherent drawbacks of the present study, such as using the CCS method for making the MEAs and not using the thinnest membrane available. Additionally, the MPL, the hot press conditions, and the Nafion^{TM} content in the ink are not optimized as the optimization of any of these parameters requires its own independent study when working with a novel material such as the catalysts produced in this work.

Nonetheless, these activity results do match closely other novel iron-based catalysts from various research groups. As summarized by Dicks *et al.*[141], Liu *et al.*[142] used a template-assisted ultrasonic spray pyrolysis method to synthesize a non-precious metal electroconductive polymer of iron polypyrrole mesoporous spheres. When tested in a PEMFC with hydrogen and air, they reported a current density of ~ 60 mA cm^{-2} at a voltage of 0.5 V. However, no information was given to any of the testing parameters to be able to directly compare the results (i.e. gas flow rates, temperatures, humidity, back pressure, MPL composition, anode catalyst composition, MEA preparation technique, catalyst loading, or membrane thickness). Wei *et al.* [143] produced an ORR catalyst of iron supported on nitrogen-doped carbon aerogels. When used as the cathode catalyst of a direct methanol fuel cell, the current density at 0.5 volts was ~10 mA cm^{-2}. A.H.A. Monteverde Videla *et al.* [144] presented a catalyst made by impregnating iron acetate coordinated with TPTZ as their nitrogen source onto a carbon nano-network that was synthesized by the chemical vapor deposition of ethane over cobalt nanoparticles. Their catalyst produced a current density of ~ 80 mA cm^{-2} at 0.5 Volts.

The comparison of the results of different studies of PEMFCs described in the literature has to be done with great caution because each study is carried out using different operating conditions and preparation techniques, with each of them having an effect on the performance of the cell, thereby making it challenging to determine if the catalyst is the cause. In order to eliminate this in the present study, an MEA with the platinum catalyst on both the cathode and anode was prepared and tested with the same operating conditions as the iron catalyst (Figure

38). For the platinum catalyst, the max power density was in the expected voltage range. Using this polarization curve for comparison, the current density of the iron catalyst is 9.25% that of platinum at 0.4 V and the max power density is 11.84% that of platinum.

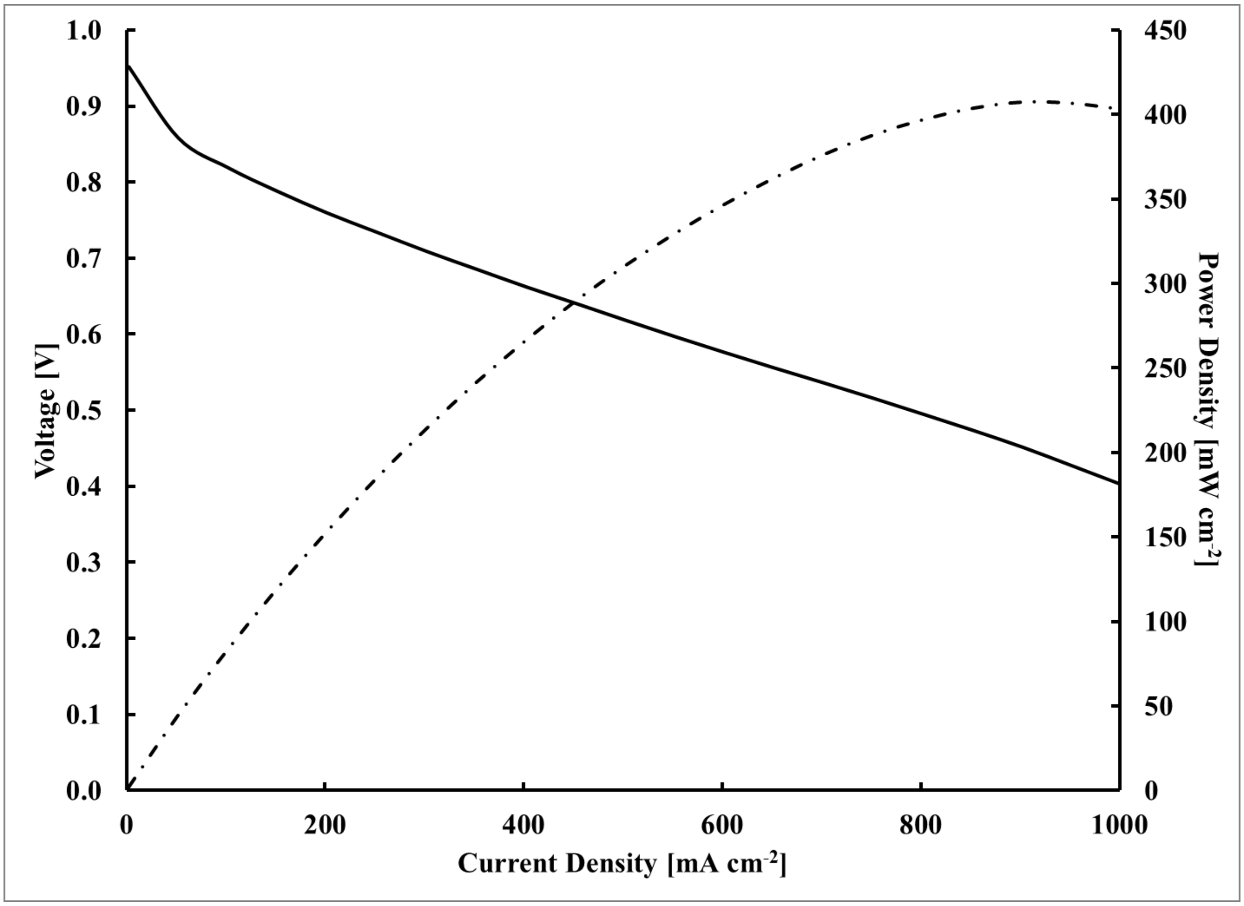

Figure 38. Polarization (–) and power density (--) curves of Platinum catalyst MEAs

A comparison of the catalytic performance for the ORR between the iron catalysts in the present study and platinum is through a normalization of the activity values with respect to their metallic mass contents. Using the NAA results, the current density at an applied voltage of 0.4 V is normalized with respect to the amount of iron and presented in Table 10. Recalling that the catalysts all produced relatively similar current density values per cm^2, the result of Fe-Low normalized to the mass of iron is impressively high because of the low amount of iron present within its bulk structure. When compared to the platinum catalyst where the mass of platinum is considered, the performance of Fe-Low is now up to 92.5% of platinum. It should be noted however that the loading of platinum was exceptionally high in the present study (0.5 mg cm^{-2}) and that a similar current density value could be achieved by Gasteiger *et al.* with a loading of around 0.2 mg of platinum [133], leading in this last case to a Fe-Low performance at 37% that of platinum. The normalized current density shows that the introduction of iron at elevated concentration levels does not boost the performance of the catalyst. In other words, the current density that can be drawn from a given GDE with these catalysts is not scalable with respect to their iron mass. The absolute currents measured in this study for the catalysts are still relatively low because of the lack of iron on the surface, which further corroborates previous work concluding that although iron is present within the graphene-nitrogen framework, the majority of the iron is not expected to be bonded with nitrogen and forming active sites dispersed at the atomic level for the oxygen reduction reaction [124,132,145,146]. It is clear however that following the values from Table 10, cost considerations make the iron-based catalyst an extremely attractive alternative to platinum, provided that the catalyst stability is maintained over long enough time periods.

Table 10. Normalized current density

Sample Name	**Current Density [mA cm^{-2} mg^{-1}]**
Fe-Low	1 855
Fe-Medium	585
Fe-High	117
Platinum	2 006

6.4.2 Catalyst stability

After performing the polarization curves for the iron catalysts, Fe-Medium was selected to carry out a stability test where the current density was recorded every 10 seconds at an applied voltage of 0.3 V for 200 hours (Figure 39). After the 200-hour time period, the current density was at 96.8% of its value at the beginning of the test. This result is considered a major achievement in the field of non-precious metal catalysts, as only a handful of researchers have been able to synthesize stable catalysts [39,147]. The more common result in this field of study is a relatively low stability that is characterized by a rapid initial loss in activity (~ 20% loss in performance during the first 2 hours of operation) followed by a gradual decrease resulting in some cases in a total loss of activity [26,28,148]. The current density did fluctuate throughout the experimental run, dropping to a low of 86.6% of its starting value; however, these fluctuations match up perfectly with the small changes and deviations observed in the cell temperature, which proved difficult to control throughout the experiment (Figure 39).

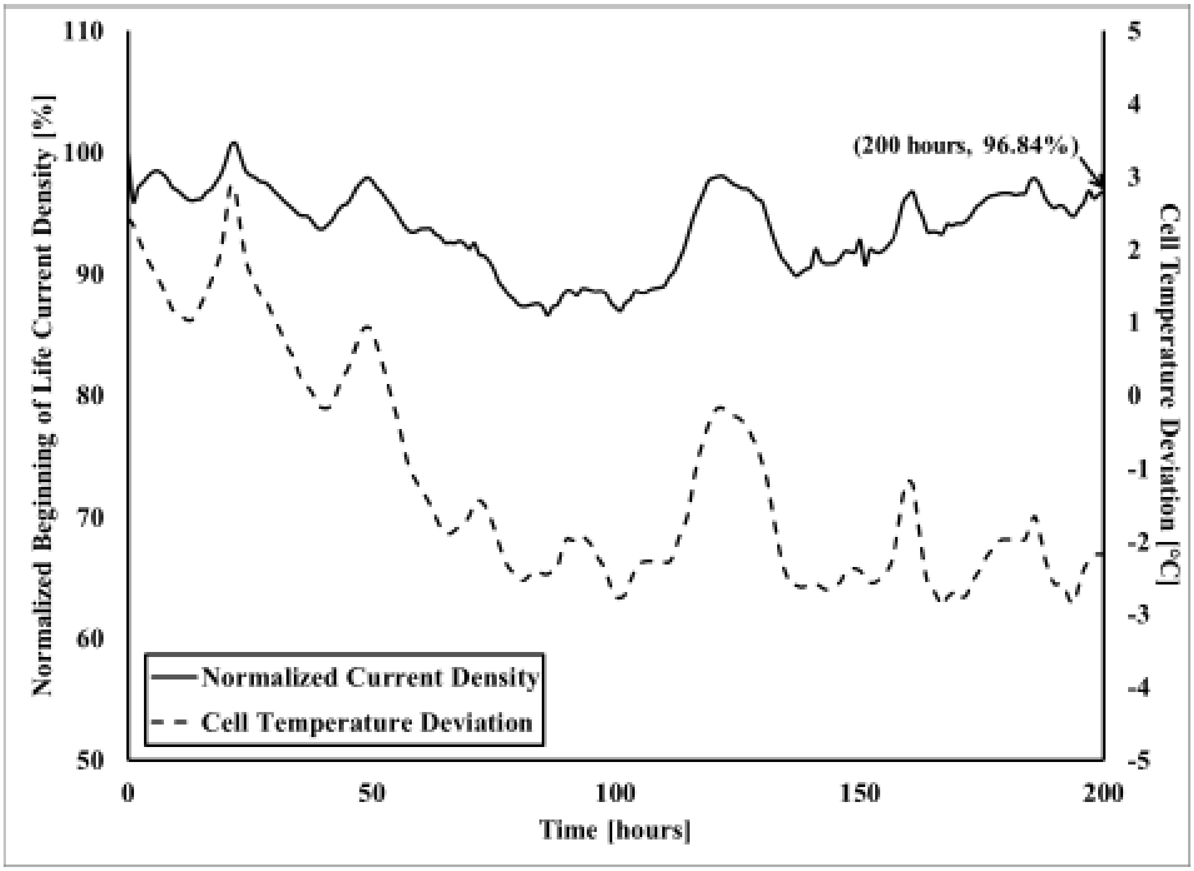

Figure 39. Time evolution of the normalized PEMFC current density and cell temperature deviations for Fe-Medium

Understanding the stability displayed in our iron-GNF catalysts is possible when considering instability mechanisms proposed in the literature. A common reported mechanism of instability is the leaching of the metal species [149,150]. In the present study, the graphene sheets probably form a protective layer that shields the metal from the acidic environment [39]; this hypothesis was already reported as a major finding in our previous study [132]. Another instability mechanism is the oxidative attack by hydrogen peroxide that is formed as a by-product during the reduction of oxygen [148]. The iron-GNF catalysts in this work have already been shown to be good catalysts for the reduction of hydrogen peroxide [105], making it all the more likely that this attack is not occurring.

6.5 Conclusions

Graphene nanoflakes with high amounts of nitrogen functionalization were synthesized by the plasma decomposition of methane and nitrogen and then exposed to an iron salt to obtain different iron weight percent. The unique non-precious metal catalysts were tested in a PEMFC to determine their suitability for the ORR. When compared to a commercial platinum catalyst that was prepared and evaluated in the exact same manner in order to eliminate the effect of all operational parameters and MEA preparation techniques, the iron catalysts generated achieve around 10% the performance of platinum. If the mass of metal present in the catalyst is further considered for normalizing the current density, the performance increases to 37% that of platinum. Most importantly, the produced catalyst shows remarkable stability as evidenced by its ability to maintain its current density after 200 hours in the PEMFC environment. This finding is uncommon for non-precious metal catalysts and confirms the interest in HN-GNFs as a catalyst support system for PEMFC catalysts. The nature of the stacked graphene provides the catalyst stability in the harsh PEMFC environment, but further adjustments to the iron-incorporation method must be done to increase the number of active sites for the ORR on the graphene surface and improve the activity.

Acknowledgments

The authors would like to acknowledge the funding contributions of the *Fonds de*

Recherche Nature et Technologie du Québec (FRNTQ) and the *Natural Science and Engineering Research Council* (NSERC) of Canada. Additionally, the authors would like to thank Dr. Lefèvre, Matthew Kok, and Mathew Evans for useful discussions, Dr. Gostick for providing advice and materials, and Dr. Maric for allowing access to the hot press machine.

Chapter 7: Fuel Cell Performance of other Graphene Nanoflakes Catalysts

7.1 Introduction

This chapter presents the polarization curves in the same fuel cell environment as in Chapter 6 for three additional graphene nanoflake-based catalysts of interest. The results of these experiments were not included in the manuscript presented in Chapter 6 as the catalysts either do not contain iron or were generated from the preliminary synthesis work at the basis of the present research project [4,104]. The three samples presented in this chapter are the GNF and HN-GNF structures generated from the plasma-based process without the iron addition step, and a GNF-based catalyst with iron incorporated using the thermo-mechanical treatment developed by Lefèvre *et al.*. Such an evaluation, together with the results of Chapter 6, is important to assess if the main contribution to the catalytic activity of these materials is effectively the iron or if the graphene support nanostructure with or without nitrogen also contributes substantially to the overall activity. Additionally, the improvement of the catalytic activity with regards to the new iron incorporation method can be determined.

7.2 Materials and methods

As indicated above, the GNF and HN-GNF powder structures are obtained directly from the plasma reactor with no further manipulation and integrated in the cathode catalyst ink to prepare a MEA. The third sample contains iron incorporated using the thermo-mechanical treatment described below and is labeled here as TM/Fe-GNF.

A batch of TM/Fe-GNF catalyst is made by first mixing 75 mL of water, 25 mL of ethanol, and 500 mg of phenanthroline in a beaker with a magnetic stir rod for 5 minutes. At this point, 32 mg of iron acetate is added and the solution is left to stir for an additional 5 minutes. After this time, 500 mg of GNF powders with low amounts (less than 2 atomic percent) of nitrogen functionalization on its surface is added and the solution stirred for an additional 2 hours. The beaker is then transferred to an oven and heated to 95°C for 24 hours, allowing the liquid to evaporate. The remaining solid sample is then collected off the beaker walls and inside a nitrogen glove box to minimize the presence of oxygen. The material is then placed in a 100 mL grinding jar and filled with 20 quarter-inch diameter chrome steel balls. The grinding jar is a component of a planetary ball miller, in which a grinding jar rotates on a stand in one direction while the main stand rotates in the opposite direction at a different speed. Ball milling occurs for three hours at a rotation velocity of 400 rpm. Following ball milling, a two-stage pyrolysis is performed on the catalyst: (1) 2 hours at 1 050°C in argon gas, followed by (2) 5 minutes at 950°C.

For all fuel cell experiments, the same materials and methods were used for the preparation of the MEA as described in chapter 6. The anode catalyst inks were made using 40% platinum on Vulcan carbon black powder (FuelCellsEtc) and catalyst inks made with GNF catalysts and a Nafion^{TM} mass content of 24.24% are used throughout this chapter. The MEAs are made using the CCS method on a gas diffusion layer (Toray carbon paper with 20% wet proofing and a micro-porous layer, TGP 090 20%, MPL) with Nafion 115 and hot pressed at 5 860 kPa for 2 minutes. The cathodes have a concentration of 4 mg/cm^2 of active area and the anodes have a concentration of 0.5 mg Platinum/cm^2. A university test station (Fuel Cell

Technologies) with a DC electronic load module (0-60 V, 60A, 300 W, Agilent Technologies) and a 5 cm^2 active area PEMFC was also used for all experiments. The fuel cell was operated at 80 °C with 100% relative humidity and absolute back pressures of 200 kPa and 190 kPa for the anode and cathode respectively.

7.3 Results and discussion

Figure 40 displays the polarization curves of the three samples with Figure 41 showing their corresponding power densities. Although the overall current density values obtained in these experiments are relatively low in all cases, a comparison of their performance reveals important differences. The performance of TM/Fe-GNF, an iron-containing catalyst, far surpasses the other two catalysts. As mentioned in Section 2.5, the literature indicates some catalysts are being developed that rely solely on carbon and nitrogen. The HN-GNF is actually showing here the lowest performance, being in fact slightly lower than non-functionalized GNFs. This result highlights the importance of iron inclusion within the structure to obtain some appreciable activity improvement towards the ORR and that GNFs and HN-GNFs are not active enough to be considered an alternative non-metal catalyst.

Recalling in Section 1.1, this doctorate project seeks to modify the iron incorporation method used to produce TM/Fe-GNF to improve the activity towards the ORR in a PEMFC. Therefore, the results of TM/Fe-GNF must be compared to the activity of the catalysts produced in Chapter 6 (Figure 36 and Figure 37). The new improved catalysts are almost 2.5 times higher than the performance observed here for the TM/Fe-GNF (16.92 mA cm^{-2} at 0.5 V (Figure 40), and a maximum power density of 18.93 mW cm^{-2} (Figure 41)). It seems that the thermo-mechanical treatment used by Lefèvre *et al.* on porous carbon black particles for generating a very active catalyst, but with low stability, does not generate a similarly high activity when used with GNFs. The stability of GNF-based catalysts remained, whether with the new iron incorporation method or the thermo-mechanical treatment, as evidenced in my master's work where a 100-hour study was performed [4,104].

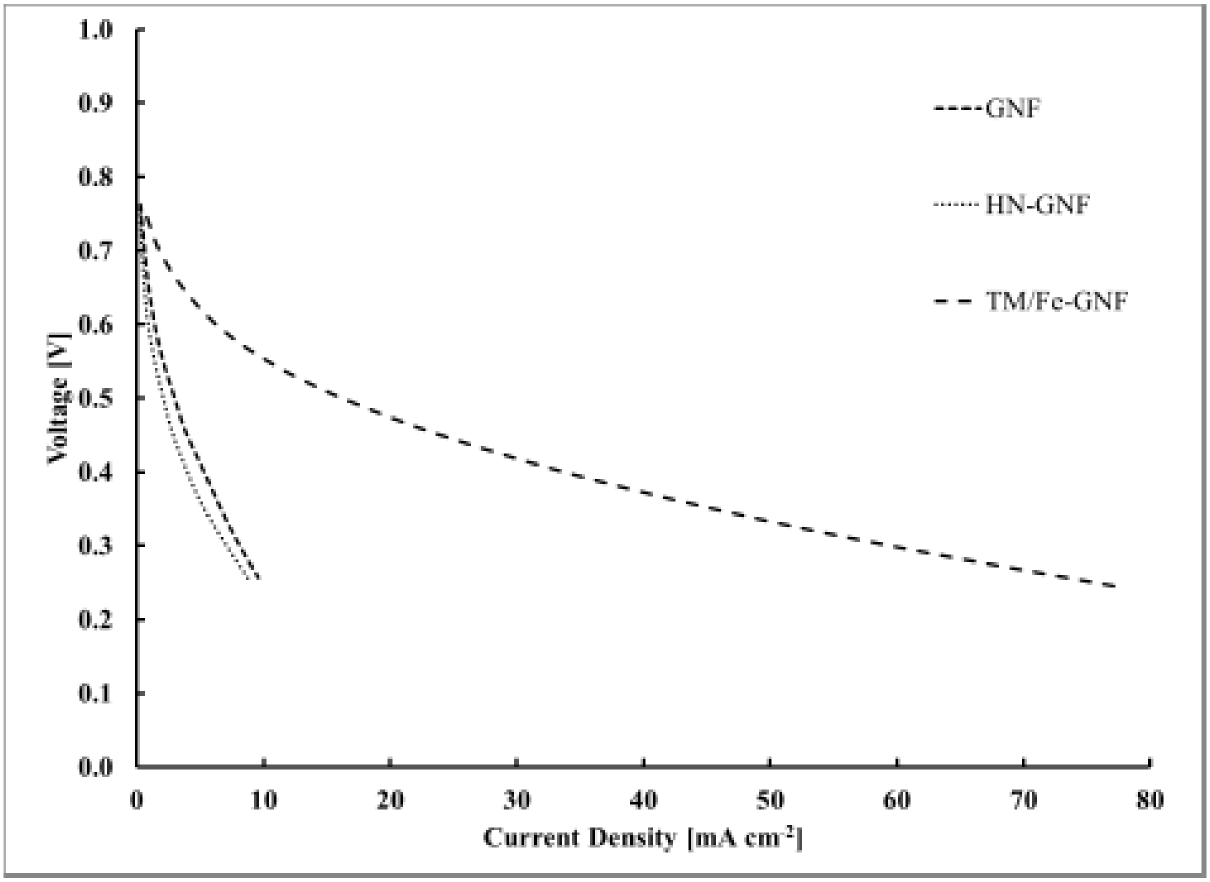

Figure 40. Polarization curves of MEAs produced with GNF-containing catalysts on the cathode and platinum on the anode

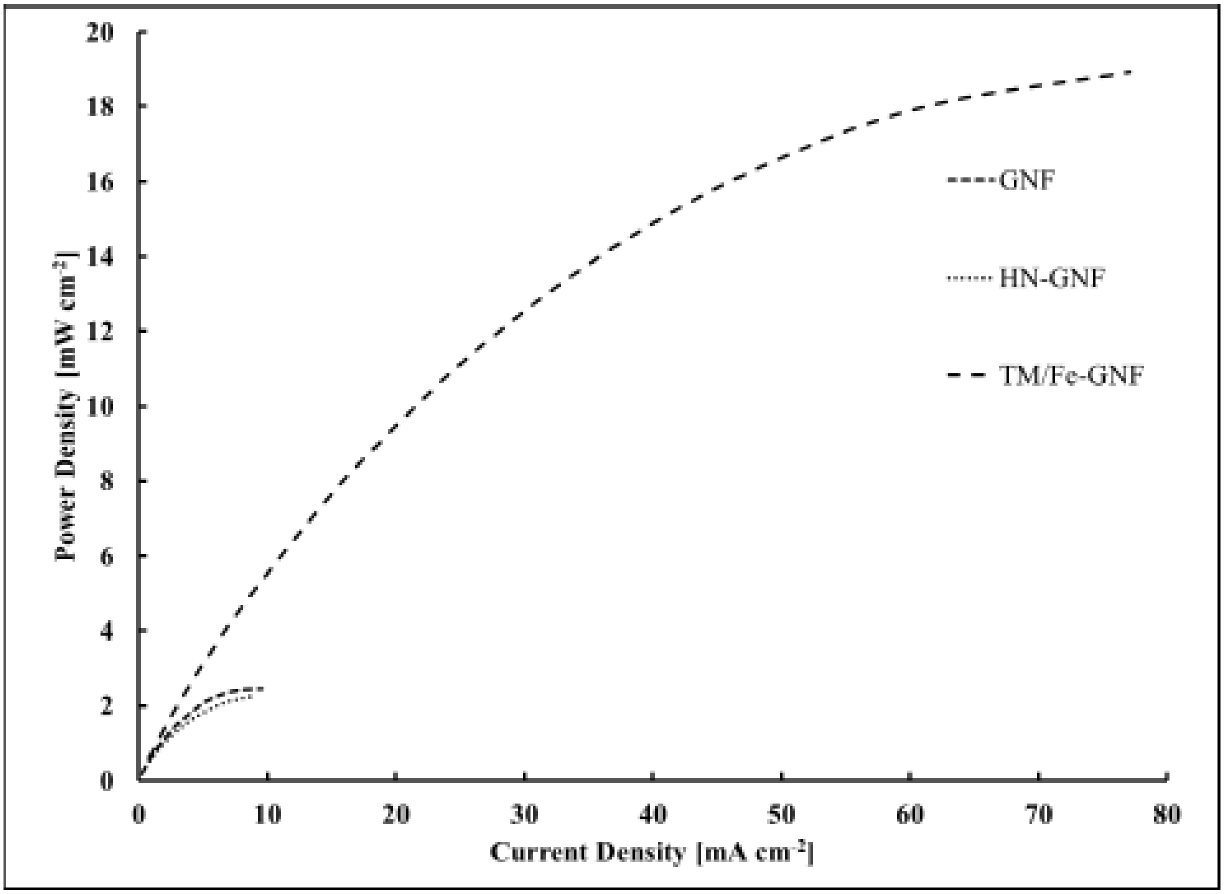

Figure 41. Power density of MEAs produced with GNF-containing catalysts on the cathode and platinum on the anode

Chapter 8: Conclusions

8.1 Summary

This doctoral work was aimed at developing and investigating the material and catalytic properties of a non-noble metal catalyst alternative to platinum for the ORR of a PEMFC. The catalyst was synthesized from a unique nanomaterial, stacked graphene with nitrogen groups functionalized to its surface and edges that is referred to as GNFs, as a carbon support system with a built-in nitrogen source as a catalyst component. The GNFs were produced in-house by the plasma decomposition of a carbon-containing feedstock using an inductively coupled plasma torch with a conical water-cooled reactor. This nanomaterial was then mixed with an iron salt and heat-treated to obtain the final catalyst structure. The final nitrogen composition, particularly the pyridinic content, of the catalyst has a tremendous effect on catalyst activity and was found to be a result of the iron incorporation method, the nitrogen functionalization during GNF growth, and the presence or absence of an additional nitrogen source. Obtaining pyridinic nitrogen is best achieved by first exposing the GNFs to nitrogen plasma in order to create active nitrogen species that react and create primary bonds with the GNF structure. This enables the generation of a large and tunable level of nitrogen functional groups on the surface. Following this nitrogen addition step, pyrolysis essentially removes the nitrogen that is either attached to amorphous carbon or weakly bonded to the GNF structures.

Iron was mainly found to be incorporated as nanoparticles within the GNF structure. This does not exclude the possibility that some atomic iron might also be inserted in the structure through a 4 to 6 nitrogen atom coordination, creating atomically dispersed catalytic sites as envisioned in the literature. If this is the case however, the level of atomic nitrogen coordination is very small and could not be detected on the surface or edges of the GNF, even at increased concentration levels. The problem of both the difficulty of detection of such sites and of separation of these from the catalytic activity generated by the iron nanoparticles still arises. The amount of iron on the surface is low and close to the detection limits of XPS, meaning that a specific iron to nitrogen bond cannot necessarily be assigned, which is an all too common problem in this field of research. The final produced catalysts are however successful in increasing the inherent catalytic properties compared to the iron-free GNFs in acidic and neutral media. When evaluated in a PEMFC environment, the activity of the catalysts is about 10% that of a platinum catalyst produced with the same MEA fabrication methodology and shows relative stability over at least 200 hour of PEMFC operation. With the cost of iron being in the vicinity of less than 10^{-5} the cost of platinum and graphene materials being only about 10^{2} the cost of carbon blacks, the catalyst can indeed be a cost-efficient alternative to platinum, but the overall performance must still be improved.

8.2 Original contributions

The contributions to the field of non-noble metal catalysts from this work are:

1) The synthesis and optimization of a non-noble metal catalyst for the ORR using stacked graphene composed of 5 to 20 single graphene sheets as the carbon support system for iron nanoparticles.
2) The development of a synthesis route to obtain a high amount of nitrogen in the pyridinic state on the catalyst surface.

3) The experimental demonstration that an iron-based catalyst can be both stable and active in a PEMFC environment and that this stability arises mainly from a change of the carbon support structure towards the strongly reduced defect concentration of the graphene nanosheets.

8.3 Recommendations for future work

The work in this project was on the development and study of stacked-graphene as a carbon support system for iron catalysts, but much more can be done with this material for the present application. The recommendations for future work are:

1) The current method for producing HN-GNFs requires the already grown GNFs to be exposed to nitrogen plasma, resulting in nitrogen levels of 15 to 25 atomic percent on the surface. The pyrolysis step of the catalyst synthesis then diminishes this amount to levels in the 3 to 6 atomic percent range, but with an increased level of nitrogen in the pyridinic state as the nitrogen attached to amorphous carbon is being primarily removed. Ideally, the starting material for iron incorporation would be HN-GNFs with a nitrogen functionalization around 16.67 atomic percent (one sixth of all atoms and all the nitrogen in the pyridinic state). One way to develop this could be to perform multiple cycles of nitrogen functionalization and pyrolysis to see if this ideal scenario could be obtained. If nitrogen functionalization must be performed more than once, the current method should be altered as the post-treatment of powders is problematic in the conical plasma reactor. Therefore, performing the nitrogen functionalization step on a simpler plasma setup (i.e. a nitrogen corona discharge in a closed vessel at atmospheric pressure) could be explored

as an alternative. Another modification could be to have a reactor that doubles as a furnace so that losses between functionalization and pyrolysis can be minimized and everything accomplished in one setup. Having more nitrogen on the surface should lead to more iron and improved performance.

2) A challenge faced by many researchers in the field of non-noble metal catalysts is the inability to verify the presence of active catalyst sites and reconcile the placement of iron and nitrogen on the catalyst surface. Observation using synchrotron radiation would provide structural and chemical properties of the materials at the molecular level. This would allow imaging of iron and nitrogen atoms within the catalyst structure and the coupling of this data to the knowledge we have of the structures and concentrations from XPS, NAA, and electron microscopy.
3) The pyrolysis temperature and time should be optimized to the specific material of GNF. It was shown that temperatures over 900°C damaged the carbon material, thus the pyrolysis temperature used in this study was set to 700°C in order to avoid GNF degradation. A detailed study should however be performed on both the temperature and the duration of the pyrolysis treatment to maximize both the removal of nitrogen attached to amorphous carbon and the amount of pyridinic nitrogen on the catalyst surface.
4) The MEA preparation method used throughout this work was adequate for a first attempt at PEMFC studies, but the PEMFC preparation technique should ideally be improved. Switching to the catalyst coated membrane method for fabricating MEAs would immediately improve performance. Additionally, when working with one specific catalyst, the catalyst ink composition can be tuned to optimize its performance. If enough

material is available, one could conduct a study looking at the viscosity of the catalyst ink with respect to its Nafion^{TM}, alcohol, and water content to achieve a uniform deposition and ideal drying conditions. Having a better control of the catalyst layer would open the door to performing a modelling study to look at the porosity and volume which would also provide useful information on increasing the overall performance of the catalyst.

References

[1] S. Gupta, D. Tryk, I. Bae, W. Aldred, E. Yeager, Heat-treated polyacrylonitrile-based catalysts for oxygen electroreduction, Journal of Applied Electrochemistry. 19 (1989) 19–27.

[2] Structure of Fe-porphyrin subunit of heme B., (n.d.). https://en.wikipedia.org/wiki/Heme#/media/File:Heme_b.svg.

[3] R. Pristavita, N.Y. Mendoza-Gonzalez, J.L. Meunier, D. Berk, Carbon blacks produced by thermal plasma: The influence of the reactor geometry on the product morphology, Plasma Chemistry and Plasma Processing. 30 (2010) 267–279.

[4] P.-A. Pascone, Synthesis, characterization, and performance of graphene nanoflakes as a non-noble metal catalyst in polymer electrolyte membrane fuel cells, McGill University, 2013.

[5] M. Lefèvre, E. Proietti, F. Jaouen, J.-P. Dodelet, Iron-based catalysts with improved oxygen reduction activity in polymer electrolyte fuel cells., Science (New York, N.Y.). 324 (2009) 71–74.

[6] B. Scrosati, History of lithium batteries, Journal of Solid State Electrochemistry. 15 (2011) 1623–1630.

[7] P. Hurley, Build Your Own Fuel Cells, Wheelock Mountain Publications, 2002.

[8] F.T. Bacon, “The Fuel Cell: Some Thoughts and Recollections,” Journal of The Electrochemical Society. 126 (1979) 7C–17C.

[9] J.W. Fairbanks, Engine Maturity, Efficiency, and Potential Improvements, 2004.

[10] J. Zhang, H. Zhang, J. Wu, J. Zhang, PEM Fuel Cell Testing and Diagnosis, 1st ed.,

Elsevier B.V, 2013.

[11] S. Litster, G. McLean, PEM fuel cell electrodes, Journal of Power Sources. 130 (2004) 61–76.

[12] Overview - History; Principle of fuel cell technology, (2012). http://www.nptel.ac.in/courses/103102015/2.

[13] J. Garche, L. Jörissen, Applications of Fuel Cell Technology : Status and Perspectives, The Electrochemical Society Interface. (2015) 39–43.

[14] J.H. Wee, Applications of proton exchange membrane fuel cell systems, Renewable and Sustainable Energy Reviews. 11 (2007) 1720–1738.

[15] D. Banham, S. Ye, K. Pei, J.I. Ozaki, T. Kishimoto, Y. Imashiro, A review of the stability and durability of non-precious metal catalysts for the oxygen reduction reaction in proton exchange membrane fuel cells, Journal of Power Sources. 285 (2015) 334–348.

[16] M.T.M. Koper, ed., Fuel Cell Catalysis: A Surface Science Approach, Hoboken, New Jersey, 2009.

[17] M. Wakisaka, H. Suzuki, S. Mitsui, H. Uchida, M. Watanabe, Increased oxygen coverage at Pt-Fe alloy cathode for the enhanced oxygen reduction reaction studied by EC-XPS, Journal of Physical Chemistry C. 112 (2008) 2750–2755.

[18] I.E.L. Stephens, A.S. Bondarenko, U. Grønbjerg, J. Rossmeisl, I. Chorkendorff, Understanding the electrocatalysis of oxygen reduction on platinum and its alloys, Energy & Environmental Science. 5 (2012) 6744–6762.

[19] J.X. Wang, H. Inada, L. Wu, Y. Zhu, Y.Y.M.M. Choi, P. Liu, et al., Oxygen Reduction on Well-Defined Core- Shell Nanocatalysts: Particle Size, Facet, and Pt Shell Thickness

Effects, Journal of the American Chemical Society. 131 (2009) 17298–17302.

[20] L. Gan, C. Cui, S. Rudi, P. Strasser, Core-shell and nanoporous particle architectures and their effect on the activity and stability of Pt ORR electrocatalysts, Topics in Catalysis. 57 (2014) 236–244.

[21] R. Jasinski, A New Fuel Cell Cathode Catalyst, Nature. 201 (1964) 1212–1213.

[22] U.I. Kramm, J. Herranz, N. Larouche, T.M. Arruda, M. Lefèvre, F. Jaouen, et al., Structure of the catalytic sites in Fe/N/C-catalysts for O2-reduction in PEM fuel cells, Physical Chemistry Chemical Physics. 14 (2012) 11673–11688.

[23] H. Isago, Making a Molecule Functional, (n.d.). http://www.nims.go.jp/molfunc/English/English_summy.htm.

[24] T. Sun, B. Tian, J. Lu, C. Su, Recent advances in Fe (or Co)/N/C electrocatalysts for the oxygen reduction reaction in polymer electrolyte membrane fuel cells, Journal of Materials Chemistry A. 5 (2017) 18933–18950.

[25] A. Zitolo, V. Goellner, V. Armel, M.-T. Sougrati, T. Mineva, L. Stievano, et al., Identification of catalytic sites for oxygen reduction in iron- and nitrogen-doped graphene materials, Nature Materials. 14 (2015) 937–942.

[26] H. Alt, H. Binder, G. Sandstede, Mechanism of the electrocatalytic reduction of oxygen on metal chelates, Journal of Catalysis. 28 (1973) 8–19.

[27] G. Faubert, R. Côté, D. Guay, J.P. Dodelet, G. Dénès, P. Bertrandc, Iron catalysts prepared by high-temperature pyrolysis of tetraphenylporphyrins adsorbed on carbon black for oxygen reduction in polymer electrolyte fuel cells, Electrochimica Acta. 43 (1998) 341–353.

[28] G. Faubert, G. Lalande, R. Cote, D. Guay, J.P. Dodelet, L.T. Weng, et al., Heat-treated iron and cobalt tetraphenylporphyrins adsorbed on carbon black: physical characterization and catalytic properties of these materials for the reduction of oxygen in polymer electrolyte fuel cells, Electrochim. Acta. 41 (1996) 1689–1701.

[29] J. Herranz, F. Jaouen, M. Lefèvre, U.I. Kramm, E. Proietti, J.-P. Dodelet, et al., Unveiling N-Protonation and Anion-Binding Effects on Fe / N / C Catalysts for O 2 Reduction in Proton-Exchange-Membrane Fuel Cells, Journal of Physical Chemistry C. 115 (2011) 16087–16097.

[30] F. Jaouen, M. Lefèvre, J.-P. Dodelet, M. Cai, Heat-Treated Fe / N / C Catalysts for O 2 Electroreduction : Are Active Sites Hosted in Micropores ?, Journal of Physical Chemistry B. 110 (2006) 5553–5558.

[31] F. Jaouen, S. Marcotte, J.P. Dodelet, G. Lindbergh, Oxygen reduction catalysts for polymer electrolyte fuel cells from the pyrolysis of iron acetate adsorbed on various carbon supports, Journal of Physical Chemistry B. 107 (2003) 1376–1386.

[32] N. Larouche, R. Chenitz, M. Lefèvre, E. Proietti, J.P. Dodelet, Activity and stability in proton exchange membrane fuel cells of iron-based cathode catalysts synthesized with addition of carbon fibers, Electrochimica Acta. 115 (2014) 170–182.

[33] N. Larouche, B.L. Stansfield, Classifying nanostructured carbons using graphitic indices derived from Raman spectra, Carbon. 48 (2010) 620–629.

[34] M. Lefèvre, J.P. Dodelet, P. Bertrand, O2 Reduction in PEM Fuel Cells : Activity and Active Site Structural Information for Catalysts Obtained by the Pyrolysis at High Temperature of Fe Precursors O2 Reduction in PEM Fuel Cells : Activity and Active Site

Structural Information for Cata, Journal of Physical Chemistry B. 104 (2000) 11238–11247.

[35] M. Lefèvre, J.P. Dodelet, Fe-based electrocatalysts made with microporous pristine carbon black supports for the reduction of oxygen in PEM fuel cells, Electrochimica Acta. 53 (2008) 8269–8276.

[36] M. Lefèvre, J.-P. Dodelet, P. Bertrand, Molecular oxygen reduction in PEM fuel cells: Evidence for the simultaneous presence of two active sites in Fe-based catalysts, Journal of Physical Chemistry B. 106 (2002) 8705–8713.

[37] C. Médard, M. Lefèvre, J.P. Dodelet, F. Jaouen, G. Lindbergh, Oxygen reduction by Fe-based catalysts in PEM fuel cell conditions: Activity and selectivity of the catalysts obtained with two Fe precursors and various carbon supports, Electrochimica Acta. 51 (2006) 3202–3213.

[38] E. Proietti, F. Jaouen, M. Lefèvre, N. Larouche, J. Tian, J. Herranz, et al., Iron-based cathode catalyst with enhanced power density in polymer electrolyte membrane fuel cells., Nature Communications. 2 (2011) 416–424.

[39] G. Wu, K.L. More, C.M. Johnston, P. Zelenay, High-Performance Electrocatalysts, Science. 332 (2011) 443–448.

[40] Polyaniline structure, (2015). https://commons.wikimedia.org/wiki/File:Polyaniline_structure.svg.

[41] X. Fu, P. Zamani, J.Y. Choi, F.M. Hassan, G. Jiang, D.C. Higgins, et al., In Situ Polymer Graphenization Ingrained with Nanoporosity in a Nitrogenous Electrocatalyst Boosting the Performance of Polymer-Electrolyte-Membrane Fuel Cells, Advanced Materials. 29

(2017) 1–8.

[42] A. Peigney, C. Laurent, E. Flahaut, R.R. Bacsa, A. Rousset, Specific surface area of carbon nanotubes and bundles of carbon nanotubes, Carbon. 39 (2001) 507–514.

[43] T.W. Odom, J.-L. Huang, P. Kim, C.M. Lieber, Structure and Electronic Properties of Carbon Nanotubes, The Journal of Physical Chemistry B. 104 (2000) 2794–2809.

[44] E. Boysen, N.C. Muir, Nanotechnology for Dummies, 2nd ed., 2011.

[45] B. Merzougui, A. Hachimi, A. Akinpelu, S. Bukola, M. Shao, A Pt-free catalyst for oxygen reduction reaction based on Fe-N multiwalled carbon nanotube composites, Electrochimica Acta. 107 (2013) 126–132.

[46] S. Yasuda, A. Furuya, Y. Uchibori, J. Kim, K. Murakoshi, Iron-nitrogen-doped vertically aligned carbon nanotube electrocatalyst for the oxygen reduction reaction, Advanced Functional Materials. 26 (2016) 738–744.

[47] Graphene Oxide: Introduction and Market News, (n.d.). https://www.graphene-info.com/graphene-oxide.

[48] H.R. Byon, J. Suntivich, Y. Shao-Horn, Graphene-based non-noble-metal catalysts for oxygen reduction reaction in acid, Chemistry of Materials. 23 (2011) 3421–3428.

[49] C.H. Choi, M.W. Chung, H.C. Kwon, S.H. Park, S.I. Woo, B, N- and P, N-doped graphene as highly active catalysts for oxygen reduction reactions in acidic media, Journal of Materials Chemistry A. 1 (2013) 3694–3699.

[50] J. de la Fuente, Graphene Applications & Uses, (n.d.). https://www.graphenea.com/pages/graphene-properties#.WlUu7qinGUk.

[51] R. Pristavita, The Synthesis and Functionalization of Nanostructured Carbon Black by

Thermal Plasma for Use in PEM Fuel Cells, McGill University, 2011.

[52] D.M. Binny, Plasma Functionalization of Graphene Nanoflakes for Non-noble Catalyst in Fuel Cells, McGill University, 2013.

[53] Tekna, Induction Plasma Torch PL-35 & PL-50, Operations and Service Manual, (2004).

[54] R. Pristavita, J.L. Meunier, D. Berk, Carbon nano-flakes produced by an inductively coupled thermal plasma system for catalyst applications, Plasma Chemistry and Plasma Processing. 31 (2011) 393–403.

[55] J.L. Meunier, N.Y. Mendoza-Gonzalez, R. Pristavita, D. Binny, D. Berk, Two-Dimensional Geometry Control of Graphene Nanoflakes Produced by Thermal Plasma for Catalyst Applications, Plasma Chemistry and Plasma Processing. (2014) 505–521.

[56] M. Bron, J. Radnik, M. Fieber-Erdmann, P. Bogdanoff, S. Fiechter, EXAFS, XPS and electrochemical studies on oxygen reduction catalysts obtained by heat treatment of iron phenanthroline complexes supported on high surface area carbon black, Journal of Electroanalytical Chemistry. 535 (2002) 113–119.

[57] P. Burg, P. Fydrych, D. Cagniant, G. Nanse, J. Bimer, A. Jankowska, The characterization of nitrogen-enriched activated carbons by IR, XPS and LSER methods, Carbon. 40 (2002) 1521–1531.

[58] J.F. Moulder, W.F. Stickle, P.E. Sobol, K.D. Bomben, Handbook of X-ray Photoelectron Spectroscopy, Physical Electronis USA, Inc., 1995.

[59] L.A.N. Laboratory, XPS works, (2011). http://www.lanl.gov/orgs/nmt/nmtdo/AQarchive/04summer/XPS.html.

[60] NIST X-ray Photoelectron Spectroscopy Database, Version 4.1 (National Institute of

Standards and Technology, Gaithersburg, 2012)), (n.d.). http://srdata.nist.gov/xps/.

[61] C.V. Raman, K.S. Krishnan, A New Type of Secondary Radiation, Nature. 121 (1928) 501–502.

[62] E. Smith, G. Dent, Modern Raman Spectroscopy: A Practical Approach, John Wiley & Sons LTD, 2005.

[63] A.C. Ferrari, D.M. Basko, Raman spectroscopy as a versatile tool for studying the properties of graphene, Nat Nanotechnol. 8 (2013) 235–246.

[64] A.C. Ferrari, J.C. Meyer, V. Scardaci, C. Casiraghi, M. Lazzeri, F. Mauri, et al., Raman spectrum of graphene and graphene layers, Physical Review Letters. 97 (2006) 1–4.

[65] A.C. Ferrari, Raman spectroscopy of graphene and graphite: Disorder, electron-phonon coupling, doping and nonadiabatic effects, Solid State Communications. 143 (2007) 47–57.

[66] D.S. Knight, W.B. White, Characterization of diamond films by Raman spectroscopy, Journal of Materials Research. 4 (1989) 385–393.

[67] A. Cuesta, P. Dhamelincourt, J. Laureyns, A. Martinez-Alonso, J.M.D. Tascon, Comparative performance of X-ray diffraction and Raman microprobe techniques for the study of carbon materials, Journal of Materials Chemistry. 8 (1998) 2875–2879.

[68] R.F. Egerton, Physical Principles of Electron Microscopy, Second, Springer, 2005.

[69] S. Brunauer, P. Emmet, E. Teller, Adsorption of gases in multimolecular layers, J. Am. Chem. Soc. 60 (1938) 309–319.

[70] NMI3, For chemical analysis: Neutron Activation Analysis, (2012). http://nmi3.eu/neutron-research/techniques-for-/chemical-analysis.html.

[71] G. Instruments, Two, Three and Four Electrode Experiments, (2017). https://www.gamry.com/application-notes/electrodes-cells/two-three-and-four-electrode-experiments/.

[72] F. Opekar, P. Beran, Rotating disk electrodes, Journal of Electroanalytical Chemistry. 69 (1976) 1–105.

[73] J. Nikolic, E. Expósito, J. Iniesta, J. González-Garcia, V. Montiel, Theoretical Concepts and Applications of a Rotating Disk Electrode, Journal of Chemical Education. 77 (2000) 1191.

[74] H. Zhang, X. Wang, J. Zhang, J. Zhang, Conventional catalyst ink, catalyst layer and MEA preparation, in: PEM Fuel Cell Electrocatalysts and Catalyst Layers: Fundamentals and Applications, 2008: pp. 889–916.

[75] J.H. Cho, J.M. Kim, J. Prabhuram, S.Y. Hwang, D.J. Ahn, H.Y. Ha, et al., Fabrication and evaluation of membrane electrode assemblies by low-temperature decal methods for direct methanol fuel cells, Journal of Power Sources. 187 (2009) 378–386.

[76] G. Tsotridis, A. Pilenga, G. De Marco, T. Malkow, EU Harmonised Test Protocols for PEMFC MEA Testing in Single Cell Configuration for Automotive Applications; JRC Science for Policy report, 2015.

[77] A.K. Geim, A.H. MacDonald, Graphene: Exploring carbon flatland, Physics Today. 60 (2007) 35–41.

[78] U. Legrand, N.-Y. Mendoza Gonzalez, P. Pascone, J.-L. Meunier, D. Berk, Synthesis and in-situ oxygen functionalization of deposited graphene nanoflakes for nanofluid generation, Carbon. 102 (2016) 216–223.

[79] A. Yoo,J.J.; Balakrishnan, K.; Huang, J.; Meunier, V.; Sumpter, B.G.; Strivastava, Ultrathin Planar Graphene Supercapacitors., Nano Lett. 11 (2011) 1423–7.

[80] L. Qu, Y. Liu, J.B. Baek, L. Dai, Nitrogen-doped graphene as efficient metal-free electrocatalyst for oxygen reduction in fuel cells, ACS Nano. 4 (2010) 1321–1326.

[81] D.M. Binny, J.L. Meunier, D. Berk, Nitrogen doping of graphene nanoflakes by thermal plasma as catalyst for oxygen reduction in Proton Exchange Membrane fuel cells, Proceedings of the IEEE Conference on Nanotechnology. (2012) 8–13.

[82] Y. Shao, J. Sui, G. Yin, Y. Gao, Nitrogen-doped carbon nanostructures and their composites as catalytic materials for proton exchange membrane fuel cell, Applied Catalysis B: Environmental. 79 (2008) 89–99.

[83] C. Han, X. Bo, Y. Zhang, M. Li, A. Wang, L. Guo, Dicobalt phosphide nanoparticles encased in boron and nitrogen co-doped graphitic layers as novel non-precious metal oxygen reduction electrocatalysts in alkaline media, Chem. Commun. 51 (2015) 15015–15018.

[84] F. Jaouen, J. Herranz, M. Lefèvre, J.-P. Dodelet, U.I. Kramm, I. Herrmann, et al., Cross-laboratory experimental study of non-noble-metal electrocatalysts for the oxygen reduction reaction, ACS Applied Materials and Interfaces. 1 (2009) 1623–1639.

[85] M. Manzoli, F. Boccuzzi, Characterisation of Co-based electrocatalytic materials for O2 reduction in fuel cells, Journal of Power Sources. 145 (2005) 161–168.

[86] T.S. Olson, S. Pylypenko, J.E. Fulghum, P. Atanassov, Bifunctional Oxygen Reduction Reaction Mechanism on Non-Platinum Catalysts Derived from Pyrolyzed Porphyrins, Journal of The Electrochemical Society. 157 (2010) B54–B63.

[87] I. Roche, K. Scott, Carbon-supported manganese oxide nanoparticles as electrocatalysts for oxygen reduction reaction (orr) in neutral solution, Journal of Applied Electrochemistry. 39 (2009) 197–204.

[88] Y. Si, Z. Xiong, X. Liu, M. Li, A Highly Active Nitrogen-Containing Non-Precious Metal Catalyst CoHMTA / C for Oxygen Reduction Reaction, International Journal of Electrochemical Science. 10 (2015) 5212–5221.

[89] R. Sirirak, T. Sarakonsri, M. Medhesuwakul, Non-platinum nanocatalyst on porous nitrogen-doped carbon fabricated by cathodic vacuum arc plasma technique, Applied Surface Science. 356 (2015) 512–520.

[90] S. Tang, H. Huangfu, Z. Dai, L. Sui, Z. Zhu, Preparation of Fe-N-Carbon Nanocoils as Catalyst for Oxygen Reduction Reaction, International Journal of Electrochemical Science. 10 (2015) 7180–7191.

[91] G. Wang, W. Wang, L.-K. Wang, W.-T. Yao, P.-F. Yao, W.-K. Zhu, et al., A N-, Fe- and Co-tridoped carbon nanotube/nanoporous carbon nanocomposite with synergistically enhanced activity for oxygen reduction in acidic media, J. Mater. Chem. A. 3 (2015) 17866–17873.

[92] J. Wu, Y. Wang, D. Zhang, B. Hou, Studies on the electrochemical reduction of oxygen catalyzed by reduced graphene sheets in neutral media, Journal of Power Sources. 196 (2011) 1141–1144.

[93] Z.-Y. Yang, Y.-X. Zhang, L. Jing, Y.-F. Zhao, Y.-M. Yan, K.-N. Sun, Beanpod-shaped Fe–C–N composite as promising ORR catalyst for fuel cells operated in neutral media, Journal of Materials Chemistry A. 2 (2014) 2623–2627.

[94] X. Zhang, W. Ouyang, D. Zeng, Y. Zhan, F. Xie, W. Zhang, et al., Nitrogen doped sublimed carbon as non-noble metal catalyst for oxygen reduction reaction, Catalysis Today. 264 (2016) 206–213.

[95] F. Bidault, D.J.L. Brett, P.H. Middleton, N.P. Brandon, Review of gas diffusion cathodes for alkaline fuel cells, Journal of Power Sources. 187 (2009) 39–48.

[96] Q. He, Q. Li, S. Khene, X. Ren, F.E. Lopez-Suarez, D. Lozano-Castello, et al., High-loading cobalt oxide coupled with nitrogen-doped graphene for oxygen reduction in anion-exchange-membrane alkaline fuel cells, Journal of Physical Chemistry C. 117 (2013) 8697–8707.

[97] I. Kruusenberg, L. Matisen, Q. Shah, A.M. Kannan, K. Tammeveski, Non-platinum cathode catalysts for alkaline membrane fuel cells, International Journal of Hydrogen Energy. 37 (2012) 4406–4412.

[98] M. Liu, R. Zhang, W. Chen, Graphene-supported nanoelectrocatalysts for fuel cells: Synthesis, properties, and applications, Chemical Reviews. 114 (2014) 5117–5160.

[99] R. Liu, D. Wu, X. Feng, K. Müllen, Nitrogen-doped ordered mesoporous graphitic arrays with high electrocatalytic activity for oxygen reduction, Angewandte Chemie - International Edition. 49 (2010) 2565–2569.

[100] Z. Mo, S. Liao, Y. Zheng, Z. Fu, Preparation of nitrogen-doped carbon nanotube arrays and their catalysis towards cathodic oxygen reduction in acidic and alkaline media, Carbon. 50 (2012) 2620–2627.

[101] K. Niu, B. Yang, J. Cui, J. Jin, X. Fu, Q. Zhao, et al., Graphene-based non-noble-metal Co/N/C catalyst for oxygen reduction reaction in alkaline solution, Journal of Power

Sources. 243 (2013) 65–71.

[102] E.H. Yu, X. Wang, U. Krewer, L. Li, K. Scott, Direct oxidation alkaline fuel cells: from materials to systems, Energy & Environmental Science. 5 (2012) 5668–5680.

[103] E.H. Yu, U. Krewer, K. Scott, Principles and materials aspects of direct alkaline alcohol fuel cells, Energies. 3 (2010) 1499–1528.

[104] P.-A. Pascone, D. Berk, J.-L. Meunier, A stable and active iron catalyst supported on graphene nano-flakes for the oxygen reduction reaction in polymer electrolyte membrane fuel cells, Catalysis Today. 211 (2013) 162–167.

[105] S.J. Amirfakhri, P.-A. Pascone, J.-L. Meunier, D. Berk, Fe–N-doped graphene as a superior catalyst for H2O2 reduction reaction in neutral solution, Journal of Catalysis. 323 (2015) 55–64.

[106] V.H. Luan, H.N. Tien, L.T. Hoa, N.T.M. Hien, E. Oh, J.S. Chung, et al., Synthesis of a highly conductive and large surface area graphene oxide hydrogel and its use in a supercapacitor, Journal of Materials Chemistry A. 1 (2013) 208–211.

[107] M.A. Worsley, S.O. Kucheyev, H.E. Mason, M.D. Merrill, B.P. Mayer, J. Lewicki, et al., Mechanically robust 3D graphene macroassembly with high surface area, Chemical Communications. 48 (2012) 8428–8430.

[108] S. Yang, L. Zhi, K. Tang, X. Feng, J. Maier, K. Müllen, Efficient synthesis of heteroatom (N or S)-doped graphene based on ultrathin graphene oxide-porous silica sheets for oxygen reduction reactions, Advanced Functional Materials. 22 (2012) 3634–3640.

[109] M.D. Stoller, S. Park, Y. Zhu, J. An, R.S. Ruoff, Graphene-Based Ultracapacitors, Nano Letters. 8 (2008) 3498–3502.

[110] C. Castiglioni, C. Mapelli, F. Negri, G. Zerbi, Origin of the D line in the Raman spectrum of graphite: A study based on Raman frequencies and intensities of polycyclic aromatic hydrocarbon molecules, Journal of Chemical Physics. 114 (2001) 963–974.

[111] T. Jawhari, A. Roid, J. Casado, Raman spectroscopic characterization of some commercially available carbon black materials, Carbon. 33 (1995) 1561–1565.

[112] Y. Wang, D.C. Alsmeyer, R.L. Mccreery, Raman Spectroscopy of Carbon Materials: Structural Basis of Observed Spectra, Chemistry of Materials. 2 (1990) 557–563.

[113] C. Song, J. Zhang, Electrocatalytic Oxygen Reduction Reaction, 2008.

[114] J. Spendelow, J. Marcinkoski, DOE Fuel Cell Technologies Office Record 14012: Fuel Cell System Cost - 2013, 2014.

[115] C.W.B. Bezerra, L. Zhang, K. Lee, H. Liu, A.L.B. Marques, E.P. Marques, et al., A review of Fe-N/C and Co-N/C catalysts for the oxygen reduction reaction, Electrochimica Acta. 53 (2008) 4937–4951.

[116] U.I. Kramm, I. Herrmann-Geppert, J. Behrends, K. Lips, S. Fiechter, P. Bogdanoff, On an Easy Way To Prepare Metal–Nitrogen Doped Carbon with Exclusive Presence of MeN 4 -type Sites Active for the ORR, Journal of the American Chemical Society. 138 (2016) 635–640.

[117] S. Pylypenko, S. Mukherjee, T.S. Olson, P. Atanassov, Non-platinum oxygen reduction electrocatalysts based on pyrolyzed transition metal macrocycles, Electrochimica Acta. 53 (2008) 7875–7883.

[118] Z. Wu, S. Yang, Y. Sun, K. Parvez, X. Feng, 3D Nitrogen-Doped Graphene Aerogel-Supported Fe 3 O 4 Nanoparticles as Efficient Electrocatalysts for the Oxygen Reduction

Reaction, Journal of the American Chemical Society. (2012) 10–13.

[119] X. Li, G. Liu, B.N. Popov, Activity and stability of non-precious metal catalysts for oxygen reduction in acid and alkaline electrolytes, Journal of Power Sources. 195 (2010) 6373–6378.

[120] S. Jiang, C. Zhu, S. Dong, Cobalt and nitrogen-cofunctionalized graphene as a durable non-precious metal catalyst with enhanced ORR activity, Journal of Materials Chemistry A. 1 (2013) 3593–3599.

[121] K. Elumeeva, J. Ren, M. Antonietti, T.P. Fellinger, High Surface Iron/Cobalt-Containing Nitrogen-Doped Carbon Aerogels as Non-Precious Advanced Electrocatalysts for Oxygen Reduction, ChemElectroChem. 2 (2015) 584–591.

[122] Y. Liu, X. Yue, K. Li, J. Qiao, D.P. Wilkinson, J. Zhang, PEM fuel cell electrocatalysts based on transition metal macrocyclic compounds, Coordination Chemistry Reviews. 315 (2016) 153–177.

[123] D. Singh, J. Tian, K. Mamtani, J. King, J.T. Miller, U.S. Ozkan, A comparison of N-containing carbon nanostructures (CNx) and N-coordinated iron-carbon catalysts (FeNC) for the oxygen reduction reaction in acidic media, Journal of Catalysis. 317 (2014) 30–43.

[124] P.-A. Pascone, J. de Campos, J.-L. Meunier, D. Berk, Iron Incorporation on Graphene Nanoflakes for the Synthesis of a Non-noble Metal Fuel Cell Catalyst, Applied Catalysis B: Environmental. 193 (2016) 9–15.

[125] C. Chilian, G. Kennedy, The NAA method at Polytechnique Montreal: an efficient alternative way to use the k 0 NAA models, Journal of Radioanalytical and Nuclear Chemistry. 300 (2014) 533–538.

[126] S.S. Kocha, Y. Garsany, D. Myers, Testing Oxygen Reduction Reaction Activity with the Rotating Disc Electrode Technique, DOE Webinar. (2013).

[127] A. Bard, R. Parson, J. Jordan, Standard potentials in aqueous solution, 1985.

[128] K.A. Kurak, A.B. Anderson, Nitrogen-Treated Graphite and Oxygen Electroreduction on Pyridinic Edge Sites, J. Phys. Chem. C. 113 (2009) 6730–6734.

[129] A. Serov, M.H. Robson, K. Artyushkova, P. Atanassov, Templated non-PGM cathode catalysts derived from iron and poly(ethyleneimine) precursors, Applied Catalysis B: Environmental. 127 (2012) 300–306.

[130] M.K. Debe, Electrocatalyst approaches and challenges for automotive fuel cells, Nature. 486 (2012) 43–51.

[131] J. Tollefson, Hydrogen vehicles: Fuel of the future?, Nature. 464 (2010) 1262–1264.

[132] P.-A. Pascone, J.-L. Meunier, D. Berk, Influence of iron on structure and catalyst activity of nitrogen-functionalized graphene nanoflakes, Materials Today Communications. 9 (2016) 54–59.

[133] H.A. Gasteiger, S.S. Kocha, B. Sompalli, F.T. Wagner, Activity benchmarks and requirements for Pt, Pt-alloy, and non-Pt oxygen reduction catalysts for PEMFCs, Applied Catalysis B: Environmental. 56 (2005) 9–35.

[134] K.C. Neyerlin, W. Gu, J. Jorne, H.A. Gasteiger, Study of the Exchange Current Density for the Hydrogen Oxidation and Evolution Reactions, Journal of The Electrochemical Society. 154 (2007) B631–B635.

[135] H.Y. Jung, J.W. Kim, Role of the glass transition temperature of Nafion 117 membrane in the preparation of the membrane electrode assembly in a direct methanol fuel cell

(DMFC), International Journal of Hydrogen Energy. 37 (2012) 12580–12585.

[136] R. O’Hayre, S.-W. Cha, W. Colella, F.B. Prinz, Fuel Cell Fundamentals, 3rd ed., Wiley, 2016.

[137] R. Perry, D. Green, J. Maloney, eds., Chemical Engineers’ Handbook, Seventh Ed, McGraw Hill, 1997.

[138] J.Y. Cheon, T. Kim, Y. Choi, H.Y. Jeong, M.G. Kim, Y.J. Sa, et al., Ordered mesoporous porphyrinic carbons with very high electrocatalytic activity for the oxygen reduction reaction, Scientific Reports. 3.2715 (2013) 1–8.

[139] K. Strickland, E. Miner, Q. Jia, U. Tylus, N. Ramaswamy, W. Liang, et al., Highly active oxygen reduction non-platinum group metal electrocatalyst without direct metal–nitrogen coordination, Nature Communications. 6.7343 (2015) 1–8.

[140] D. Zhao, J.L. Shui, L.R. Grabstanowicz, C. Chen, S.M. Commet, T. Xu, et al., Highly efficient non-precious metal electrocatalysts prepared from one-pot synthesized zeolitic imidazolate frameworks, Advanced Materials. 26 (2014) 1093–1097.

[141] A.L. Dicks, R. Othman, Z. Zhu, Non precious metal catalysts for the PEM fuel cell cathode, International Journal of Hydrogen Energy. 37 (2012) 357–372.

[142] H. Liu, Z. Shi, J. Zhang, L. Zhang, J. Zhang, Ultrasonic spray pyrolyzed iron-polypyrrole mesoporous spheres for fuel celloxygen reduction electrocatalysts, J. Mater. Chem. 19 (2009) 468–470.

[143] Y. Wei, C. Shengzhou, L. Weiming, Oxygen reduction on non-noble metal electrocatalysts supported on N-doped carbon aerogel composites, International Journal of Hydrogen Energy. 37 (2012) 942–945.

[144] A.H.A. Monteverde Videla, L. Osmieri, S. Specchia, Non-noble Metal (NNM) Catalysts for Fuel Cells: Tuning the Activity by a Rational Step-by-Step Single Variable Evolution, in: Electrochemistry of N4 Macrocyclic Metal Complexes: Volume 1: Energy, Second Edition, 2016: pp. 69–101.

[145] P.-A. Pascone, D. Berk, J.-L. Meunier, A stable and active iron catalyst supported on graphene nano-flakes for the oxygen reduction reaction in polymer electrolyte membrane fuel cells, Catalysis Today. 211 (2013) 162–167.

[146] U. Legrand, J.L. Meunier, D. Berk, Iron functionalization on graphene nanoflakes using thermal plasma for catalyst applications, Applied Catalysis A: General. 528 (2016) 36–43.

[147] R. Bashyam, P. Zelenay, A class of non-precious metal composite catalysts for fuel cells, Nature. 443 (2006) 63–66.

[148] H. Schulenburg, S. Stankov, V. Schunemann, J. Radnik, I. Dorbandt, S. Fiechter, et al., Catalysts for the oxygen reduction from heat-treated iron(III) tetramethoxyphenylporphyrin chloride: Structure and stability of active sites, Journal of Physical Chemistry B. 107 (2003) 9034–9041.

[149] B. Wang, Recent development of non-platinum catalysts for oxygen reduction reaction, Journal of Power Sources. 152 (2005) 1–15.

[150] D. Deng, L. Yu, X. Chen, G. Wang, L. Jin, X. Pan, et al., Iron Encapsulated within Pod-like Carbon Nanotubes for Oxygen Reduction Reaction, Angewandte Chemie - International Edition. 52 (2013) 371–375.

Appendix A: Operation Procedure for the Tekna System

This procedure describes how to start the utilities for the Tekna system with argon as central, sheath and powder gases.

Start up procedure:

- Verify that the RF generator breaker (found in the center corridor between lab 5310 and 5150) is in the off position.
- Verify the torch and the connections (Figure 1) in the Faraday cage. Make sure that the cage is properly closed.

Figure 1

- Open the right side panel of the main system in lab 5130 and verify that the switch is in the "B" position (Figure 2).

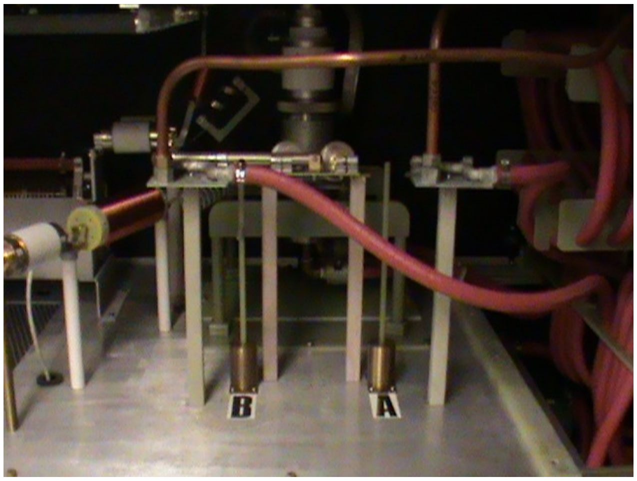

Figure 2

- Lift the reactor bottom plate and close the reactor.
- Switch the RF console control breaker, situated behind the generator (next to the electrode erosion system) to the ON position, and rotate 90 deg clockwise the yellow knob located on the control console (next to the rotameters). The computer monitor should be on after a few seconds. If not, a manual start must be done using the computer found in the Automatisation Panel (use the key to open door located on the same side of the control console).
- Log into the Plasma program.
- Verify that valve 1 on the gas exit line is pointing towards the ceiling, i.e. the "B" position (Figure 3).

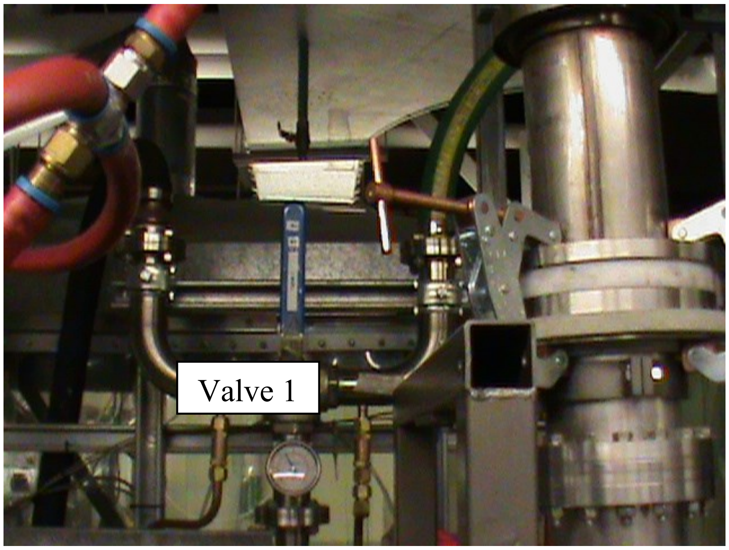

Figure 3

- Verify that the argon tank connection, labeled "Valve 2" is attached to the argon tank.
- Open valve 3 to allow argon to the control console. The ideal operating conditions will require 100 – 120 psig of gas as the inlet operating pressure. If the pressure reading exceeds 120 psig don't adjust any pressure because these readings will decrease when the vacuum is on. If the pressure is below 100 psig, increase the pressure by turning the pressure adjusting valve on the argon tank.
- Verify that valve 4 is closed, preventing the argon from draining.

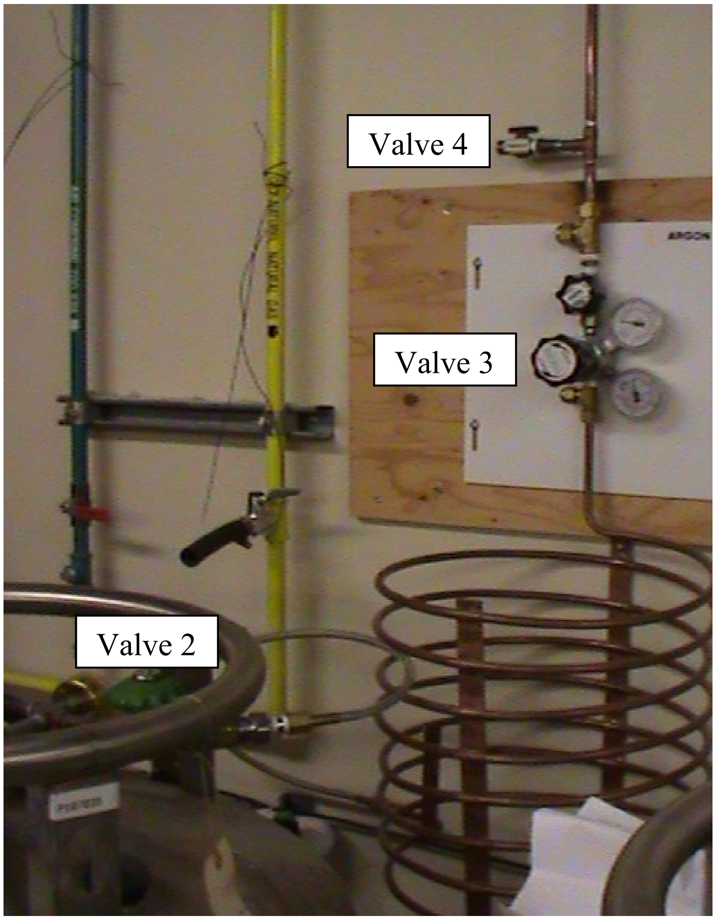

Figure 4

- Open valve 5, Argon Inlet to allow the gas flow into the system and check again the pressure reading on the argon tank regulator
- Verify that valve 6, for the auxiliary gas 1, is closed.
- Verify that valve 7, the hydrogen inlet, is closed.
- Verify that valve 8, compressed air inlet, is opened.

  NOTE: All the valves in the compressed air line, green line, must always be open. There is no need to adjust them.

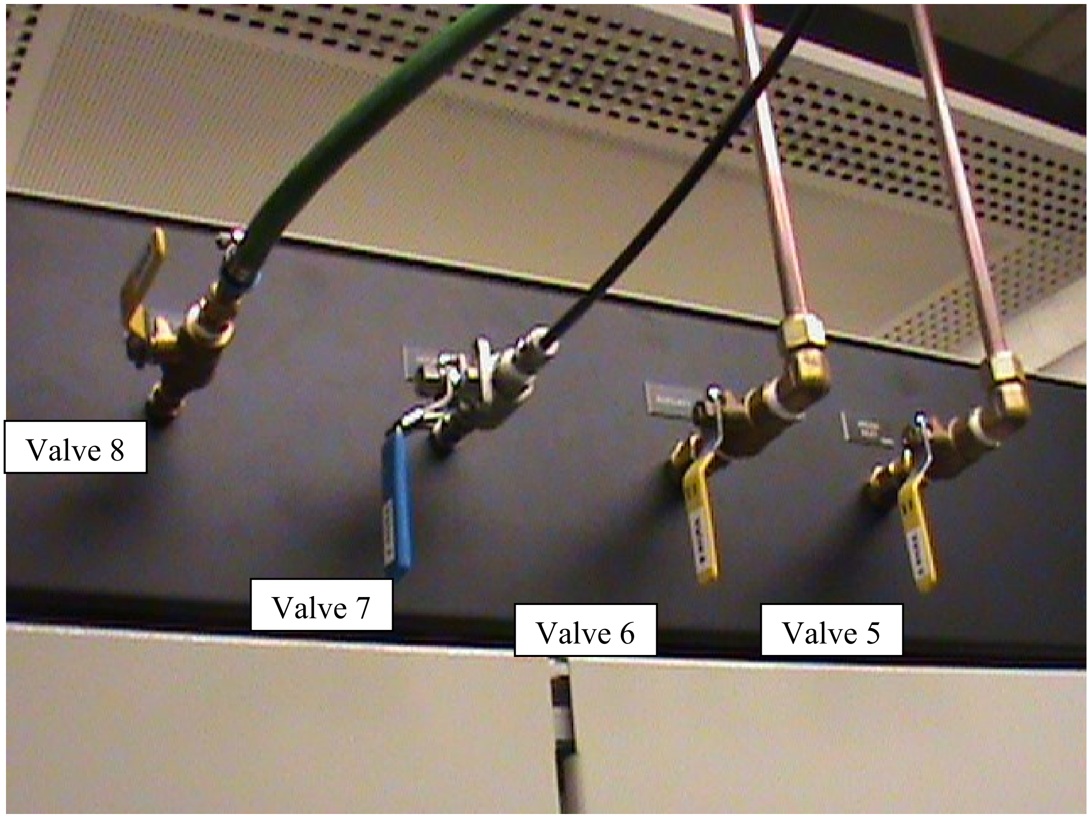

Figure 5

- Adjust all the valves to the vacuum pump: open valves 10, 11 that help to control the strength of the vacuum. It has been adjusted and it should only be re-adjusted if a vacuum lower than 2 psig is needed. Valve 12 should always be closed.
- Close valves 13 and 14 that allow the exhaust of gas from the DC system (Figure 6). This is very important in order to prevent contamination from DC system to the ICP system.
- Verify that valve 15 is open (Figure 7). This valve opens the vacuum line from the ICP system to the vacuum pump.
- Verify that valve 16 is opened (this valve should always be opened).
- Verify that valve 17 (valve used for the DC system), is closed.
- Open valve 18.
- The vacuum pump needs water to operate. Verify that valve 19, the drain valve of the vacuum pump water reservoir is closed (this valve should always be closed and should be opened only when a drain of the vacuum pump water reservoir is necessary). You need to go to the other side of the lab (underneath the DC plasma system) to control these valves.

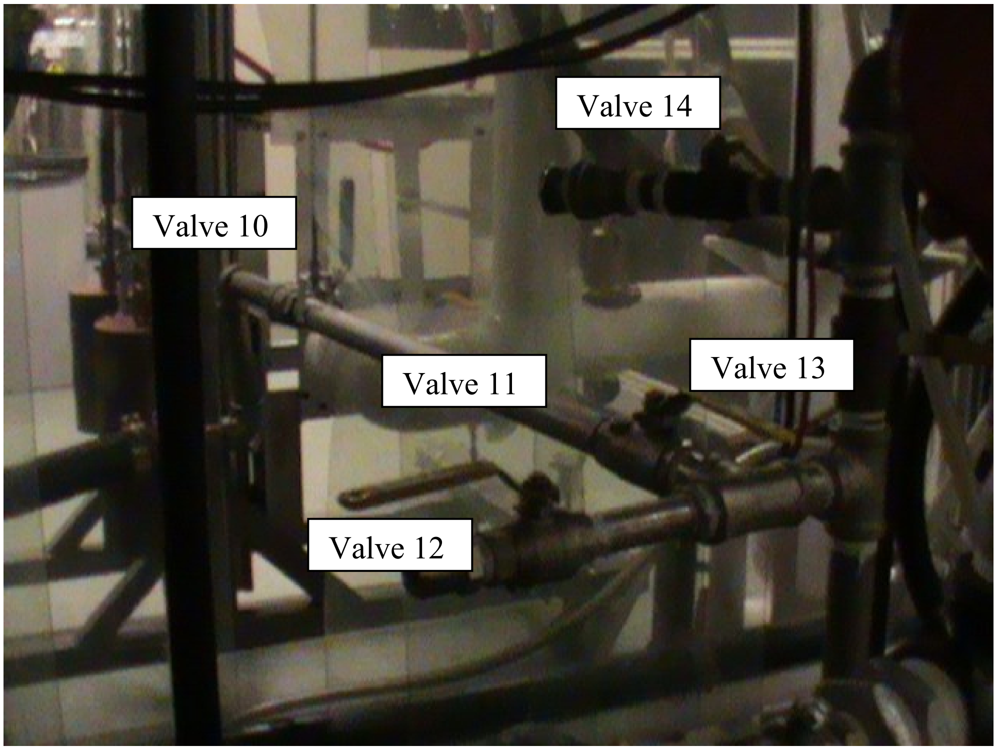

Figure 6

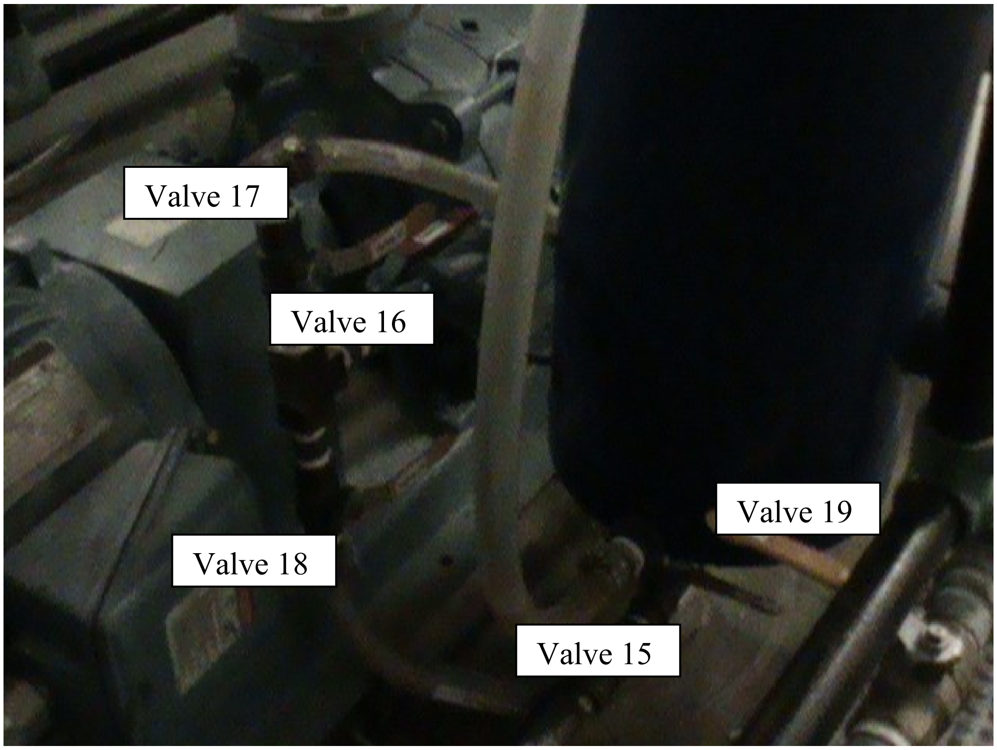

Figure 7

- Before starting the cooling water in the lab, check that valve 9 for the system cooling water tank drain is closed.
- Slightly open valve 20 to start the lab cooling water.
- Open the drain valve 21 to check that there is cooling water running in the line and, in case the system was not run in the last few weeks let the water run for about 1 minute to clean any dirt and deposit from the line. Then close the drain valve 21.
- Open valve 20 completely (**Do it slowly!**)
- Verify that valve 23 (dirty drain) and valve 24 (clean drain) of the generator supply water tank are closed.
- Verify that valve 25 (situated on top of the water tank) is about 1 turn away from being completely closed.
- Open valve 22 to allow cooling water from the lab line to fill the water tank. **This valve has a safety switch. Don't force it. Pull the switch before turning.**
- Wait for the water to fill up the tank. When water starts coming out the top, close valve 25 quickly. The filter should be full.
- Open slowly valve 26 to let water into the ICP system. **This valve has a safety switch, too.**
- This water line is used by the system for the cooling on the torch and probe.
- For the cooling of the reactor, the system uses another water tank, situated inside the control console, on the other side of the lab, next to the argon tank. Open the back door and close the water tank valve (valve 9). Open valves 27 and 28 (on the left side of the reactor) to allow water to fill the tank.
- The lab is equipped with a booster pump that you need to turn on after the cooling water has been started. Turn the switch breaker labeled "booster pump" and then rotate the knob located in the adjacent controller to AUTO position (remember that the breaker must always be turned on first). The breaker and the controller are situated on the corner wall of the lab, next to the DC plasma system.

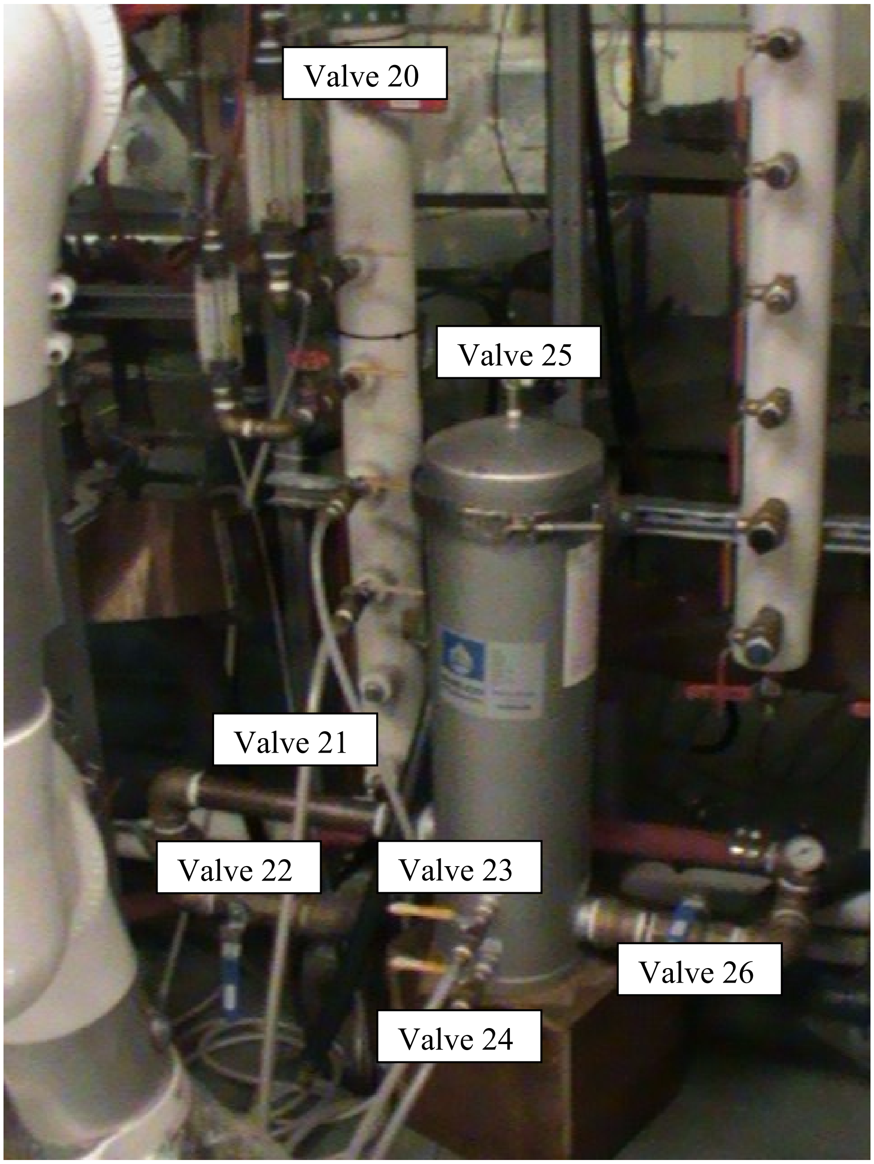

Figure 8

- Switch the RF generator breaker found in the center corridor.
- Turn on the high voltage switch situated on the main control console, next to the computer screen.
- Turn on filament, situated also on the main control console. The filament needs 15 minutes to heat.
- Log on the system and open a work session. Be sure you choose the B side of reactor.

- In the window on the touch pad screen, set the initial pressure, PID values, and gas flows (Table 1).

Table 1

Item	Value
Pressure	2.0 psig
K	7.6
I	6.6
D	1.1
Central gas flow rate	45 slpm
Sheath gas flow rate	13 slpm
Torch and probe flow rate	4.5 slpm

- The vacuum pump can now be turned on. First open valve 29 to allow water flow to the vacuum pump. **Verify that there is a flow of at least 9 gpm for the needed by the vacuum pump for safe operation.**
- Then press “Vacuum”.
- Switch the vacuum pump breaker on and then press the green start button on the controller underneath the breaker. These breakers are situated next to the breakers for the booster pump.
- Now it is time to start the gas flow. On the computer monitor press “Gas flow”.
- Adjust valve 12 to “help” the PID controller reach the desired pressure. Ideally, the control valve should be closed about 80% for a stable operation of the controller.
- When the pressure reached 2 psig and the controller is stable, the system is ready for plasma ignition.
- On the computer monitor select “Standby”. Check the time elapsed for filament heating.
- Adjust the grid to a value of 7.2.
- Pull “RF On” button.
- Turn the power knob to a value of approximately 28. At this point the plasma should be on.
- Using the grid, power knob, gauges on the panel, and the power reading on the computer monitor, adjust till the power reaches a value of approximately 20 KW. Ideally, plate amperes value should be 10 times greater than the grid amperes value.

- When system is stable for a few minutes, it is time for the carbon source injection. On the computer monitor, set the pressure to the desired operation value and also change the PID values (Table 2).

Table 2

Item	Value
Pressure	8.0 psig
K	1.8
I	11.4
D	1.9

- Adjust valve 12 to "help" the PID controller reach the desired pressure. Ideally, the control valve should be opened 80%.
- Set the gas flow rates for Methane and Nitrogen on the mass flow controller (Table 3).

Table 3

Gas	Mass Flow Controller Setting
Methane	1slpm
Nitrogen	0.1 slpm

- When the system is stable and it reached the desired experimental pressure, introduce methane and nitrogen into the system. First open the cylinders regulators (cylinders are situated in the right side of the lab, next to the blue cabinet) and then turn on the mass flow meters.
- ***If you intend to only grow this type of GNF,*** to obtain uniform powder morphology it is advised to run experiments for no more than 30 minutes.

High Nitrogen Functionalization

- Turn on valve 6.
- Turn off methane flow and change the Nitrogen flow to 5 slpm.
- Increase power to 28 kW to compensate for the power drop that will occur to ensure that the plasma doesn't go out.

- On the control panel, swap the sheath gas control from Ar to Ar/Aux. Set the Aux gas flow rate of sheath gas to 45 and the Ar to 0. This will mean that for a few seconds, both gases are on, so try to minimize this time.
- Change the probe flow to 0 slpm.
- Drop the pressure to 2 psia using the same PID values in Table 1.
- Increase the power to 25 kW.
- For this stage, run for 30 minutes.

Shut down procedure:

- Turn off the methane and nitrogen flows by closing the tank valves.
- Decrease power knob to 0.
- Push “RF On” button
- Turn filament off.
- **Turn off the RF generator breaker.**
- On the computer monitor select “Manual”.
- Turn off the high voltage switch.
- Set the pressure to 14 psig and open valve 12 completely to “help” the system reach atmospheric pressure.
- When close enough to 14, turn off the vacuum pump controller and then the switch breaker. Make sure that you stop the flow of gas to the reactor immediately (by pressing the “Gas flow” button on the computer screen) after you stop the vacuum pump. You may have to run across the lab to do this otherwise the pressure in the reactor will build up quite fast.
- Close valve 29 to stop the water flow to the vacuum pump.
- Similarly, the lab booster pump must be switched off. Turn the controller to the middle position. i.e. between auto and manual and then switch off the breaker.
- The vacuum valve must be closed thus isolating the ICP system from the DC system (valve 19).
- Close valve 18.
- Wait about 5 minutes, then press “Water cooling” and “Torch and Probe”.
- Close valves 27 and 28 and open the water tank drain valve 9.
- Stop the main lab water line supply by closing valve 20.

- Close valves 22 and 26 to stop water entering the ICP system.
- Open drain valves 23 and 24 to drain the water tank. For this you need to vent the tank by opening valve 25.
- The gas flow rates can be stopped by closing the valve 5 first. Then close the tank valve and open valve 4 to vent the system.
- On the computer monitor, exit the plasma program.
- Turn off the yellow knob located on the control console (next to the rotameters).
- Switch the RF console control breaker to the OFF position.
- Let the reactor cool for over 2 hours before retrieving sample inside. **Wear HEPA mask when opening the full reactor.**

NOTE: If you hear an unusual noise or alarm, check that all utilities are running properly.